Universidad del País Vasco

Euskal Herriko Unibertsitatea

Nonequilibrium Dynamics and Molecular Mobility in Polymer Glasses: From Bulk to 3-D Confinement

Doctoral Thesis submitted by

Natalia Gutiérrez Pérez de Eulate

to the

University of the Basque Country

Supervised by

Dr. Daniele Cangialosi

Polymers and Soft Matter Group

Physics Department – Faculty of Chemistry

Donostia – San Sebastián, 2018

INSTITUTIONS

Materials Physics Center
Centro de Física de Materiales
(CSIC-UPV/EHU)
Donostia – San Sebastián (España)

Université Libre de Bruxelles (ULB)
Bruselas (Bélgica)

Ministerio de Economía,
Industria y Competitividad

“La ciencia, muchacho, está hecha de errores, pero de errores útiles de cometer, pues poco a poco, conducen a la verdad”

Julio Verne

ABSTRACT

Since the discovery of polymers in the past century, their use has become ubiquitous in our everyday lives. Until recently, applications have focused on the use of polymers where the bulk characteristics of the macromolecules have been of primary interest. Within the wide variety of polymers, an important sub-class is represented by glass-forming polymers. The main characteristic of these materials is that they can exist in an amorphous phase below the melting point and, when they are cooled to the glassy state, they exhibit the rigidity of a solid but without long-range molecular order of crystals. With respect to polymer glasses, their main advantage is that they are light and easy to manufacture, while possessing high transparency and reasonable rigidity. Given all these important practical uses as well as the need for a fundamental understanding of their properties, polymer glasses have been studied for decades.

Within the search for a comprehensive understanding of glasses, given their non-equilibrium nature, there has been an intense research in understanding the thermodynamics of polymer glasses and the kinetics of equilibrium recovery at a fundamental level, and their connection to the glass transition. These aspects of polymers glasses are shared with glasses of any nature. In this sense, there have been many theories trying to explain the origin of the slowdown of molecular dynamics close to the glass transition. Recently, the possibility of confining polymer glasses at the nanoscale has opened new strategies to shed light on the so-far unanswered questions on the glass transition and the non-equilibrium glassy state.

Abstract

Nowadays, shifts in the glass transition temperature, is a well-documented effect of confinement, which for more than 20 years have been fascinating a broad community of researchers. This thesis aims to provide novel insights on non-equilibrium phenomena of polymer glasses confined at the nanoscale. To this end, we have established an optimal methodology, ranging from the preparation and characterization to the study of glass transition related phenomena of bulk and confined systems. Specifically, the research was focused on the non-equilibrium effects below the glass transition temperature (T_g). Furthermore, in the framework of non-equilibrium effects, in this work it is also shown how in confinement these can be of utmost importance even above T_g.

This thesis is divided into seven different chapters going from the state of the art to the future perspectives on the dynamics and thermodynamics of confined polymer glasses.

In Chapter 1, we start providing a general introduction to the thermodynamics and dynamics of glass-forming systems, followed by a summary on recent advancements in the research on confined polymer glasses. We conclude Chapter 1 with the aim and the outline of this thesis.

In Chapter 2, we introduce the main experimental techniques employed in this thesis. In particular, *standard* Differential Scanning Calorimetry (DSC), Fast Scanning Calorimetry (FSC) and Spectroscopic Ellipsometry are described with particular emphasis on how they can be exploited to characterize vitrification and non-equilibrium phenomena. Furthermore, complementary techniques such as Dynamic Light Scattering (DLS) and Atomic Force Microscopy (AFM) are described, showing how they can be employed to characterize the morphology of the obtained confined systems object of the present study, that is, polymer nanospheres and thin films.

In Chapter 3, we present results on the characterization of different aspects of the glass transition of poly(styrene) (PS) nanospheres and its bulk homologue by FSC. The aim of this chapter was to provide information on the molecular mobility and the way vitrification takes places. The most interesting aspects that emerged from this study were that (i) when decreasing the diameter of PS nanospheres, a decrease in T_g was observed. On the other hand, (ii) the molecular mobility was shown not to be affected by the size of the nanospheres, displaying bulk-like behavior for all systems. These results point toward a decoupling between vitrification and molecular mobility and a more efficient ability of maintaining equilibrium in PS nanospheres in comparison to the bulk.

In Chapter 4, we present physical aging experiments of bulk and PS nanospheres performed by FSC. In accordance with the previous results obtained from Chapter 3, it was found that these systems maintained more efficiently the thermodynamic equilibrium in comparison to the bulk homologue. This was evidenced by the observation of accelerated physical aging in PS nanospheres. Furthermore, our aging experiments showed a complex behavior of equilibrium recovery, supporting the existence of two mechanisms of equilibration, in ways analogous to bulk polymer glasses. However, the acceleration of physical aging in PS nanospheres allows detecting the two mechanisms of equilibration in considerably shorter time scales than in bulk.

In Chapter 5, we show how complex equilibrium recovery behavior obtained in PS nanospheres, with two steps of equilibration, can also be found in very long-term physically aged bulk polymers glasses. In this section, we monitored the physical aging of three types of polymers such as poly(arylate) (PAr), poly(carbonate) (PC) and poly(sulfone) (PSU) aged at room temperature for up to 30 years by *standard* DSC.

In Chapter 6, we focus on the non-equilibrium dynamics in confined polymer glasses by studying the kinetics of equilibrium recovery in polymers supported on a substrate above T_g. For that purpose, we studied poly(tert-butylstyrene) (PTBS) supported thin films, an analog of PS, by means of Spectroscopic Ellipsometry. These thin films were subjected to an annealing temperature (T_a) of 50 K higher than bulk T_g. The aim of this study was to observe the evolution of T_g with annealing time and film thickness. It was highlighted the importance of the adsorbed layer between the polymer and substrate in producing an increase of T_g toward the bulk value.

Finally, in Chapter 7 we summarize the main results and conclusions obtained from this thesis. The general objective of this work was to reach a deep understanding of the aspects that influence the glass transition of amorphous or glassy materials based on polymers, with special attention to those systems subjected to geometrical confinement. Hence, this thesis contributes to the progress of understanding the non-equilibrium effects at the nanoscale level and in bulk amorphous polymers.

RESUMEN

Desde el descubrimiento de los polímeros en el siglo pasado, su uso se ha vuelto omnipresente en nuestra vida cotidiana, dando lugar al desarrollo de numerosas aplicaciones tecnológicas. Dentro de la amplia variedad de polímeros, una sub-clase importante son los polímeros capaces de formar vidrios. La principal características de dichos materiales es que pueden existir en el estado amorfo por debajo del punto de fusión, y cuando son enfriados hacia el estado vítreo, exhiben una rigidez similar a la de un sólido con la excepción de no poseer el orden molecular de largo alcance propio de los materiales cristalinos. Con respecto a los polímeros formadores de vidrio o amorfos, sus principales ventajas radican en que son livianos y fáciles de fabricar, a la vez que poseen una gran transparencia y razonable rigidez. Teniendo en cuenta dichos aspectos, los vidrios poliméricos han sido sujeto de estudio durante décadas.

Con la finalidad de poder entender la naturaleza de los sistemas formadores de vidrio, la ciencia del estado vítreo sigue siendo un campo de investigación continua que pretende alcanzar una comprensión profunda de los procesos cinéticos y termodinámicos que influyen en la transición vítrea. Los polímeros amorfos, son materiales que por debajo de la temperatura de transición vítrea, se encuentran en un estado de no-equilibrio termodinámico. En este sentido, numerosas teorías continúan intentando explicar el origen de la ralentización de la dinámica molecular de dichos materiales cuando se encuentran cerca de la transición vítrea. En la actualidad, la posibilidad de confinar materiales poliméricos amorfos a nivel de la nanoescala ha puesto de manifiesto nuevas

estrategias de investigación, que permiten arrojar luz sobre preguntas anteriormente sin respuesta, en lo referente a la transición vítrea y al estado vítreo de no-equilibrio.

Uno de los efectos más documentados y que más han fascinado durante más de 20 años a la comunidad científica, es la modificación de la temperatura de transición vítrea de los poliméricos amorfos con el confinamiento. Este trabajo pretende proporcionar nuevos conocimientos sobre los fenómenos de no-equilibrio presentes en vidrios poliméricos confinados. Con dicho fin, se ha establecido una metodología óptima que abarca desde la preparación y caracterización, hasta el estudio físico de dichos sistemas en el estado 'bulk' y confinado. Específicamente, la investigación se ha centrado en los efectos de no-equilibrio por debajo de la temperatura de transición vítrea (T_g). Así mismo, se ha mostrado cómo el efecto del confinamiento provoca igualmente, efectos de no-equilibrio termodinámico incluso por encima de la T_g.

Esta tesis se divide en siete capítulos, que van desde el estado del arte hasta las perspectivas futuras sobre la dinámica y la termodinámica de los vidrios poliméricos confinados.

En el Capítulo 1, comenzamos proporcionando una introducción general a la termodinámica y la dinámica de los sistemas formadores de vidrio, seguido de un resumen de los recientes avances sobre vidrios poliméricos confinados. Concluimos el Capítulo 1 con el objetivo y la descripción general de esta tesis.

En el Capítulo 2, presentamos las principales técnicas experimentales empleadas en este trabajo. En particular, se han descrito detalladamente la calorimetría diferencial de barrido (DSC) estándar, la calorimetría de barrido rápido (FSC) y la elipsometría espectroscópica, haciendo especial énfasis en la explotación de dichas técnicas para la caracterización de fenómenos de vitrificación y de no-equilibrio. Además, se describen técnicas complementarias como Dynamic Light Scattering (DLS) y Atomic Force

Microscopy (AFM), empleadas para la caracterización morfológica de los sistemas confinados obtenidos en el presente estudio, es decir, nanoesferas y películas delgadas basadas en polímeros amorfos.

En el Capítulo 3, presentamos resultados sobre la caracterización de diferentes aspectos de la transición vítrea de nanoesferas de poli(estireno) (PS) y de su homólogo 'bulk' mediante FSC. El objetivo de este capítulo ha sido discernir sobre la naturaleza del fenómeno de vitrificación y de la movilidad molecular. Los aspectos más interesantes que surgieron del presente estudio fueron que (i) al disminuir el diámetro de las nanoesferas de PS, se observó una disminución progresiva del valor de la T_g comparada con el sistema 'bulk'. Por otro lado, (ii) se demostró que la movilidad molecular no se veía afectada por el tamaño de las nanoesferas y mostraba un comportamiento tipo 'bulk' para todos los niveles de confinamiento. Estos resultados apuntan a una capacidad más eficiente de mantener el equilibrio termodinámico en sistemas confinados, en comparación con sistemas 'bulk'.

En el Capítulo 4, presentamos experimentos de envejecimiento físico de nanoesferas de PS y 'bulk' por medio de FSC. De acuerdo con los resultados previos obtenidos en el Capítulo 3, se encontró que estos sistemas mantenían más eficientemente el equilibrio termodinámico. Esto fue evidenciado por la observación del envejecimiento físico acelerado en nanoesferas de PS. Además, nuestros experimentos de envejecimiento físico mostraron un comportamiento complejo de recuperación del equilibrio, confirmando la existencia de múltiples mecanismos de equilibrado, análogo a otros materiales formadores de vidrio.

En el Capítulo 5, mostramos cómo dicho comportamiento complejo de recuperación de equilibrio, observado en el capítulo anterior para las nanoesferas de PS, también pudo encontrarse en polímeros amorfos 'bulk' envejecidos físicamente a tiempos muy largos. En esta sección, monitorizamos el envejecimiento físico de tres tipos de polímeros como, poli(arilato) (PAr),

poli(carbonato) (PC) y poli(sulfona) (PSU) envejecidos a temperatura ambiente hasta aproximadamente 30 años mediante DSC.

En el Capítulo 6, nos centramos en la dinámica de no-equilibrio de sistemas confinados, mediante el estudio de la cinética de recuperación del equilibrio de polímeros amorfos soportados sobre un sustrato por encima de T_g. Para tal fin, se estudiaron películas delgadas de poli(tert-butilestireno) (PTBS), un análogo del PS, por medio de elipsometría espectroscópica. Estas películas delgadas se sometieron a una temperatura de recocido (T_a) de 50 K por encima de la T_g del sistema 'bulk'. El objetivo de este estudio, fue observar la evolución de la temperatura de transición vítrea con al tiempo de recocido y el grosor película. Se destacó la importancia de la capa adsorbida entre el polímero y el sustrato, promotora del efecto del aumento de la T_g hacia valores cercanos al 'bulk'.

Finalmente, en el Capítulo 7 resumimos los principales resultados y conclusiones extraídas de esta tesis. El objetivo general de este trabajo fue llegar a una comprensión profunda de los aspectos que influyen en la transición vítrea de materiales amorfos o vidrios basados en polímeros, con especial atención en los sistemas sometidos al confinamiento geométrico. Por lo tanto, esta tesis contribuye al progreso de la comprensión de los efectos de no-equilibrio a nivel de la nanoescala y en polímeros amorfos en estado 'bulk'.

Contents

1. INTRODUCTION – THE GLASS TRANSITION IN BULK POLYMERS AND UNDER GEOMETRICAL CONFINEMENT 1
1.1. POLYMERS AND THE GLASS TRANSITION 1
1.1.1.BASIC PROPERTIES OF POLYMERS 1
1.1.2.THE GLASS TRANSITION 3
1.1.3.PHYSICAL AGING 10
1.1.4.GLASS TRANSITION AND PHYSICAL AGING VERSUS MOLECULAR MOBILITY 14
1.2. POLYMER GLASSES UNDER CONFINEMENT 14
1.2.1.GLASS TRANSITION IN CONFINED POLYMERS 15
1.2.2.PHYSICAL AGING IN CONFINED POLYMERS 19
1.2.3.DECOUPLING BETWEEN T_G AND MOLECULAR MOBILITY 20
1.3. AIM AND OUTLINE OF THIS THESIS 23
1.4. REFERENCES 25

2. EXPERIMENTAL TECHNIQUES AND DATA ANALYSIS 33
2.1. THERMAL ANALYSIS 33
2.1.1. CALORIMETRY 34
2.1.1.1. STANDARD DSC 35
2.1.1.2. FAST SCANNING CALORIMETRY (FSC) 37
2.1.1.3. DATA ANALYSIS 40
2.1.2. SPECTROSCOPIC ELLIPSOMETRY 46
2.1.2.1. DATA ANALYSIS 49
2.2. MORPHOLOGICAL ANALYSIS 50
2.2.1. DYNAMIC LIGHT SCATTERING 50
2.2.2. ATOMIC FORCE MICROSCOPY 52
2.2.2.1. AMPLITUDE MODULATION IMAGING 53
2.3. REFERENCES 55

3. VITRIFICATION AND MOLECULAR MOBILITY IN POLYSTYRENE NANOSPHERES AND IN BULK 59
3.1. INTRODUCTION 59
3.2. SAMPLES AND EXPERIMENTAL DETAILS 62
3.2.1. SAMPLES 62
3.2.2. DETERMINATION OF TF AND STEP RESPONSE ANALYSIS 65
3.3. RESULTS AND DISCUSSION 66
3.3.1. SAMPLES MORPHOLOGY 66
3.3.2. VITRIFICATION KINETICS AND MOLECULAR MOBILITY 70
3.4. CHAPTER SUMMARY 78
3.5. REFERENCES 80

4. STRUCTURAL RECOVERY IN POLYSTYRENE NANOSPHERES AND IN BULK 85
4.1. INTRODUCTION 85
4.2. SAMPLES AND EXPERIMENTAL DETAILS 87
4.2.1. SAMPLES 87
4.2.2. PHYSICAL AGING MEASUREMENTS 87
4.3. RESULTS AND DISCUSSION 88
4.3.1. ISOCHRONAL AGING 89
4.3.2. ISOTHERMAL AGING 92
4.4. CHAPTER SUMMARY 99
4.5. REFERENCES 100

5. VERY LONG-TERM PHYSICAL AGING OF GLASSY POLYMERS 105
5.1. INTRODUCTION 106
5.2. SAMPLES AND EXPERIMENTAL DETAILS 107
5.2.1. SAMPLES 108
5.2.2. PHYSICAL AGING MEASUREMENTS 110
5.3. RESULTS AND DISCUSSION 111
5.4. CHAPTER SUMMARY 116
5.5. REFERENCES 118

6. TUNING CONFINEMENT EFFECTS ON POLY(TERT-BUTYLSTYRENE) THIN FILMS 121
6.1 INTRODUCTION 121
6.2 SAMPLES AND EXPERIMENTAL DETAILS 124
6.2.1. SAMPLES 124
6.2.2. SPECTROSCOPIC ELLIPSOMETRY 127
6.3 RESULTS AND DISCUSSION 128
6.3.1. FORMATION OF THE ADSORBED LAYER 128
6.3.2. IMPACT OF THICKNESS AND THERMAL ANNEALING ON T_G 130
6.4 CHAPTER SUMMARY 140
6.5 REFERENCES 140

7. CONCLUSIONS 145

A. APPENDIX 149

PUBLICATIONS 155

1

INTRODUCTION – THE GLASS TRANSITION IN BULK POLYMERS AND UNDER GEOMETRICAL CONFINEMENT

This chapter introduces the topic of the glass transition. Particular emphasis is devoted to thermodynamic and dynamic aspects of glasses below the glass transition temperature. After a general description of the glass transition in bulk, attention is devoted to the specific effects due to geometrical confinement. In the first part, concepts on the glass transition and physical aging of glass-forming systems are introduced. Subsequently, the effects arising from confining polymer glasses in at the nanoscale level are discussed, followed by a review of recent results and paying special attention to the non-equilibrium dynamics. To conclude, the experimental activity showing deviations from bulk behavior, in terms of glass transition temperature and physical aging, are discussed.

1.1. POLYMERS AND THE GLASS TRANSITION

1.1.1. BASIC PROPERTIES OF POLYMERS

In 1922 the German organic chemist, Hermann Staudinger, presented how to obtain high molecular weight molecules linked by a large number of small molecules. This reaction, called *'polymerization'*, was achieved by the repetition of individual units joined together by covalent bonds,[1] as is schematized in Figure 1.1. Thus, polymers are essentially long molecules, or macromolecules, consisting of a large number of basic units chemically joined together to form one entity.[2]

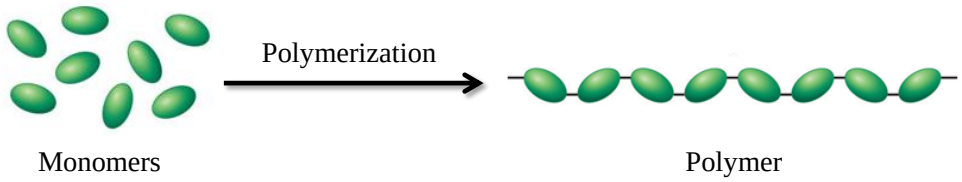

Figure 1.1 Schematic representation of the polymerization process

Most polymers are typically based on hydrogens and carbons. The number of monomers in a polymer chain determines the degree of polymerization. In a polymeric system, chains of different sizes are usually found, therefore, rather than relating polymers to a unique degree of polymerization, it has to be referred to molecular weight distribution functions. The most commonly used distributions are defined as follows: (i) the ***number-average molecular weight*** (M_n) and (ii) the ***weight-average molecular weight*** (M_w), respectively defined as (1.1):

$$M_n = \frac{\sum_i N_i M_i}{\sum_i N_i} \quad \text{and} \quad M_w = \frac{\sum_i N_i M_i^2}{\sum_i N_i M_i} \qquad (1.1)$$

where N_i is the number of molecules of molecular weight M_i. These averages are equal only for perfectly monodisperse polymer, whereas in general $M_w > M_n$ and the ratio between M_w/M_n gives the ***polydispersity index*** (PDI). This parameter is used as a measure of the broadness of a molecular weight distribution of a polymer.[3,4]

Polymers can be classified in two main classes: (i) fully amorphous and (ii) semi-crystalline ones. In amorphous polymers, chains are randomly disposed throughout the whole material. However, in semi-crystalline polymers, apart from an amorphous part, a fraction of the chains exhibit long-range order. Due to the constraints imposed by chain connectivity and, in some case, the presence of conformational disorder, polymers do not exist in a fully crystalline configuration, see Figure 1.2.

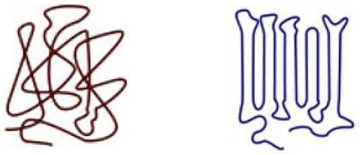

Figure 1.2 Schematization of a) amorphous and b) semi-crystalline polymers.

1.1.2. THE GLASS TRANSITION

The existence of systems thermodynamically in non-equilibrium is ubiquitous in nature. These systems spontaneously evolve toward the most sable thermodynamic state, that is, the one with the lowest free energy.[5] Among the numerous examples of non-equilibrium systems, glasses are an important class given their use in nature since the beginning of civilization. The essential requirement to form a glass is the ability of a disordered liquid to avoid, when cooled down, the thermodynamic most favorable state corresponding to the ordered crystal.[6–8] Moreover, another important class, given their technological relevance, is represented by glass-forming polymers. These are those kinds of polymers that can be easily supercooled below their melting temperature.[9] Apart from these systems, a wide range of materials can also be obtained as glasses such as silicates, oxides and chalcogenides (oxygen, sulphur, selenium), halides, metals or glass-forming organic compounds (alcohols, acids, oxoacids, aromatics).

1.1.2.1. Thermodynamic aspects

Slow kinetics of transformation of a liquid into the ordered crystal below the melting temperature, allows maintaining the system in the disordered state over long-time scales. On further cooling, the supercooled liquid transforms into a non-equilibrium glass.[10] This is sketched in Figure 1.3, where a

schematic representation of the thermodynamic quantities of glass-forming system at constant pressure and cooling rate is provided.

Figure 1.3 (right panel) shows the stability plots of the free energy of the configurational space. The left panel shows how, at a given applied cooling rate, the supercooled metastable state cannot be followed and the system falls into a non-equilibrium glassy state, that is, a 'frozen' liquid within the experimental observation time. This phenomenon is known as the glass transition[11,12] and takes place in a temperature range that depends on the experimental cooling conditions. Below the glass transition temperature (T_g) the glassy state is unstable with respect not only to the supercooled liquid, but also to the crystalline solid. Figure 1.3 also shows the so-called fictive temperature (T_f), defined as the temperature at which a glass in a generic thermodynamic state would be at the equilibrium.[13] The concept of the fictive temperature represents a common way to define the thermodynamic state of a glass, which was introduced by Tool[13] in 1946.

As previously mentioned, glasses belong to the category of non-equilibrium systems; therefore, they will spontaneously evolve with time toward the closest free energy minimum. This evolution is known as physical aging (see Figure 1.3) and implies a reduction of the T_f of the glass.

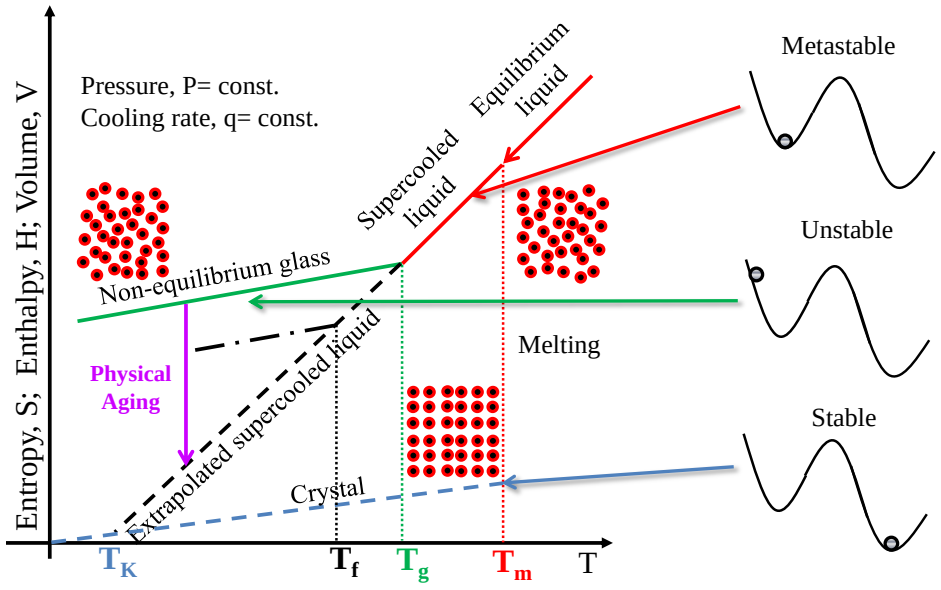

Figure 1.3 Left Panel: Schematic representation of the temperature dependence of thermodynamic properties (entropy, enthalpy, volume) in glass-forming systems at constant pressure. The indicated temperatures are defined as: (i) T_m, the melting temperature; (ii) T_g, the glass transition temperature; (iii) T_f, the fictive temperature and (iv) T_k, the Kauzmann temperature, which is the temperature at which entropy of the 'supercooled liquid' equals that of the corresponding crystal. Right Panel: The stability plots of the thermodynamic potential.

From a thermodynamic point of view, the typical signature of the liquid-glass transition is based on the observation of a jump in the thermodynamic coefficients. This is reminiscent of a second-order thermodynamic transition according to the classification made by Ehrenfest in 1933.[14] This is sketched in the following Figure 1.4.

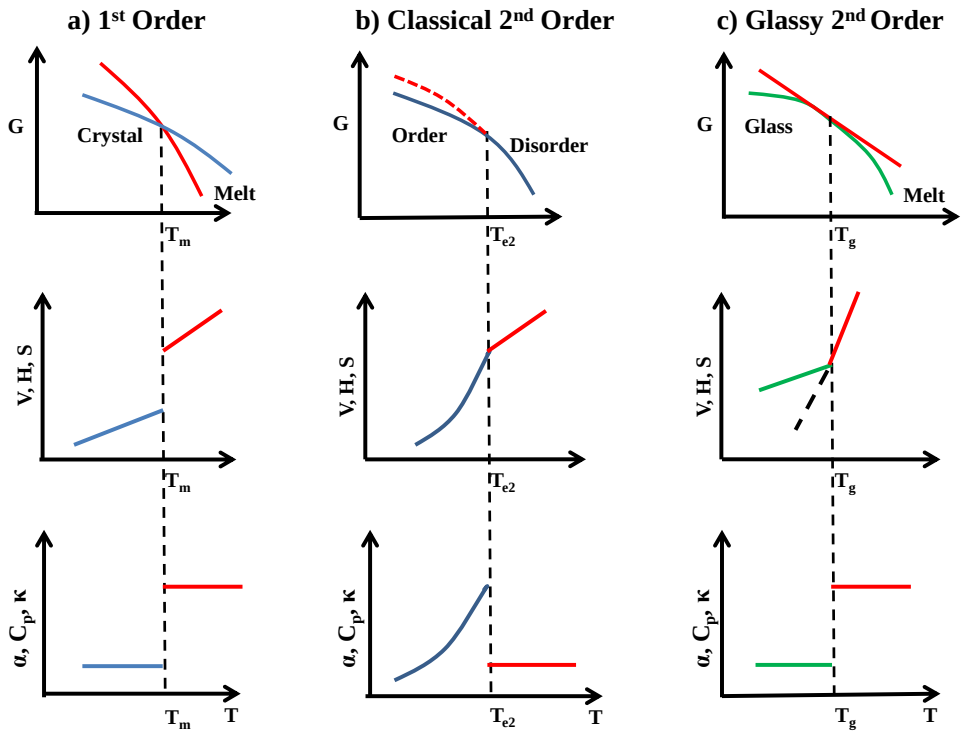

Figure 1.4 Schematization of thermodynamic transitions: (a) First-order phase transition; (b) Second-order phase transition; c) Second-order glass transition.

Figure 1.4 shows the temperature dependences of the different thermodynamic quantities, that is, *G*, Gibbs free energy; *V*, volume; *H*, enthalpy; *S*, entropy; α, *k* thermal expansion and compressibility coefficients and C_p, heat capacity at constant pressure. First-order transitions show a discontinuity in the first partial derivative of the free energy as a function of temperature or pressure, defined in equation (1.2):

$$\left(\frac{\partial G}{\partial T}\right)_P = -S;\ \left(\frac{\partial G}{\partial P}\right)_T = V;\ \left[\frac{\partial\left(\frac{G}{T}\right)}{\partial\left(\frac{1}{T}\right)}\right]_P = H \qquad (1.2)$$

In second-order transitions, there is no discontinuity in *V*, *H*, *S* at the transition, but there is in the heat capacity C_p, the thermal expansion α, and the compressibility *k*, defined by the following relationships (1.3):

$$\left(\frac{\partial H}{\partial T}\right)_P = C_p;\ \frac{1}{V}\left(\frac{\partial V}{\partial T}\right)_P = \alpha;\ -\frac{1}{V}\left(\frac{\partial V}{\partial P}\right)_T = k \qquad (1.3)$$

In other words, a second-order transition exhibits changes of the susceptibilities, that is, the response of the system to a parameter changes implies a discontinuity in the second partial derivative of the free energy,[7,15,16] as observed in Figure 1.4.

Given this general thermodynamic description, it is noteworthy to mention that the glass transition is not a true second order thermodynamic phase transition, despite exhibiting a discontinuity of α, C_p and *k*. One reason is that, in a classical second order transition, the values of α, C_p or *k* are larger than in the liquid one (see Figure 1.4), whereas, at the glass transition, the opposite behavior is observed. This difference is reflected in the so-called Prigogine – Defay ratio (Π), which should fulfill the following relationship:[17]

$$\Pi = \frac{1}{VT}\frac{\Delta c_p \Delta k}{(\Delta\alpha)^2} = 1 \qquad (1.4)$$

where *V* is the specific volume; Δc_p, Δk, $\Delta\alpha$ are the jumps at the transition of the specific heat, the compressibility and the thermal expansion coefficients, respectively. At the glass transition the Prigogine – Defay ratio is generally found to be larger than the unity.[17]

Furthermore, a straightforward indication that the glass transition cannot be considered a thermodynamic transition resides in its cooling rate dependent T_g or T_f. In this sense, Figure 1.5 illustrates the change in the value of T_f depending on the cooling rate (*e.g.* $q_{1cool} > q_{2cool}$).[18,19] It is noticeable that the lower the T_f is, the lower in the energy landscape the glass is located.

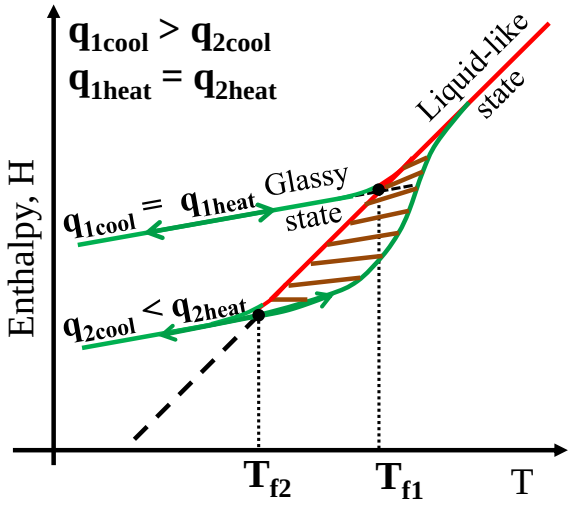

Figure 1.5 Schematic plot of the enthalpy vs temperature for a glass cooled and immediately reheated for two different cooling rates ($q_{1cool} > q_{2cool}$).

In particular, T_g increases when the observation time of the experiment decreases, that is, at higher cooling rates. Thus, in order to understand the cooling rate dependence of the T_g, its intimate link with the molecular mobility must be recalled, as will be seen in the following section.

1.1.2.2. Dynamic aspects

A liquid cooled down below the melting temperature is characterized by a dramatic increase of the viscosity with decreasing temperature. Thus, such increase implies a slowing down of the typical relaxation time (τ) of the associated spontaneous fluctuations. The phenomenon related to such τ is commonly called α-process. In particular, a glass is formed when the typical relaxation time of spontaneous fluctuations is of the order of the observation time of the experiment. At that point, the system is not able to maintain the equilibrium anymore and a glass is formed.

Angell[20] classified different types of glass-forming systems according to the temperature dependence of the relaxation time (or the viscosity). In particular, only for the so-called *strong* glass former τ can be described by a simple Arrhenius law (1.5) (see Figure 1.6).

$$\tau = \tau_0 \exp\left(\frac{E_\mathrm{a}}{k_\mathrm{B} T}\right) \qquad (1.5)$$

where τ_0 is the pre-exponential factor, E_a is the apparent activation energy of a thermally activate process and k_B is the Boltzman constant.

For *fragile* glasses, as shown in Figure 1.6, the activation energy increases with decreasing temperature. An appropriate description of τ is based on the employment of the Vogel-Fulcher-Tammann (VFT) equation:[21–23]

$$\tau = \tau_0 \exp\left(\frac{B}{T - T_0}\right) \qquad (1.6)$$

where τ_0 is the pre-exponential factor, T_0 is the so-called Vogel temperature and B is the Vogel activation energy. The VFT equation insinuates divergence of the relaxation time at T_0.

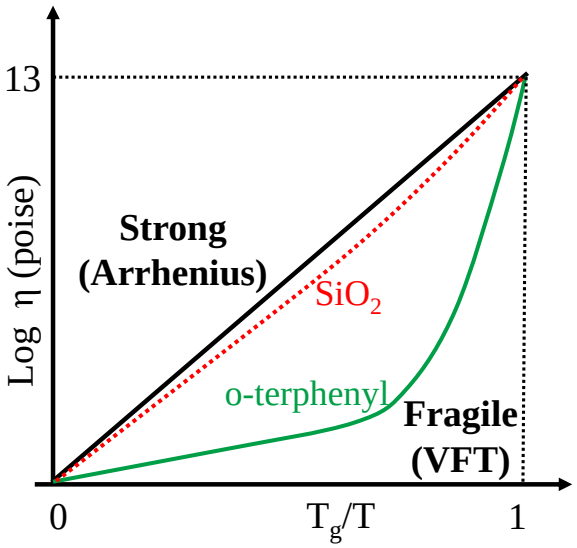

Figure 1.6 Angell's plot (log η versus T_g/T) for two glass-forming materials. *Strong* glass formers show Arrhenius-like (linear) temperature dependence, while *fragile* glass formers show a highly non-Arrhenius-like curvature indicative of a very rapid slowing down of molecular mobility with decreasing temperature. The latter behavior is typical for most amorphous polymers.

Several methods such as dynamic mechanical analysis,[24] light scattering,[25] neutron scattering,[26] nuclear magnetic resonance,[27] specific heat spectroscopy[28] and broadband dielectric spectroscopy,[29] allow measuring the molecular mobility. This is done by the application of a linear perturbation to the glass-forming system.

1.1.3. PHYSICAL AGING

From the previous considerations on the kinetic nature of the glass transition, it is clear that the thermodynamic state of a glass is such that, there exists an excess of thermodynamic properties (*S, H, V*) in comparison to the supercooled liquid state. This situation implies a spontaneous evolution of thermodynamic properties toward the closest free energy minimum. This

phenomenon is known as physical aging or structural relaxation.[30] One consequence of such phenomenon is the densification of the system, which implies a variation of the dimensions of objects made of glass. The kinetics of recovery of equilibrium generally depends on (i) the time scale of spontaneous fluctuations, and (ii) the distance of the instantaneous thermodynamic state of the glass from equilibrium. Given the fact that during the course of physical aging a change of the thermodynamic state occurs, its description must include the dependence of τ on the thermodynamic state of the glass. This aspect of equilibrium recovery is generally known as non-linearity.[31]

One way to explore the fate of the dynamics below T_g consists of following the kinetics of equilibrium recovery of the glass in the physical aging regime. This can be performed by monitoring the time evolution of thermodynamic properties, for instance the enthalpy by means of calorimetry. Figure 1.7 (upper panel) shows the way the enthalpy of a glass, previously aged below T_g, recovers equilibrium on heating. As can be observed from the lower panel of Figure 1.7, the natural consequence of such recovery is that an overshoot emerges in the heat capacity trace. This overshoot is related to the enthalpy recovery and gives information of the energy released upon aging. The fictive temperature T_f[13] is a common way to identify the thermodynamic state of a glass, defined by the intersection of the glass line, traced from the thermodynamic state of a given glass and the supecooled liquid equilibrium line (see Figure 1.7, upper panel). Given this definition, a low enthalpy/entropy or equivalent high density glass will exhibit low T_f.

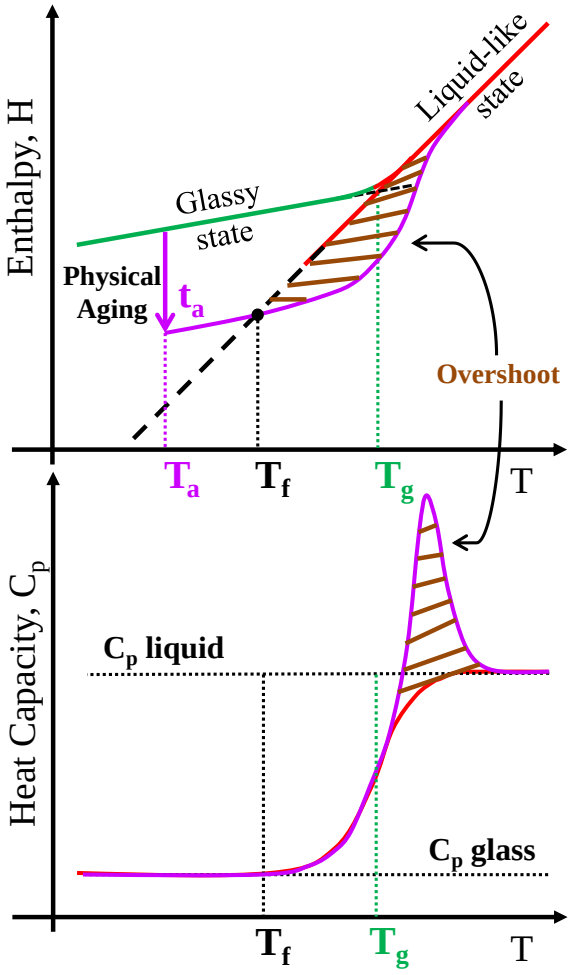

Figure 1.7 Schematic representation of the enthalpy (upper panel) and the heat capacity (lower panel) versus temperature for a glass-forming system upon physical aging. Black dashed line represents the thermodynamic equilibrium. T_a is the aging temperature at a given aging time (t_a). T_f is the fictive temperature. Purple line is the aged sample heating scan.

In the upper panel of Figure 1.7, purple line depicts the recovered enthalpy to the liquid-like state upon heating, when a glass is isothermally held below T_g for given temperature and time (T_a, t_a). In the lower panel of Figure 1.7, the

purple line shows an endothermic peak of the heat capacity trace superimposed to the T_g.[32] Usually the enthalpy recovery of a glass is measured using differential scanning calorimetry (DSC) by the evaluation of the enthalpic departure (ΔH) from the equilibrium obtained from the integral area of each overshoot, as shown in Figure 1.8.

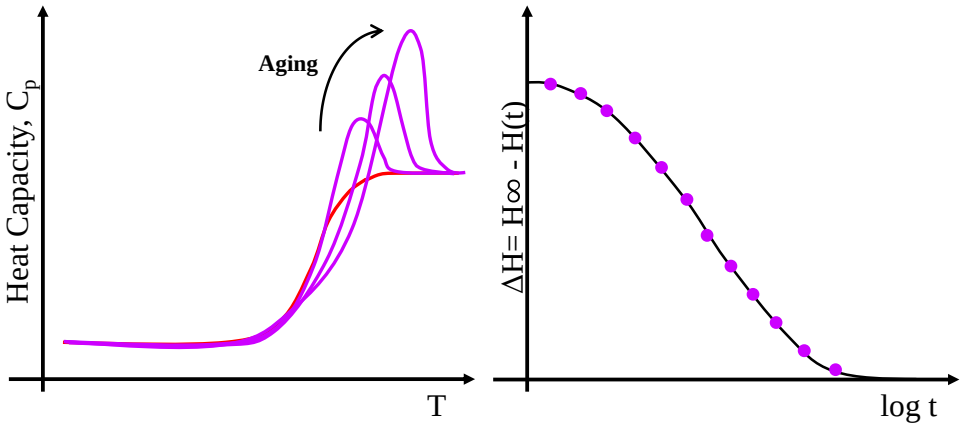

Figure 1.8 Left Panel: Schematic representation of DSC heat capacity curves collected on heating after different aging times at a given temperature. Right Panel: Relaxation curve obtained from the individual measurements at different aging times. H_∞: Expected total enthalpy extrapolated from the equilibrium melt; H(t): enthalpy recovery as a function of aging time at T_a.

To close this section, it is worth mentioning that recent experiments, where the recovery of equilibrium was followed well below T_g and for aging times larger than days, showed the presence of multiple mechanisms of equilibrium recovery in polymeric,[33,34] chalcogenide,[35] metallic,[36] and low molecular weight organic glasses.[37] These results require revisiting the paradigmatic view of physical aging, based on a single monotonous approach to equilibrium. As will be seen in the next chapters, this aspect has been central in the development of the present thesis.

1.1.4. GLASS TRANSITION AND PHYSICAL AGING VERSUS MOLECULAR MOBILITY

Despite the intimate link between the *non-equilibrium glass dynamics* – the transition from liquid to glass (the so-called "thermal glass transition") and the physical aging – and the *equilibrium dynamics* – (the so-called "dynamic glass transition") – in terms of the molecular mobility, it is important to point out that these two aspects are conceptually different.[38] In the case of glassy dynamics, the rate of spontaneous fluctuations can only be determined if the experimental protocol fulfill the fluctuation dissipation theorem (FDT)[39] by the application of a linear perturbation. On the other hand, measuring the T_g, for instance by calorimetry, via the application of a ramp in the temperature scan or the equilibrium recovery of glasses, entails the use of large perturbations well beyond the linear regime.[40]

In most cases, the conceptual difference between the non-equilibrium and equilibrium glass dynamics does not imply that, differences in the temperature dependence of the two characteristic times of these aspects exist.[41,42] However, there exist several "bad actors" among bulk glasses exhibiting different behavior of the temperature dependence of the T_g and the molecular mobility.[43] As will be seen in next section of the chapter, the conceptual difference between equilibrium and non-equilibrium dynamics is of utmost importance in particular conditions of confinement.

1.2. POLYMER GLASSES UNDER CONFINEMENT

In this section the influence of nanoscale confinement on different aspects of glass dynamics of glass-forming polymers is highlighted.

The study of confined polymer glasses under different configurations such as thin films, nanotubes and nanoparticles have attracted a huge interest from both fundamental and technological viewpoints in recent years. Regarding the

latter aspect, thin films are used in applications as templates in microelectronic,[44] active layers in photovoltaic cells,[45] non-biofouling protective coatings[46] or membranes in separation technologies.[47] Nanotubes or nanowires are used as a filler for polymer nanocomposites, becoming structural materials for the aerospace industry and automotive or railway among others.[48] Polymer nanoparticles or nanospheres are used as vehicles in drug delivery,[49] components in fluorescent imaging,[50] performance reinforcing additives[51] or components in photonic structures.[52]

This technological interest has generated an intense research in understanding how properties of confined systems are modified by the presence of the polymer/external world interface. Given the large surface area of such interface to volume of polymer ratio, physical properties of confined polymers can dramatically deviate from those of the corresponding bulk homologues. When a macromolecule is confined at the nanoscale level, new unexpected phenomena affecting the glass transition, interfacial interactions and irreversible adsorption onto the substrate appear to play a large role in the materials' properties.[53–57] In this sense, numerous studies have reported large T_g shifts.[55,58–61] In the following sections, we will review the recent activity of how nanoconfined polymeric systems, in particular thin films, nanospheres and nanocomposites, show deviations from bulk T_g[58,62] and physical aging.[63]

1.2.1. GLASS TRANSITION IN CONFINED POLYMERS

Thin films are by far the most investigated systems in confined polymer glasses. In the mid 90's Keddie *et al.* investigated the T_g variation of silicon oxide (SiO_2) supported polystyrene (PS)[58] and poly(methyl-methacrylate) (PMMA)[62] thin films, where a reduction and an increase in T_g was detected respectively. Conversely, when PMMA was supported onto a gold substrate its T_g decreased with confinement, showing that those changes in T_g could be related to the interactions between the confined polymer and the interface. In this context, it has been reported that T_g variations (ΔT_g) are directly related to

the polymer-substrate interfacial interactions for the case of supported polymeric thin films. Regarding these interactions, three different scenarios can be observed: (i) $\Delta T_g > 0$ due to the attractive interactions between the polymer and the interface, (ii) $\Delta T_g < 0$ when repulsive or free/soft interfaces are taken place or (iii) $\Delta T_g \sim 0$.[58,62,64–68] Figure 1.9 shows such T_g variation as a function of thickness for three representative polymers; PS, PMMA, and poly(2-vinyl pyridine) (P2VP).

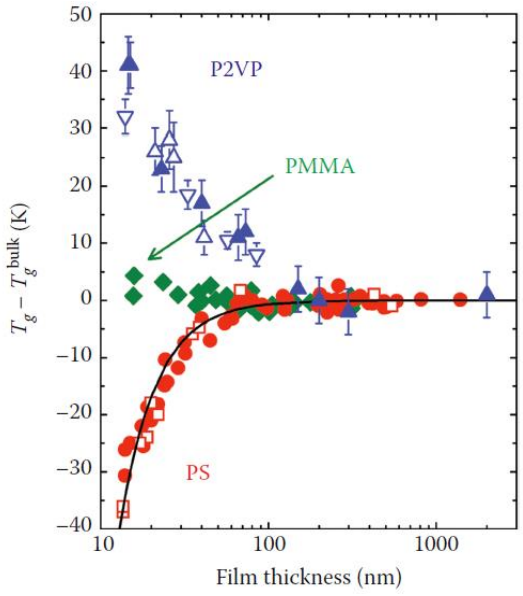

Figure 1.9 $T_g - T_g^{bulk}$ as a function of film thickness for three characteristic polymers all supported on silica substrates. PS measured by fluorescence;[69,70] PMMA by ellipsometry;[62] and P2VP by fluorescence, X-ray reflectivity[64] an ellipsometry.[71] Reprinted from Ref.[72]

The first factor affecting the magnitude of T_g depression in glassy polymers under confinement is the nature of the interface. In particular, freestanding films exhibit significantly larger T_g depression in comparison to supported or capped ones. This was first shown by Forrest *et al.*,[73] where T_g depression as large as 70 K was detected at about 30 nm PS thickness. In contrast, in supported PS films, the depression has been found to be no larger than 30 – 40

K for films as thin as 10 nm.[74] In the case of capped films, these effects are even more limited.[75,76]

The cooling rate is an important key factor beyond the film thickness that plays a determining role in the magnitude of T_g deviations. Studies in this sense were promoted by Efremov *et al.*,[77] performing specific heat measurements on thin PS films supported on platinum at cooling rates as large as thousands of K/s. Surprisingly, in that work no discernible deviations of the T_g from bulk behavior were found. Subsequently, Fakhraai and Forrest,[78] by employing ellipsometry showed that, deviations from bulk T_g become less pronounced when the cooling rate was increased. However, ellipsometry experiments were unable to close the gap with calorimetry investigations at high cooling rates, therefore, advances in fast scanning calorimetry (FSC) technique[79] allowed to fill the cooling rate gap. Studies performed on PS and PC thin films[80,81] confirm the observed trend of larger T_g depression as cooling rate decreases.

Other important factors determining the T_g deviation are the polymer chain architecture and the tacticity. For instance, Glynos *et al.*[54,82] showed how the T_g of 16-arms star-shaped PS thin films was higher than the bulk one, demonstrating the importance of the chain architecture on the thickness dependence on the T_g. Moreover, Grohens *et al.*[65,83] focused on the role of chain tacticity, showing that isotactic PMMA (i-PMMA) exhibits increase of the T_g with decreasing films thicknesses, opposite to the syndiotatic (s-PMMA) polymer behavior.

Gathering all these findings, it is important to notice that interfacial interactions and the surface to volume ratio are not sufficient factors to describe the thermodynamic state of a confined polymeric system.[84] The change of the local density due to the chain adsorption, which propagates from the irreversibly adsorbed layer to the interior part of the film, has been recently shown to be a parameter of utmost importance to describe the thickness

dependence of T_g on supported thin films. In particular, experiments have been shown that deviations from bulk T_g are intimately related to the amount of interfacial free volume.[85,86] This can be tuned by irreversibly adsorbing polymer chains via annealing well above T_g.[57]

Importantly, the phenomenology found in thin films is qualitatively encountered in other kind of geometrical confinements. Among them, polymer nanospheres have gained increasing importance in recent years. The first report on polymer nanospheres T_g was presented by Gaur and Wunderlich[87] in 1980. They revealed a broadening of the T_g region and a decrease in the heat capacity (ΔC_p) calorimetric scans. More recently, Feng *et al.* studied the effect of the interface in PS[88] and PMMA[89] aqueous dispersed nanospheres by tuning the amount of surfactant. Their work revealed that in both cases surfactant-free PS and PMMA nanospheres exhibit T_g depression with confinement. However, in the surfactant covered nanospheres the deviations from T_g bulk were less pronounced. Altogether, these results indicate that the kind of interface is a key factor in governing the deviations in T_g of polymer nanospheres.

Recent developments on nanoprecipitation techniques[90–92] allow the fabrication of surfactant-free nanospheres. Zhang *et al.*[60] presented T_g suppression for PS nanospheres exposed to air or into a fluid with weak interfacial interactions. On the contrary, that reduction was strongly suppressed when PS nanospheres were capped into core-shell silica. It is worth mentioning that an increase in T_g with nanosphere confinement has also been shown by Martinez-Tong *et al.*,[93,94] basing their results on entropic arguments. They proposed a decrease in the system entropy due to the subtraction of configurational degrees of freedom for chain arrangements, as a result of the curvature at the interface in 3-D confinement.

Finally, the T_g of polymer nanocomposites has been the subject of intense research in the last years. In the plethora of studies reported in the literature, it

is possible to find examples of polymer nanocomposites exhibiting decrease, increase or no-change in T_g. Generally, the former two results are found in nanocomposites with strong interaction polymer/nanoparticles. In contrast, T_g reduction is normally found in those cases in which nanoparticles are grafted by organic hair, whose nature is similar to that of polymer. This makes the interaction of polymer/nanoparticles essentially neutral. Given the large amount of work regarding the T_g of polymer nanocomposites, the reader is addressed reviews on the topic.[55,95]

1.2.2. PHYSICAL AGING IN CONFINED POLYMERS

As discussed previously, physical aging is tied to the glass transition. Hence, several experiments on sub-100 nm thick polymer films were carried out. Pioneering in this sense is the work developed by Kawana and Jones,[96] who studied the physical aging for PS supported thin films on silicon oxide wafers by ellipsometry. Their results showed that the achievement of equilibrium was accelerated when decreasing the film thickness. However, in the most extreme case, 10 nm thick films, aging was so rapid that the system remained in the metastable supercooled liquid without any sign of glass transition. In other words, the equilibrium was maintained throughout the temperature scan without sign of discontinuity in the temperature dependence of the thickness, normally observed at T_g. Moreover, physical aging of thin films was investigated by fluorescence spectroscopy, which provides information on the change of the local free volume.[97,98] The main outcome of these studies, generally agrees with that of ellipsometry. Similar results were presented employing calorimetric techniques in the study of PS films. It has been shown that the equilibrium was progressively achieved at shorter times when reducing the film thickness.[99,100] Boucher *et al.*[101] investigated the kinetics of the enthalpy recovery in stacked glassy PS films from 30 to 95 nm[102] in a temperature range below the T_g. Their results, apart from the acceleration of physical aging, showed the existence two mechanisms of equilibration toward equilibrium. These two mechanisms can be defined as: (i) a fast mechanism –

the first one at shorter times – providing partial enthalpy recovery with Arrhenius temperature dependence and (ii) a slow mechanism that follows the VFT temperature dependence.

In recent years the influence of confinement on the physical aging of polymer nanospheres has received increasing interest. Generally, from the sign of T_g deviations from bulk behaviour, it is possible to deduce whether physical aging proceeds faster or slower than in the bulk homologue. Concerning a relevant work performed by Guo *et al*,[103] they have investigated the structural relaxation or physical aging of aqueous-suspended and silica-capped PS nanospheres under isobaric (constant pressure) and isochoric (constant volume) conditions. In line with what was observed in other configurations,[95,99,100,104,105] their results showed how nanospheres confined by a soft medium – such as water[60,88] or air[106,107] – also exhibit accelerated physical aging with decreasing the size of confinement. In contrast, if polymer nanospheres are surrounded by hard medium such as silica, values of T_g are observed to be similar to the bulk ones.[60,108]

Finally, the way polymers ages in nanocomposites is summarized in relevant reviews on the topic.[55,63,95] Similarly to polymer nanospheres, also the physical aging of polymer nanocomposites is intimately related to the T_g. Hence, generally speaking, acceleration of physical aging is found in polymer nanocomposites exhibiting T_g lower than the bulk, whereas the opposite is observed for nanocomposite with positive deviation of the T_g with respect to the bulk. In those cases where T_g is found approximately bulk-like, examples of acceleration of physical aging can be found.[104]

1.2.3. DECOUPLING BETWEEN T_G AND MOLECULAR MOBILITY

The important aspect arising from the investigation of physical aging of confined polymers exhibiting T_g depression is that the acceleration of such phenomenon is, in a wide range of conditions, not originated from a

concomitant acceleration of the polymer molecular mobility. In section 1.1.4, the connection between the glass transition and molecular mobility has been discussed pointing out that, the T_g and the molecular mobility are two different aspects of glass dynamics. In this context, recent studies in polymer thin films and nanospheres have revealed a decoupling between segmental mobility and T_g. In this context, several recent works[75,106] suggest that the equilibrium and non-equilibrium glassy dynamics are not one-to-one related in nanostructured glasses unlike in bulk systems. An example of these studies was presented by Boucher *et al.*[75] They studied the molecular dynamics and thermal T_g of thin films by broadband dielectric spectroscopy and calorimetry. In such study, it was found a marked decoupling between the molecular mobility and T_g. This is shown in Figure 1.10, where the former, obtained from the specific heat spectroscopy experiments in the linear regime, in terms of the real part of the complex specific heat, is found to be invariant with the thickness in PS films (right axe), whereas a clear T_g depression is observed when decreasing film thickness (left axe), in line with other findings in different confined polymers.[55,109]

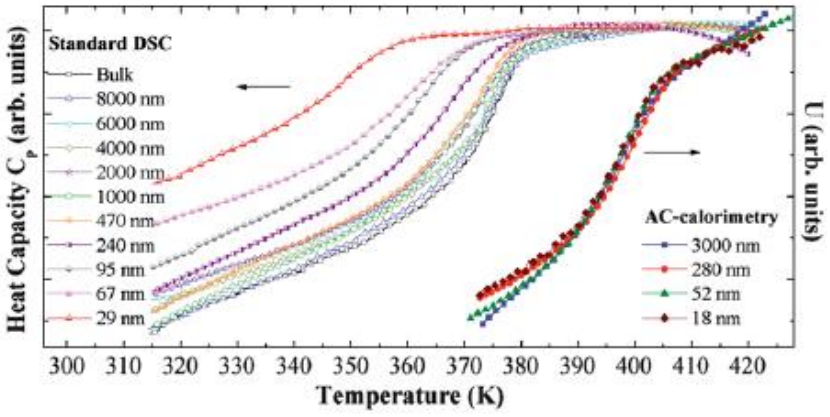

Figure 1.10 Left axes: Temperature dependence of the specific heat and obtained from DSC at a cooling rate of 20 K/min. Right axes: Temperature dependence of the amplitude of the complex differential voltage at a scanning rate of 2 K/min and a frequency of 160 Hz measured by AC-calorimetry. Reprinted from ref.[75]

These results point toward a decoupling between the non-equilibrium dynamics – in terms of T_g and physical aging – and the molecular mobility. Such decoupling implies that, the time to reach equilibrium (τ_{eq}) in the physical aging regime can be found to be shorter in confinement than in bulk, without any change of the polymer molecular mobility. This has been actually shown to be the case in several glassy polymers in different kinds of confinement.[100,110,111]

1.3. AIM AND OUTLINE OF THIS THESIS

The aim of this thesis is to gain insights in the understanding of dynamics and thermodynamics of polymer glasses. Investigations in the knowledge of the glassy state are still a field of continuous research from both experimental and theoretical viewpoints. This research entails the study of the glass molecular mobility and the way a supercooled liquid transforms into a glass, a phenomenon well-known as glass transition.

Recently, it has been shown that polymer glasses, under particular conditions of geometrical confinement, exhibit reduced glass transition temperature (T_g). In this framework, it has been furthermore shown that: (i) the equilibrium molecular mobility of the polymer in different kinds of confinement is equal to that of the bulk polymer; (ii) faster recovery of equilibrium in the glassy state when compared with the bulk counterpart, that is, in the physical aging regime is found; (iii) given the fact the equilibrium liquid line is followed to lower temperatures than the bulk, due to the reduced T_g and the faster recovered in the physical aging regime, glasses with low energy can be achieved in relatively short time scales in polymers under geometrical confinement. These results indicate that, beyond the polymer intrinsic molecular mobility in confinement, geometric factors play an essential role in determining the deviations from bulk behavior of the non-equilibrium dynamics, in terms of T_g reduction and acceleration of physical aging.

To shed light on the origin of the deviations of non-equilibrium dynamics from bulk behavior and its relation to the molecular mobility in confined polymer glasses, in the present thesis calorimetric methods have been employed. Specifically, apart from the standard differential scanning calorimetry, fast scanning calorimetry based on chip technology, allowing exploring times scales as short as microseconds, has been used. Furthermore, this technique also allows the application of linear perturbations in order to get information on the molecular mobility. For this purpose, a simple model based

on poly(styrene) nanospheres, has been selected. In particular, insights on all aspects of glass dynamics, including the molecular mobility, the glass transition and physical aging in the glassy state of these systems, have been presented. Regarding the latter aspect, the analogy with very long-term aged bulk polymer glasses will be emphasized, showing how the same phenomenology can be observed in both bulk and confinement, though on largely different aging time scales.

Finally, in the framework of non-equilibrium dynamics in confined polymer glasses, this thesis is complemented with studies on the kinetics of equilibrium recovery in supported polymeric films above T_g. For that purpose, poly(tert-butylstyrene) (PTBS) thin films supported on silicon oxide have been studied. In particular, the way T_g evolved when applying suitable annealing protocols above T_g have been investigated. PTBS was particularly suitable for this study thanks to its extremely large T_g suppression in comparison to its bulk analogue.

1.4. REFERENCES

(1) American Chemical Society International Historic Chemical Landmarks. http://www.acs.org/content/acs/en/education/whatischemistry/landmarks/staudingerpolymerscience.html.

(2) Gompper, G.; Schick, M. An Introduction to Soft Matter. In *Soft Matter*; Gompper, G., Schick, M., Eds.; Wiley-VCH Verlag GmbH & Co. KGaA, 2005; pp 1–16.

(3) Bower, D. I. *An Introduction to Polymer Physics*; Cambridge University Press, 2002.

(4) Strobl, G. R. *The Physics of Polymers - Concepts for Understanding Their Structures and Behavior*, 3rd ed.; Springer-Verlag Berlin Heidelberg, 2007.

(5) Demirel, Y. *Nonequilibrium Thermodynamics: Transport and Rate Processes in Physical, Chemical and Biological Systems*; Elsevier, 2007.

(6) Debenedetti, P. G. *Metastable Liquids: Concepts and Principles*; Physical Chemistry: Science and Engineering; Princeton University Press, 1996.

(7) Gutzow, I. S.; Schmelzer, J. W. P.; Schmelzer, J. W. P.; Gutzow, I. S.; Mazurin, O. V.; Priven, A. I.; Todorova, S. V.; Petroff, B. P. Basic Properties and the Nature of Glasses: An Overview. In *Glasses and the Glass Transition*; Wiley-VCH Verlag GmbH & Co. KGaA, 2011; pp 9–89.

(8) Tropin, T. V.; Schmelzer, J. W.; Aksenov, V. L. Modern Aspects of the Kinetic Theory of Glass Transition. *Phys.-Uspekhi* **2016**, *59* (1), 42.

(9) Cangialosi, D. Dynamics and Thermodynamics of Polymer Glasses. *J. Phys. Condens. Matter* **2014**, *26* (15), 153101.

(10) Cangialosi, D. Chapter 8 - Glass Transition and Physical Aging of Confined Polymers Investigated by Calorimetric Techniques. In *Handbook of Thermal Analysis and Calorimetry*; Sergey Vyazovkin, N. K. and C. S., Ed.; Recent Advances, Techniques and Applications; Elsevier Science B.V., 2018; Vol. 6, pp 301–337.

(11) Ediger, M. D.; Angell, C. A.; Nagel, S. R. Supercooled Liquids and Glasses. *J. Phys. Chem.* **1996**, *100* (31), 13200–13212.

(12) Angell, C. A.; Ngai, K. L.; McKenna, G. B.; McMillan, P. F.; Martin, S. W. Relaxation in Glassforming Liquids and Amorphous Solids. *J. Appl. Phys.* **2000**, *88* (6), 3113–3157.

(13) Tool, A. Relation between Inelastic Deformability and Thermal Expansion of Glass in Its Annealing Range. *J. Am. Ceram. Soc.* **1946**, *29* (9), 240–253.

(14) Jaeger, G. The Ehrenfest Classification of Phase Transitions: Introduction and Evolution. *Arch. Hist. Exact Sci.* **1998**, *53* (1), 51–81.

(15) *Handbook of Thermal Analysis and Calorimetry: Applications to Polymers and Plastics*; Cheng, S. Z. D., Ed.; Handbook of Thermal Analysis and Calorimetry; Elsevier Science, 2002.

(16) Menczel, J. D.; Prime, R. B. *Thermal Analysis of Polymers: Fundamentals and Applications*; Wiley, 2014.

(17) Schmelzer, J. W. P.; Gutzow, I. S.; Schmelzer, J. W. P.; Gutzow, I. S.; Mazurin, O. V.; Priven, A. I.; Todorova, S. V.; Petroff, B. P. Generic Theory of Vitrification of Glass-

Forming Melts. In *Glasses and the Glass Transition*; Wiley-VCH Verlag GmbH & Co. KGaA, 2011; pp 91–164.
(18) Moynihan, C. T.; Easteal, A. J.; De Bolt, M. A.; Tucker, J. Dependence of the Fictive Temperature of Glass on Cooling Rate. *J. Am. Ceram. Soc.* **1976**, *59*, 12–16.
(19) Yue, Y.; von der Ohe, R.; Jensen, S. L. Fictive Temperature, Cooling Rate, and Viscosity of Glasses. *J. Chem. Phys.* **2004**, *120* (17), 8053–8059.
(20) Angell, C. A. Spectroscopy Simulation and Scattering, and the Medium Range Order Problem in Glass. *J. Non-Cryst. Solids* **1985**, *73* (1), 1–17.
(21) Vogel, H. *Phys Zeit* **1921**, *22*, 645–646.
(22) Fulcher, G. S. *J. Am. Ceram. Soc.* **1925**, *8* (6), 339–355.
(23) Tammann, G.; Hesse, W. *Z. Für Anorg. Allg. Chem.* **1926**, *156* (1), 245–257.
(24) Zuza, E.; Ugartemendia, J. M.; Lopez, A.; Meaurio, E.; Lejardi, A.; Sarasua, J.-R. Glass Transition Behavior and Dynamic Fragility in Polylactides Containing Mobile and Rigid Amorphous Fractions. *Polymer* **2008**, *49* (20), 4427–4432.
(25) Fitz, B. D.; Mijovic, J. Segmental Dynamics and Density Fluctuations in Polymer Networks during Chemical Vitrification. *Macromolecules* **1999**, *32* (12), 4134–4140.
(26) Frick, B.; Richter, D. The Microscopic Basis of the Glass Transition in Polymers from Neutron Scattering Studies. *Science* **1995**, *267* (5206), 1939–1945.
(27) Papon, A.; Montes, H.; Hanafi, M.; Lequeux, F.; Guy, L.; Saalwächter, K. Glass-Transition Temperature Gradient in Nanocomposites: Evidence from Nuclear Magnetic Resonance and Differential Scanning Calorimetry. *Phys. Rev. Lett.* **2012**, *108* (6), 065702.
(28) Birge, N. O.; Nagel, S. R. Specific-Heat Spectroscopy of the Glass Transition. *Phys. Rev. Lett.* **1985**, *54* (25), 2674–2677.
(29) Kremer, F.; Schönhals, A. *Broadband Dielectric Spectroscopy*, 1st ed.; Springer-Verlag Berlin Heidelberg, 2003.
(30) Struik, L. C. E. *Physical Aging In Amorphous Polymers and Other Materials*, 1st ed.; Elsevier: Amsterdam, 1978; Vol. 106.
(31) Kovacs, A. J. Transition vitreuse dans les polymères amorphes. Etude phénoménologique. In *Fortschritte Der Hochpolymeren-Forschung*; Advances in Polymer Science; Springer, Berlin, Heidelberg, 1964; pp 394–507.
(32) Hodge, I. M. Enthalpy Relaxation and Recovery in Amorphous Materials. *J. Non-Cryst. Solids* **1994**, *169* (3), 211–266.
(33) Daniele Cangialosi, V. M. B.; Angel Alegría, J. C. Direct Evidence of Two Equilibration Mechanisms in Glassy Polymers. *Phys. Rev. Lett.* **2013**, *111*, 095701.
(34) Pradipkanti, L.; Chowdhury, M.; Satapathy, D. K. Stratification and Two Glass-like Thermal Transitions in Aged Polymer Films. *Phys. Chem. Chem. Phys.* **2017**, *19* (43), 29263–29270.
(35) Golovchak, R.; Kozdras, A.; Balitska, V.; Shpotyuk, O. Step-Wise Kinetics of Natural Physical Ageing in Arsenic Selenide Glasses. *J. Phys. Condens. Matter* **2012**, *24* (50), 505106.
(36) Gallino, I.; Cangialosi, D.; Evenson, Z.; Schmitt, L.; Hechler, S.; Stolpe, M.; Ruta, B. Hierarchical Aging Pathways and Reversible Fragile-to-Strong Transition upon

Annealing of a Metallic Glass Former. *Acta Mater.* **2018**, *144* (Supplement C), 400–410.

(37) Miller, R. S.; MacPhail, R. A. Ultraslow Nonequilibrium Dynamics in Supercooled Glycerol by Stimulated Brillouin Gain Spectroscopy. *J. Chem. Phys.* **1997**, *106* (8), 3393–3401.

(38) Donth, E.-J. *The Glass Transition - Relaxation Dynamics in Liquids and Disordered Materials*; Springer Series in Materials Science; Springer-Verlag: Berlin Heidelberg, 2001; Vol. 48.

(39) Callen, H. B.; Greene, R. F. On a Theorem of Irreversible Thermodynamics. *Phys. Rev.* **1952**, *86* (5), 702–710.

(40) Johari, G. P. Specific Heat Relaxation-Based Critique of Isothermal Glass Transition, Zero Residual Entropy and Time-Average Formalism for Ergodicity Loss. *Thermochim. Acta* **2011**, *523* (1), 97–104.

(41) Schawe, J. E. K. Vitrification in a Wide Cooling Rate Range: The Relations between Cooling Rate, Relaxation Time, Transition Width, and Fragility. *J. Chem. Phys.* **2014**, *141* (18), 184905.

(42) Wang, L.-M.; Velikov, V.; Angell, C. A. Direct Determination of Kinetic Fragility Indices of Glassforming Liquids by Differential Scanning Calorimetry: Kinetic versus Thermodynamic Fragilities. *J. Chem. Phys.* **2002**, *117* (22), 10184–10192.

(43) Robertson, C. .; Santangelo, P. .; Roland, C. . Comparison of Glass Formation Kinetics and Segmental Relaxation in Polymers. *J. Non-Cryst. Solids* **2000**, *275* (3), 153–159.

(44) B. Rodríguez, A.; R. Tomlinson, M.; Khodabakhsh, S.; Chang, J.-F.; Cousin, F.; Lott, D.; Sirringhaus, H.; S. Huck, W. T.; M. Higgins, A.; Geoghegan, M. All-Polymer Field-Effect Transistors Using a Brush Gate Dielectric. *J. Mater. Chem. C* **2013**, *1* (46), 7736–7741.

(45) Yang, X.; Loos, J.; Veenstra, S. C.; Verhees, W. J. H.; Wienk, M. M.; Kroon, J. M.; Michels, M. A. J.; Janssen, R. A. J. Nanoscale Morphology of High-Performance Polymer Solar Cells. *Nano Lett.* **2005**, *5* (4), 579–583.

(46) Cho, W. K.; Kong, B.; Choi, I. S. Highly Efficient Non-Biofouling Coating of Zwitterionic Polymers: Poly((3-(Methacryloylamino)Propyl)-Dimethyl(3-Sulfopropyl)Ammonium Hydroxide). *Langmuir* **2007**, *23* (10), 5678–5682.

(47) Yave, W.; Car, A.; Wind, J.; Peinemann, K.-V. Nanometric Thin Film Membranes Manufactured on Square Meter Scale: Ultra-Thin Films for CO2 Capture. *Nanotechnology* **2010**, *21*, 395301.

(48) Kausar, A.; Rafique, I.; Muhammad, B. Review of Applications of Polymer/Carbon Nanotubes and Epoxy/CNT Composites. *Polym.-Plast. Technol. Eng.* **2016**, *55* (11), 1167–1191.

(49) Masood, F. Polymeric Nanoparticles for Targeted Drug Delivery System for Cancer Therapy. *Mater. Sci. Eng. C* **2016**, *60* (Supplement C), 569–578.

(50) De-La-Cuesta, J.; González, E.; Pomposo, J. A. Advances in Fluorescent Single-Chain Nanoparticles. *Molecules* **2017**, *22* (11), 1819.

(51) Jiang, B.; Zhu, L.; Zhao, C.; Chen, Z. An Investigation on the Bound Rubber and Dynamic Mechanical Properties of Polystyrene Particles-Filled Elastomer. *Polym. Compos.* **2017**, *38* (6), 1112–1117.

(52) Still, T.; Cheng, W.; Retsch, M.; Jonas, U.; Fytas, G. Colloidal Systems: A Promising Material Class for Tailoring Sound Propagation at High Frequencies. *J. Phys. Condens. Matter* **2008**, *20* (40), 404203.
(53) Alcoutlabi, M.; McKenna, G. B. Effects of Confinement on Material Behaviour at the Nanometre Size Scale. *J. Phys. Condens. Matter* **2005**, *17* (15), R461.
(54) Glynos, E.; Frieberg, B.; Chremos, A.; Sakellariou, G.; Gidley, D. W.; Green, P. F. Vitrification of Thin Polymer Films: From Linear Chain to Soft Colloid-like Behavior. *Macromolecules* **2015**, *48*, 2305–2312.
(55) Cangialosi, D.; Alegría, A.; Colmenero, J. Effect of Nanostructure on the Thermal Glass Transition and Physical Aging in Polymer Materials. *Prog. Polym. Sci.* **2016**, *54–55* (Supplement C), 128–147.
(56) Jeong, H.; Napolitano, S.; Arnold, C. B.; Priestley, R. D. Irreversible Adsorption Controls Crystallization in Vapor-Deposited Polymer Thin Films. *J. Phys. Chem. Lett.* **2017**, *8* (1), 229–234.
(57) Napolitano, S.; Glynos, E.; Tito, N. B. Glass Transition of Polymers in Bulk, Confined Geometries, and near Interfaces. *Rep. Prog. Phys.* **2017**, *80* (3), 036602.
(58) Keddie, J. L.; Jones, R. A. L.; Cory, R. A. Size-Dependent Depression of the Glass Transition Temperature in Polymer Films. *Europhys. Lett.* **1994**, *27*, 59–64.
(59) J. S. Sharp; J. A. Forrest. Free Surfaces Cause Reductions in the Glass Transition Temperature of Thin Polystyrene Films. *Phys. Rev. Lett.* **2003**, *91* (23), 235701.
(60) Zhang, C.; Guo, Y.; Priestley, R. D. Glass Transition Temperature of Polymer Nanoparticles under Soft and Hard Confinement. *Macromolecules* **2011**, *44* (10), 4001–4006.
(61) Ediger, M. D.; Forrest, J. A. Dynamics near Free Surfaces and the Glass Transition in Thin Polymer Films: A View to the Future. *Macromolecules* **2014**, *47*, 471–478.
(62) Keddie, J. L.; Jones, R. A. L.; Cory, R. A. Interface and Surface Effects on the Glass-Transition Temperature in Thin Polymer Films. *Faraday Discuss.* **1994**, *98* (0), 219–230.
(63) Priestley, R. D. Physical Aging of Confined Glasses. *Soft Matter* **2009**, *5* (5), 919–926.
(64) van Zanten, J. H.; Wallace, W. E.; Wu, W. Effect of Strongly Favorable Substrate Interactions on the Thermal Properties of Ultrathin Polymer Films. *Phys. Rev. E* **1996**, *53* (3), R2053–R2056.
(65) Grohens, Y.; Brogly, M.; Labbe, C.; David, M.-O.; Schultz, J. Glass Transition of Stereoregular Poly(Methyl Methacrylate) at Interfaces. *Langmuir* **1998**, *14* (11), 2929–2932.
(66) Fryer, D. S.; Peters, R. D.; Kim, E. J.; Tomaszewski, J. E.; de Pablo, J. J.; Nealey, P. F.; White, C. C.; Wu, W. Dependence of the Glass Transition Temperature of Polymer Films on Interfacial Energy and Thickness. *Macromolecules* **2001**, *34* (16), 5627–5634.
(67) Roth, C. B.; McNerny, K. L.; Jager, W. F.; Torkelson, J. M. Eliminating the Enhanced Mobility at the Free Surface of Polystyrene: Fluorescence Studies of the Glass Transition Temperature in Thin Bilayer Films of Immiscible Polymers. *Macromolecules* **2007**, *40* (7), 2568–2574.

(68) Xu, J.; Ding, L.; Chen, J.; Gao, S.; Li, L.; Zhou, D.; Li, X.; Xue, G. Sensitive Characterization of the Influence of Substrate Interfaces on Supported Thin Films. *Macromolecules* **2014**, *47* (18), 6365–6372.
(69) Ellison, C. J.; Torkelson, J. M. The Distribution of Glass-Transition Temperatures in Nanoscopically Confined Glass Formers. *Nat. Mater.* **2003**, *2* (10), 695.
(70) Ellison, C. J.; Mundra, M. K.; Torkelson, J. M. Impacts of Polystyrene Molecular Weight and Modification to the Repeat Unit Structure on the Glass Transition−Nanoconfinement Effect and the Cooperativity Length Scale. *Macromolecules* **2005**, *38*, 1767–1778.
(71) Park, C. H.; Kim, J. H.; Ree, M.; Sohn, B.-H.; Jung, J. C.; Zin, W.-C. Thickness and Composition Dependence of the Glass Transition Temperature in Thin Random Copolymer Films. *Polymer* **2004**, *45* (13), 4507–4513.
(72) Roth, C. B. *Polymer Glasses*; CRC Press; 2016.
(73) Forrest, J. A.; Dalnoki-Veress, K.; Stevens, J. R.; Dutcher, J. R. Effect of Free Surfaces on the Glass Transition Temperature of Thin Polymer Films. *Phys. Rev. Lett.* **1996**, *77*, 2002–2005.
(74) Forrest, J. A.; Dalnoki-Veress, K. The Glass Transition in Thin Polymer Films. *Adv. Colloid Interface Sci.* **2001**, *94* (1), 167–195.
(75) Boucher, V. M.; Cangialosi, D.; Yin, H.; Schönhals, A.; Alegría, A.; Colmenero, J. T g Depression and Invariant Segmental Dynamics in Polystyrene Thin Films. *Soft Matter* **2012**, *8* (19), 5119–5122.
(76) Napolitano, S.; Wübbenhorst, M. The Lifetime of the Deviations from Bulk Behaviour in Polymers Confined at the Nanoscale. *Nat. Commun.* **2011**, *2*, 260.
(77) Efremov, M. Y.; Olson, E. A.; Zhang, M.; Zhang, Z.; Allen, L. H. Probing Glass Transition of Ultrathin Polymer Films at a Time Scale of Seconds Using Fast Differential Scanning Calorimetry. *Macromolecules* **2004**, *37* (12), 4607–4616.
(78) Fakhraai, Z.; Forrest, J. A. Probing Slow Dynamics in Supported Thin Polymer Films. *Phys. Rev. Lett.* **2005**, *95* (2), 025701.
(79) *Fast Scanning Calorimetry*; Schick, C., Mathot, V., Eds.; Springer International Publishing, 2016.
(80) Shamim, N.; Koh, Y. P.; Simon, S. L.; McKenna, G. B. Glass Transition Temperature of Thin Polycarbonate Films Measured by Flash Differential Scanning Calorimetry. *J. Polym. Sci. Part B Polym. Phys.* **2014**, *52* (22), 1462–1468.
(81) Cangialosi, D.; Alegría, A.; Colmenero, J. Cooling Rate Dependent Glass Transition in Thin Polymer Films and in Bulk. In *Fast Scanning Calorimetry*; Schick, C., Mathot, V., Eds.; Springer International Publishing: Cham, 2016; pp 403–431.
(82) Glynos, E.; Frieberg, B.; Oh, H.; Liu, M.; Gidley, D. W.; Green, P. F. Role of Molecular Architecture on the Vitrification of Polymer Thin Films. *Phys. Rev. Lett.* **2011**, *106* (12), 128301.
(83) Grohens, Y.; Hamon, L.; Reiter, G.; Soldera, A.; Holl, Y. Some Relevant Parameters Affecting the Glass Transition of Supported Ultra-Thin Polymer Films. *Eur Phys J E* **2002**, *8* (2), 217–224.

(84) Napolitano, S.; Rotella, C.; Wübbenhorst, M. Can Thickness and Interfacial Interactions Univocally Determine the Behavior of Polymers Confined at the Nanoscale? *ACS Macro Lett.* **2012**, *1* (10), 1189–1193.
(85) Housmans, C.; Sferrazza, M.; Napolitano, S. Kinetics of Irreversible Chain Adsorption. *Macromolecules* **2014**, *47*, 3390–3393.
(86) Burroughs, M. J.; Napolitano, S.; Cangialosi, D.; Priestley, R. D. Direct Measurement of Glass Transition Temperature in Exposed and Buried Adsorbed Polymer Nanolayers. *Macromolecules* **2016**, *49* (12), 4647–4655.
(87) Gaur, U.; Wunderlich, B. Study of Microphase Separation in Block Copolymers of Styrene and α-Methylstyrene in the Glass Transition Region Using Quantitative Thermal Analysis. *Macromolecules* **1980**, *13* (6), 1618–1625.
(88) Feng, S.; Li, Z.; Liu, R.; Mai, B.; Wu, Q.; Liang, G.; Gao, H.; Zhu, F. Glass Transition of Polystyrene Nanospheres under Different Confined Environments in Aqueous Dispersions. *Soft Matter* **2013**, *9* (18), 4614–4620.
(89) Feng, S.; Chen, Y.; Mai, B.; Wei, W.; Zheng, C.; Wu, Q.; Liang, G.; Gao, H.; Zhu, F. Glass Transition of Poly(Methyl Methacrylate) Nanospheres in Aqueous Dispersion. *Phys. Chem. Chem. Phys.* **2014**, *16* (30), 15941–15947.
(90) Hornig, S.; Heinze, T.; Becer, C. R.; Schubert, U. S. Synthetic Polymeric Nanoparticles by Nanoprecipitation. *J. Mater. Chem.* **2009**, *19* (23), 3838–3840.
(91) Zhang, C.; Chung, J. W.; Priestley, R. D. Dialysis Nanoprecipitation of Polystyrene Nanoparticles. *Macromol. Rapid Commun.* **2012**, *33* (20), 1798–1803.
(92) Zhang, C.; Pansare, V. J.; Prud'homme, R. K.; Priestley, R. D. Flash Nanoprecipitation of Polystyrene Nanoparticles. *Soft Matter* **2011**, *8* (1), 86–93.
(93) Martínez-Tong, D. E.; Soccio, M.; Sanz, A.; García, C.; Ezquerra, T. A.; Nogales, A. Chain Arrangement and Glass Transition Temperature Variations in Polymer Nanoparticles under 3D-Confinement. *Macromolecules* **2013**, *46* (11), 4698–4705.
(94) Martínez-Tong, D. E.; Cui, J.; Soccio, M.; García, C.; Ezquerra, T. A.; Nogales, A. Does the Glass Transition of Polymers Change Upon 3D Confinement? *Macromol. Chem. Phys.* **2014**, *215* (17), 1620–1624.
(95) Cangialosi, D.; Boucher, V. M.; Alegría, A.; Colmenero, J. Physical Aging in Polymers and Polymer Nanocomposites: Recent Results and Open Questions. *Soft Matter* **2013**, *9* (36), 8619–8630.
(96) Kawana, S.; Jones, R. a. L. Effect of Physical Ageing in Thin Glassy Polymer Films. *Eur. Phys. J. E* **2003**, *10* (3), 223–230.
(97) Priestley, R. D.; Ellison, C. J.; Broadbelt, L. J.; Torkelson, J. M. Structural Relaxation of Polymer Glasses at Surfaces, Interfaces, and In Between. *Science* **2005**, *309* (5733), 456–459.
(98) Priestley, R. D.; Broadbelt, L. J.; Torkelson, J. M. Physical Aging of Ultrathin Polymer Films above and below the Bulk Glass Transition Temperature: Effects of Attractive vs Neutral Polymer−Substrate Interactions Measured by Fluorescence. *Macromolecules* **2005**, *38* (3), 654–657.
(99) Koh, Y. P.; Simon, S. L. Structural Relaxation of Stacked Ultrathin Polystyrene Films. *J. Polym. Sci. Part B Polym. Phys.* **2008**, *46* (24), 2741–2753.

(100) Boucher, V. M.; Cangialosi, D.; Alegría, A.; Colmenero, J. Enthalpy Recovery in Nanometer to Micrometer Thick Polystyrene Films. *Macromolecules* **2012**, *45* (12), 5296–5306.
(101) Boucher, V. M.; Cangialosi, D.; Alegría, A.; Colmenero, J. Complex Nonequilibrium Dynamics of Stacked Polystyrene Films Deep in the Glassy State. *J. Chem. Phys.* **2017**, *146* (20), 203312.
(102) Boucher, V. M.; Cangialosi, D.; Alegria, A.; Colmenero, J. Reaching the Ideal Glass Transition by Aging Polymer Films. *Phys. Chem. Chem. Phys.* **2017**, *19* (2), 961–965.
(103) Guo, Y.; Zhang, C.; Lai, C.; Priestley, R. D.; D'Acunzi, M.; Fytas, G. Structural Relaxation of Polymer Nanospheres under Soft and Hard Confinement: Isobaric versus Isochoric Conditions. *ACS Nano* **2011**, *5* (7), 5365–5373.
(104) Boucher, V. M.; Cangialosi, D.; Alegría, A.; Colmenero, J.; González-Irun, J.; Liz-Marzan, L. M. Accelerated Physical Aging in PMMA/Silica Nanocomposites. *Soft Matter* **2010**, *6* (14), 3306–3317.
(105) Cangialosi, D.; Boucher, V. M.; Alegría, A.; Colmenero, J. Enhanced Physical Aging of Polymer Nanocomposites: The Key Role of the Area to Volume Ratio. *Polymer* **2012**, *53* (6), 1362–1372.
(106) Zhang, C.; Boucher, V. M.; Cangialosi, D.; Priestley, R. D. Mobility and Glass Transition Temperature of Polymer Nanospheres. *Polymer* **2013**, *54* (1), 230–235.
(107) Mathlouthi, C.; Hugenell, F.; Delpech, F.; Rharbi, Y. Heat Capacity of Confined Polystyrene in Close-Packed Particles. *Macromolecules* **2017**, *50* (1), 472–481.
(108) Zhang, C.; Guo, Y.; Shepard, K. B.; Priestley, R. D. Fragility of an Isochorically Confined Polymer Glass. *J. Phys. Chem. Lett.* **2013**, *4* (3), 431–436.
(109) Priestley, R. D.; Cangialosi, D.; Napolitano, S. On the Equivalence between the Thermodynamic and Dynamic Measurements of the Glass Transition in Confined Polymers. *J. Non-Cryst. Solids* **2015**, *407*, 288–295.
(110) Boucher, V. M.; Cangialosi, D.; Alegría, A.; Colmenero, J.; Pastoriza-Santos, I.; Liz-Marzan, L. M. Physical Aging of Polystyrene/Gold Nanocomposites and Its Relation to the Calorimetric Tg Depression. *Soft Matter* **2011**, *7* (7), 3607–3620.
(111) Ramakrishnan, V.; Harsiny, S.; Goossens, J. G. P.; Hoeks, T. L.; Peters, G. W. M. Physical Aging in Polycarbonate Nanocomposites Containing Grafted Nanosilica Particles: A Comparison between Enthalpy and Yield Stress Evolution. *J. Polym. Sci. Part B Polym. Phys.* **2016**, *54* (20), 2069–2081.

2

EXPERIMENTAL TECHNIQUES AND DATA ANALYSIS

In this chapter we will focus on the description of the technical aspects and physical principles underlying different experimental techniques used in this thesis. Firstly, we will focus on the description of the techniques providing information on the thermodynamic state in terms of enthalpy and volume, with special attention to glass-forming materials. Secondly, we will describe techniques which have the ability to analyze the morphology of the investigated glass-forming systems. Finally, we will introduce the methodologies followed for the data analysis.

2.1. THERMAL ANALYSIS

Thermal analysis is based on techniques sharing a common feature: they measure a material's response as a function of the temperature, that is, when it is heated, cooled or held isotermally.[1] Different thermal methods are commonly used to analyze the behavior of glass-forming systems. Here, the main purpose is achieving information about the glass transition temperature (T_g). To do so, we have used calorimetric techniques and spectroscopic ellipsometry. The main property that is measured by differential scanning calorimetry (DSC) is the heat flow rate, that is to say, the flow of energy exchanged by the sample and the external world as a function of temperature or time.[2] Spectroscopic ellipsometry gives information on the complex refractive index,[3] which depends on the material's density. Therefore, if a system is subjected to a temperature program, a discontinuity in the thermal expansion and consequently in volume, will be observed.

Over the last 20 years, there have been an emergence of novel calorimeters fabricated with Micro-Electro-Mechanical-Systems (MEMS) processes,[4–7] which rely on the use of a thin membrane. These nanocalorimeters main purpose is to reduce the mass, thus allowing fast heat transfer and therefore, high heating/cooling rates.

2.1.1. CALORIMETRY

Generally speaking, differential scanning calorimetry measures the change of the difference in temperature between a sample and a corresponding reference, while they are subjected to a controlled temperature program. This technique uses the temperature difference developed between the sample and the reference, where such difference is used to calculate the heat flow. Conventionally, an exothermic exchange indicates heat flowing out of the sample, while an endothermic exchange indicates heat flowing in.[1] The energy changes, which occurs as a sample is heated, cooled or held isothermally – apart from providing the specific heat capacity of the sample – enable to quantify the phase transformations that occur in the sample, for example, melting processes, glass transitions and a range of more complex events.[2]

In general, considering a time independent heat capacity and sample mass for each temperature step, differentiation with respect to the time yields to:[8]

$$\frac{dQ}{dt} = C_p \frac{dT}{dt} = c_p m \frac{dT}{dt} \qquad (2.1)$$

where dQ/dt is the heat flow rate also represented by ΔHF; dT/dt is defined as the heating or cooling rate (q); C_p and c_p are the apparent heat capacity and specific heat capacity, respectively; m is the sample mass. Here an apparent quantity is considered due to the fact that, when a phase transformation takes place, such quantity contains the latent heat of such transformation. This consideration has to be kept in mind, though in the rest of the thesis for simplicity we will name such magnitude as the heat capacity, and the related

intensive property as the specific heat capacity instead of 'apparent' specific heat capacity. It is recalled that the heat capacity (C_p) is the ratio of the amount of heat transferred to a material to the resulting increase in its temperature, while the specific heat capacity (c_p), is a measure of the amount of heat necessary to raise the temperature of 1 gram of a sample by 1 degree K.[9]

2.1.1.1. Standard DSC

DSC is based on measuring the heat exchange between a substance and the external world as the temperature is varied.[2] Two types of DSC instruments exist: those based on (i) heat flux and (ii) power compensation, schematically represented in Figure 2. **1** and Figure 2. **2**, respectively. In the (i) heat flux modality, due to the heat capacity of the sample, the reference side (usually an empty pan) generally heats up faster than the sample side during heating of the DSC measuring cell, that is, the reference temperature increases a bit faster than the sample temperature. The two curves exhibit parallel behavior during heating at a constant heating rate, until a sample transformation occurs. The temperature of the sample does not change during the transformation or changes in a non-linear manner, for instance, at the glass transition. However, the temperature of the reference side remains unaffected and continues exhibiting a linear increase. When the transformation is completed, the sample temperature also begins to change again and exhibits a linear increase. The differential behavior in terms of temperature of the sample and the reference gives information about thermal properties of the sample, such as the heat capacity or the latent heat of a transformation.[1]

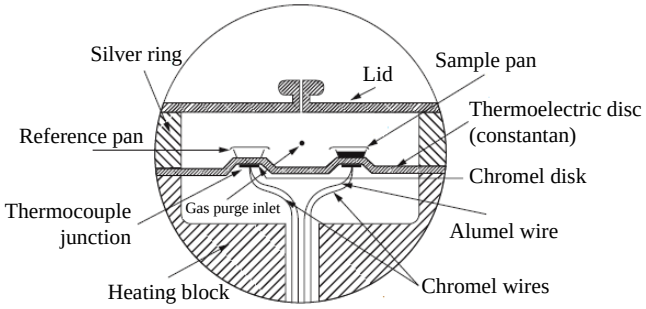

Figure 2. 1 Cross section of TA instruments DSC heat flux measuring cell.[1]

In the (ii) power compensation modality, both cells are heated independently in different furnaces as represented in Figure 2. 2.

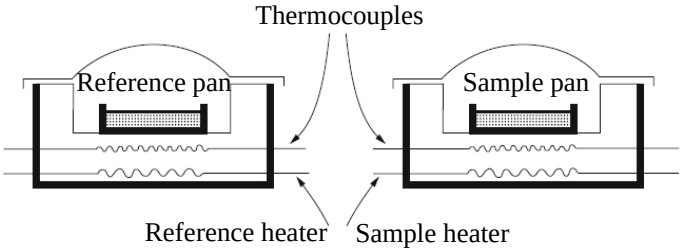

Figure 2. 2 Power compensation sample holder with twin furnaces and sensors.[9]

This DSC is based on heating/cooling the cells at a constant linear rate.[1,9] Hence, the system is based on ensuring that the recorded temperature values in the sample and reference cells are as close as possible. To do so, a differential heat flux is delivered to the sample and the reference cells, which depends on the thermal properties of the sample.

In this thesis, a heat flux modality calorimeter, that is, Q2000 from TA Instruments, is employed. Temperature control is fulfilled through a Helium (He) gas flow of 25 mL/min. Samples are generally prepared by encapsulating 2 − 10 mg of material into aluminum pans.

2.1.1.2. Fast Scanning Calorimetry (FSC)

The typical heating/cooling rates of conventional DSC are centered on the usual laboratory rates, that is, around 10 K/min,[7] and normally cover a range between 0.1 and 300 K/min.[10] Recently, to overcome the limitations in the maximum achievable heating/cooling rates, new experimental techniques based on fast scanning calorimetry (FSC) have been developed. These techniques are based on the same principles presented for standard DSC. In the direction of increasing the rate of temperature variation, 'homemade' FSC instruments, capable of reaching 10^7-10^8 K/s, are currently available.[11,12] Hence, the combination of FSC and standard DSC instruments allows accessing a heating and cooling rate range of more than eight decades. Such remarkable range can be exploited to unveil new information about structure formation and reorganization processes in materials.[7,10] Thus, FSC has recently been employed to explore systems far from thermodynamic equilibrium,[5] otherwise inaccessible by standard DSC. Typical examples are highly metastable polymorphic phases and glasses, or those materials that exhibit strong tendency to crystallize.[10]

In the present thesis, we have employed a commercial FSC, that is, the equipment 'Flash DSC 1' by 'METTLER TOLEDO'. This device makes use of a chip sensor based on MEMS processes.[4–7] Likewise in standard DSC, Flash DSC 1 consists of two separate furnaces: one for the sample and the other for the reference, which operate like a conventional DSC. The temperature range of Flash DSC 1 is from 178 to 723 K and scan rates can be varied within 0.1 to 4000 K/s on cooling and from 0.5 to 40000 K/s on heating.[13] The sensor is made of two identical squares of silicon nitride/oxide membranes, deposited on top of an aluminum core as shown in Figure 2.3. The total thickness of the membrane is ~ 2 μm. The temperature of the sample area is measured with eight thermocouples for each furnace,[7,10] as detailed in the scheme of Figure 2.4. Experiments are carried out on an inert gas atmosphere, typically N_2, though other gases can be employed,[10] in order to

avoid water condensation from the environment, and to optimize the applied program temperature. A Huber TC100 intracooler is used for temperature control.

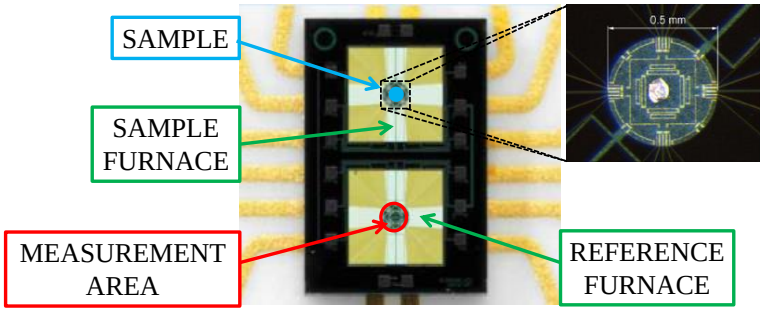

Figure 2.3 Left Panel: Chip sensor overall view. The active area of the sample and the reference, and the entire furnaces are indicated. Right Panel: Magnification of a sample on the active area.[7]

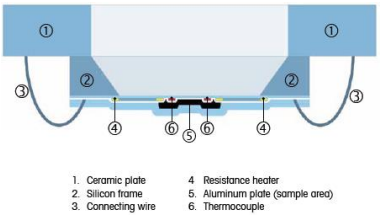

Figure 2.4 Schematic cross-section (not to scale) of the chip sensor (one membrane is shown).[7]

Calibration

The calibration of the Flash DSC 1 consists of conditioning and correction temperature procedures. The conditioning procedure is needed to erase the stress generated during the production process. It consists of heating the empty chip sensor at 100 K/s from 318 to 723 K followed by an isotherm of 4 s at this high temperature, followed by cooling at 100 K/s down to 318 K and finishing with an isotherm of 4 s. This protocol is repeated until the heat flow

rate curves of two consecutive experiments collapse. This is generally achieved after five conditioning experiments. Afterwards, the correction procedure is performed. The experiment begins by doing an isotherm of 0.1 s at 173 K, followed by a heating ramp of 550 K/s up to 723 K and holding this temperature for 1 s. The correction temperature is performed in order to correct the thermocouple signal (T_s) with respect to the sensor supporting temperature signal (T_{ss}).[10]

Thermal Lag

The thermal lag of the Flash DSC 1 is determined almost exclusively by the sample geometry and its contact with the sensor.[10] Strictly speaking, only the portion of sample in direct contact with the chip membrane exhibits the temperature registered by the thermocouple. A temperature profile is therefore generated along the direction perpendicular to the surface of the membrane. This depends on the scanning rate, the mass of the sample, its geometry and thermal conductivity. Typically for polymeric materials with mass of several hundred of nanograms and thicknesses of microns, a 2 K thermal lag is registered at heating/cooling rates of about 1000 K/s. At lower rates, such lag is generally negligible.[14,15] For geometries substantially differing from that of films, the thermal contact can be improved by introducing a medium between the sample and the chip membrane. This is the case of the study reported in this thesis, where polymer nanospheres are investigated. In such a case, a thin layer of diluted polydimethylsiloxane (PDMS) was used in order to improve the thermal contact between the sample and the chip.

Sample mass determination

The achievement of scan rates of the order of thousands of K/s can be accomplished employing sample masses lower than several hundred nanograms.[7] Weighing of such low masses is not possible even employing the most accurate balances available. Hence, thermal properties like the melting

enthalpy, the glass transition step height or the heat capacity in a given known thermodynamic state are used to estimate the sample mass.[10] In our case, the sample mass was calculated from the step of the heat flow rate jump in the range of temperature of the glass transition (ΔHF (T_g)). This is related to the total specific heat jump (Δc_p) through equation (2.1), which can be rewritten as follows:

$$\Delta HF(T_g) = m\Delta c_p(T_g)q \qquad (2.1)$$

The mass of the sample can be evaluated from such equation, once $\Delta c_p(T_g)$ is known from independent measurements by standard DSC.

2.1.1.3. Data Analysis

Estimation of the Fictive Temperature

The fictive temperature (T_f) is a measure of the thermodynamic state of a glass and is defined as the intersection of the extrapolated glass line and the extrapolated equilibrium melt line. The concept of T_f was first introduced by Tool[16] and described in details in Chapter 1. It is generally measured on heating and can be calculated following the equation developed by Moynihan:[17]

$$\int_{T_f}^{T\gg T_g}(c_{pm} - c_{pg})\mathrm{d}T = \int_{T\ll T_g}^{T\gg T_g}(c_p - c_{pg})\mathrm{d}T \qquad (2.2)$$

where c_{pm} and c_{pg} are the specific heat capacities of melt and glass respectively, and c_p is the experimental specific heat capacity.

As can be observed in the Figure 2.5 and given its definition, T_f is extracted when both areas match each other, as mathematically described by the equation (2.2).

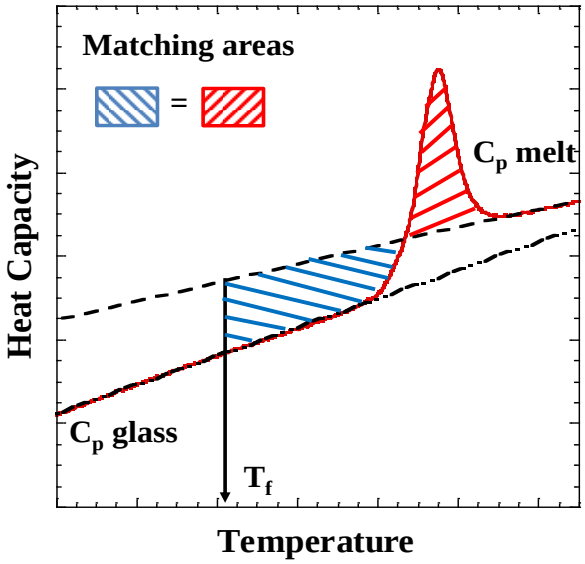

Figure 2.5 Moynihan[17] method of the matching areas to determine T_f applied to a typical calorimetric heat scan. The dashed line represents the specific heat of the melt and the dashed dotted line the specific heat of the glass.

It is important for an objective analysis, to employ the same glass and melt lines in all the scans for a given set of data. In order to do this, we have to superpose the melt and glass regions, that is, those regions where no irreversible processes related to devitrification are taking place, of a given scan to the reference scan by minimizing the mean square error, $\chi^2 = \sum\left(c_{\mathrm{p\_corrected}} - c_{\mathrm{p\_ref}}\right)^2$; where $c_{\mathrm{p\_corrected}}$ corresponds to a corrected scan in slope and in the vertical shift. The minimization is accomplished in the same specified temperature range for all scans, far away from the transition or enthalpy overshoot.

Estimation of the Enthalpy Recovery

The effect of physical aging on the enthalpy change of a glass is illustrated in Figure 2.6 (left panel), where the c_p scan of PS bulk aged at 368 K for 100000

s, and that of the reference or unaged scans are shown as a showcase. In the right panel of that figure, the c_p of the aged sample in excess to that of the reference as a function of temperature is also shown. The effect of physical aging on enthalpy recovery has been discussed in details in Chapter 1. Given the relationship between the specific heat and the enthalpy, the general procedure for the determination of the amount of relaxed enthalpy during the aging process, consists of integrating the difference between aged and unaged thermograms, according to the following equation (2.3):[18]

$$\Delta H(T_a, t_a) = \int_{T \ll T_g}^{T \gg T_g} \left(c_p^a - c_p^u\right) dT \qquad (2.3)$$

where c_p^a and c_p^u are respectively the specific heats of the aged and unaged samples.

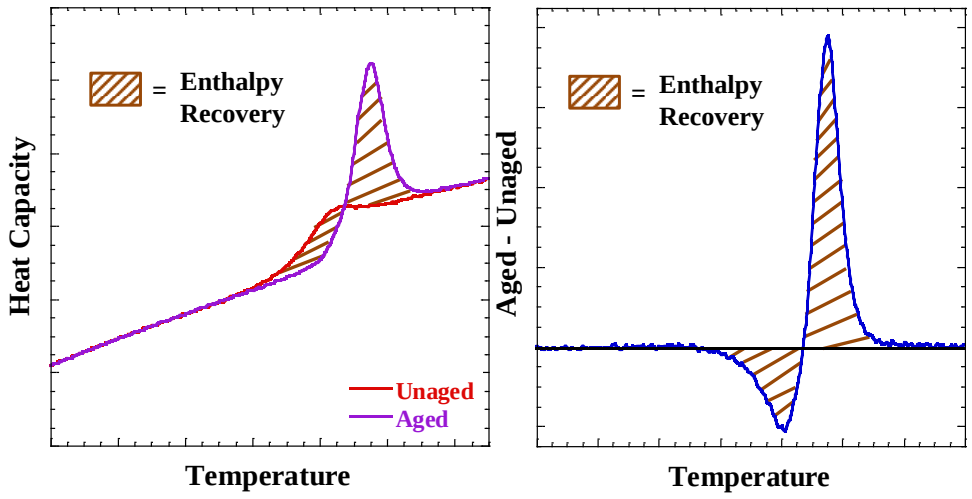

Figure 2.6 Left Panel: Calorimetric heat scans of unaged (red line) and aged (purple line) for PS bulk sample. Right Panel: Excess of the specific heat (blue line) as a function of temperature for the scans presented in the left panel. The recovered enthalpy corresponds to the brown stripped area. Data are for bulk PS aged at T_a= 368 K for t_a= 100000 s.

In this case, the same procedure as the one explained for the T_f determination, superposition of the glass and melt lines for the aged and the unaged scans has to be applied, by minimizing the mean squared error χ^2 of the excess specific heat. Thus, the difference between the specific heat of the aged and unaged scans in the region where no endothermic overshoot is presented.

Step Response Analysis

The step response method was developed by Schick and co-workers[19,20] to determine the complex heat capacity spectrum (c_p^*). The value of c_p^* depends on the frequency of temperature modulation and can be used to study the dynamic glass transition and the irreversible (non-equilibrium or non-linear) and reversible (equilibrium or linear) processes of a system,[21] as described in details in Chapter 1.

Figure 2.7 shows the thermal protocols employed to perform one (left panel) and two (right panel) steps response analysis.[20,22] The one step protocol entails a down-jump of 2 K at 2000 K/s followed by and isothermal period (t_p) of 0.1 and 1 s. The two steps protocol is based on a down-jump of 2 K at 1000 K/s and an up-jump of 1 K at 1000 K/s, both followed by a total isothermal period of t_p= 0.05 s, where both isotherms exhibit identical time length.

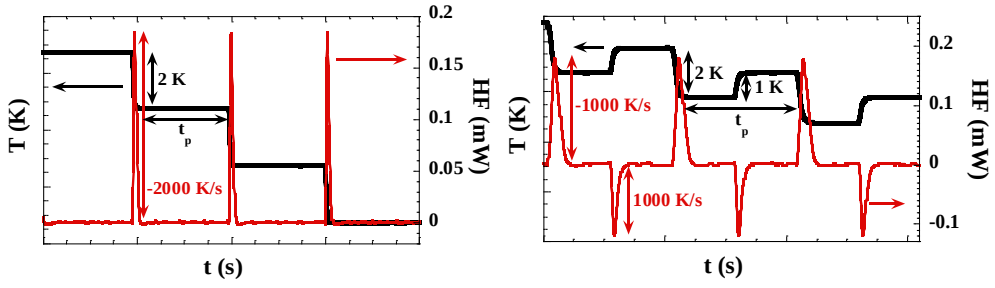

Figure 2.7 Thermal protocol to perform one (left panel) and two (right panel) steps response analysis. Black lines correspond to the programmed cooling step, whereas red lines show the heat flow rate. t_p is the period of the modulation.

The baseline has to be corrected considering that on an isotherm heat must be delivered to the sample, due to the fact that the Flash DSC 1 cold block is maintained at 170 K. Hence, the heat flow is corrected in such a way that, in the stationary state of the isotherm it is shifted to zero. As an example, Figure 2.8 shows the baseline correction for the two steps protocol down-up jump experiment. The corrected baseline was performed by taking the value of the *HF* at the end of the isotherm cicle (t_p) and subtracting it from the total *HF*.

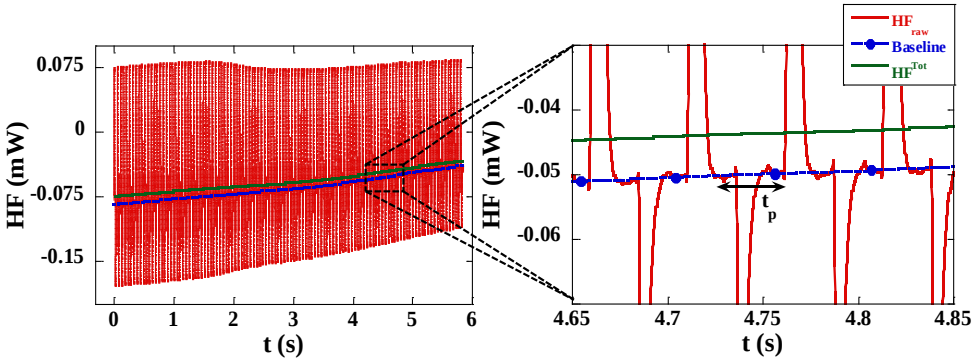

Figure 2.8 Left Panel: Heat flow rate response corresponding to the two steps down-up protocol for bulk PS in Flash DSC 1 (underlying cooling rate $\langle q \rangle$: 20 K/s; period t_p: 0.05 sec). Right Panel: Magnification of the heat flow rate response. Heat flow rate baseline (blue dashed line) and the total heat flow rate (green solid line). Blue bullet points correspond to the end of each isotherm.

By applying the Fourier transformation of the heat flow rate and the cooling/heating rate, the complex specific heat capacity can be determined as follows (2.4):[19,20]

$$c_p^*(\omega) = c_p'(\omega) - ic_p''(\omega) = \frac{\int_0^{t_p} \mathrm{HF}(t) e^{-i\omega t} \mathrm{d}t}{\int_0^{t_p} q(t) e^{-i\omega t} \mathrm{d}t} \qquad (2.4)$$

where ω is the angular frequency; c_p' the real component and c_p'' the imaginary component of the complex heat capacity and t_p the period of the oscillation.

Furthermore, this kind of measurement provides with the total heat capacity by dividing the total corrected heat flow rate and the underlying cooling/heating rate, as expressed in the following equation (2.5):

$$c_{\mathrm{p}}^{\mathrm{Tot}} = \frac{\langle \mathrm{HF} \rangle_{\mathrm{corrected}}}{\langle q \rangle} \qquad (2.5)$$

where $\langle \cdot \rangle$ is the average over one modulation period; $\langle \mathrm{HF} \rangle$ is the average or total corrected heat flow signal and $\langle q \rangle$ the underlying cooling/heating rate.

The basic features of the complex heat capacity (c_{p}^{*}) are that there is a step in a real part (c_{p}') and a peak in the imaginary part (c_{p}''), as well as a shift with frequency.[22] By means of the total and the complex heat capacity, two different responses, a non-linear and linear one, are generated simultaneously providing information respectively on (i) the thermal glass transition (vitrification – $T_{\mathrm{g}}(q)$), and (ii) the dynamic glass transition ($T_{\mathrm{g}}(\omega)$),[19–22] as depicted in Figure 2.9.

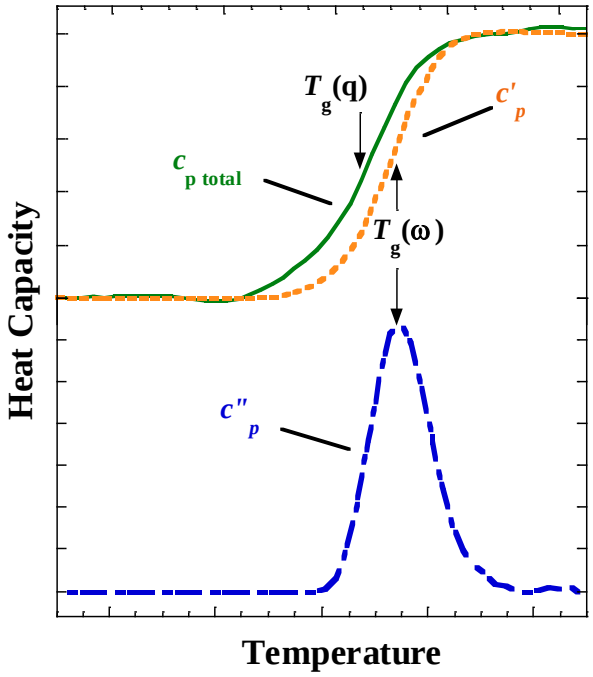

Figure 2.9 Calorimetric heat scan for PS bulk in Flash DSC1 measured by the step response method at a period of t_p= 0.1 sec. Illustration of the deconvolution of the complex heat capacity. $T_g(\omega)$, the dynamic glass transition, from $c_p^{'}$ (orange dashed line) and $c_p^{''}$(blue dashed-dotted line) and $T_g(q)$, the thermal glass transition, from c_p^{Tot} (green solid line) are shown.

2.1.2. SPECTROSCOPIC ELLIPSOMETRY

Ellipsometry is a non-destructive method for characterizing thin layers at solid and viscous liquid substrates based on their thickness (d) and complex refractive index ($\tilde{N}$).[3] Briefly, this technique measures the change in the polarization state of light reflected from a surface[23] as summarized in Figure 2.10.[24,25]

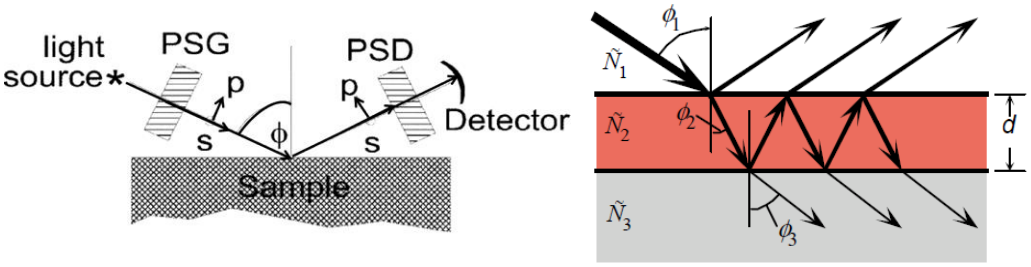

Figure 2.10 Left Panel: Schematic diagram of an ellipsometry experiment. The light beam passes through the polarization state generator (PSG) before being reflected from the sample surface. After reflection, the light beam is repolarized by the polarization state detector (PSD) before being detected. Light polarized in the plane of incidence is 'p' polarized light, while light polarized perpendicular to the plane of incidence is 's' polarized light. The ϕ is the angle of incidence.[26] Right Panel: Reflection and transmissions with multiple interfaces model of an air/thin film/substrate structure. Where $\tilde{N}_1$ is the complex refractive index in the medium 1, $\tilde{N}_2$ in the medium 2 and $\tilde{N}_3$ in the medium 3. $\emptyset_1$ is the incident and $\emptyset_2$, $\emptyset_3$ are the refracted angles.[24]

From a physical point of view, spectroscopic ellipsometry measures two values: the amplitude ratio (Ψ) and the phase difference (Δ) between the parallel (p) and the perpendicular (s) light waves with respect to the plane of incidence, after reflection from the sample surface (Figure 2.10). The general equation describing this relation is:[26]

$$\frac{R_p}{R_s} = tan\Psi e^{i\Delta} \tag{2.6}$$

where R_p and R_s are the total or the Fresnel reflection coefficients, that are expressed as:

$$R_p = \frac{r_{12}^p + r_{23}^p exp(-j2\beta)}{1 + r_{12}^p r_{23}^p \, exp(-j2\beta)}$$

$$R_s = \frac{r_{12}^s + r_{23}^s exp(-j2\beta)}{1 + r_{12}^s r_{23}^s \, exp(-j2\beta)} \tag{2.7}$$

In these last equations *r* is the amplitude reflection coefficient at the interfaces presented in the right panel of Figure 2.10, where three different media are considered to be in a layer-by-layer configuration. Specifically, $\tilde{N}_1$ is the air, $\tilde{N}_2$ the sample to be studied having a determined thickness (*d*), and $\tilde{N}_3$ the supporting substrate. Thus, in equation (2.7), the subscript '12' and '23' means that these Fresnel reflection coefficients are those for the interface between medium 1 – medium 2, and medium 2 – medium 3, respectively. Finally, in these equations β is the *film phase thickness* and is given as:[26]

$$\beta = 2\pi\left(\frac{d}{\lambda}\right)\tilde{N}_2 cos\phi_2 \qquad (2.8)$$

Then, equation (2.6) is a function of $\tilde{N}_1,\tilde{N}_2,\tilde{N}_3,\phi_2,\lambda$ and *d*, being λ the wavelength. Generally, $\tilde{N}_1$, $\tilde{N}_3$ and λ are known, ϕ_2 can be obtained from Snell's law,[25] leaving thus $\tilde{N}_2$ and *d* as unknowns. If the sample material is considered transparent, that is, if it does not absorb light at a wavelength range of the equipment, one can use the Cauchy or Sellmeier relationship[26,27] to obtain $\tilde{N}_2$, which will have exclusively a real part (*i.e.* becoming $\tilde{N}_2 \Rightarrow n_2$). Finally it becomes evident that the only parameter left for calculation is the film thickness, *d*.

In this thesis, ellipsometric measurements were performed with the spectroscopic ellipsometer (MM-16 Horiba) using a wavelength range of λ= 430 – 850 nm and 70º angle of incidence (ϕ_1), corresponding to the Brewster angle[24,25] (*i.e.* the angle of incidence at which there is no reflection of p-polarized light at an uncoated optical surface) of silicon, the material used as substrate for the determination of thin films thicknesses. For the analysis of the glass transition temperature an external temperature controller (TMS 94 Linkam Scientific Instruments Ltd.) was used, while acquiring the ellipsometric angles.

2.1.2.1. Data Analysis: Estimation of the Glass Transition Temperature

The value of T_g can be obtained by measuring the temperature dependence of the ellipsometric angles; Ψ and Δ. Given the linear dependence of Ψ on h in the studied range of thicknesses, the condition $\delta|h| \sim \delta|\Psi|$ is valid, where δ indicates a small increment of the quantity.[24] Furthermore, as in the approximation of thin films, assuming that the constraints at the supporting interface allow thermal expansion only in the normal direction, it holds that $h(T) \sim V(T)$, where V is the volume of the sample.[28] Upon heating, the material softens in proximity of T_g, which results in a neat increase in thermal expansion, $\sim \partial V/\partial T$. This quantity is directly proportional to the temperature derivative of the ellipsometric angles. The T_g is attributed to the crossing of linear regressions fits of the $\Psi(T)$ in the glassy and in the supercooled liquid state.[29] For instance, Figure 2.11 shows how the ellipsometric angles Ψ and Δ are correlated with the thickness of the film as a function of the temperature.

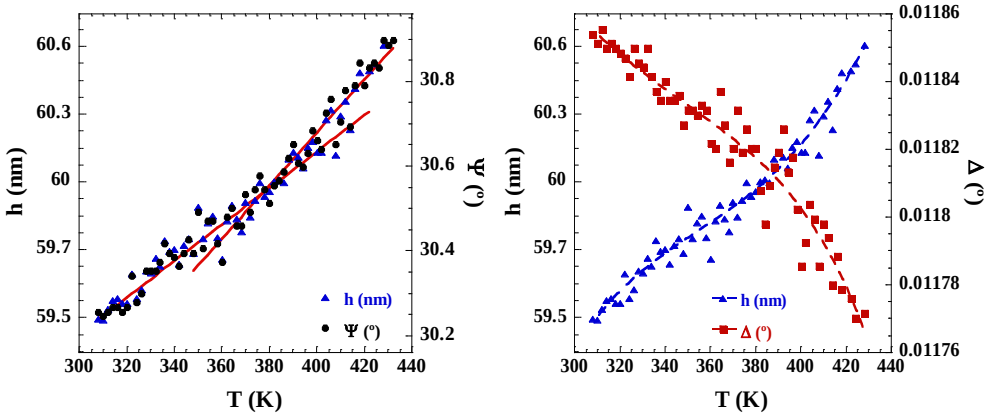

Figure 2.11 Raw data of the ellipsometric angles Ψ and Δ (at a wavelength of 600 nm and an incidence angle of 70°) for a 60 ± 1 nm PTBS thick film as a function of T compared to $h(T)$ at 2 K/min. Left Panel: h (blue triangles) and Ψ(black circles) as a function of T. The crossover between melt and liquid lines (red solid line) is taken as T_g value. Right Panel: Δ (red squares) and h (blue triangles) as a function of T. Dashed lines are third order polynomial fits of the raw data for eye guiding.

2.2. MORPHOLOGICAL ANALYSIS

The morphological characterization of the structure achieved by a material after a given preparation protocol is generally carried out by different methods. Examples are transmission electron microscopy (TEM), scanning electron microscopy (SEM), scanning transmission electron microscopy (STEM), small-angle X-ray scattering (SAXS), wide-angle X-ray scattering (WAXS), atomic force microscopy (AFM) and dynamic light scattering (DLS).

In this section, we will focus on DLS and AFM. Within the framework of the present thesis, both techniques are used to characterize the size of polystyrene (PS) nanospheres. Furthermore, AFM is employed to determine the thicknesses of poly(tert-butyl styrene) (PTBS) thin films.

2.2.1. DYNAMIC LIGHT SCATTERING

DLS is a technique employed to characterize the size of particles dispersions. It basically makes use of the illumination by a laser beam of a suspension of particles, undergoing Brownian motion.[30–32] DLS experiments are based on the analysis of the temporal fluctuations of the scattered intensity due to density or concentration fluctuations in the sample. The experimental set-up is shown in Figure 2.12, where the detector is connected to a correlator that computes the correlation function from the intensity fluctuations as a function of time. A correlator is basically a signal comparator that measures the degree of similarity between two signals, or one signal with itself at varying time intervals.[33] In general, the correlation function is defined as:[32]

$$G(\tau) = \langle I(t)I(t+\tau)\rangle \qquad (2.9)$$

Where τ is the time difference (the sample time) of the correlator, *I(t)* is the scattered intensity at time *t* and *I(t+τ)* is the scattered intensity at time *t+τ*. In homodyne detection mode, the correlation function of the scattered intensity

$G(\tau)$, is related to the electric-field correlation function $g_1(\tau)$, by the equation (2.10):[32]

$$G(\tau) = A\left[1 + B\left(g_1(\tau)\right)^2\right] \qquad (2.10)$$

where A is the normalization factor and B an instrumental factor, which reflects deviations from the ideal correlation, and $g_1(\tau)$ is the sum of all the exponential decays contained in the correlation function.

For monodisperse particles in solution the field correlation function decays exponentially as $|g_1| = 1 + exp(-\Gamma\tau)$ with a decay rate of $\Gamma = Dq^2$, where D is the diffusion coefficient of the particle and q is the magnitude of the scattering wave vector, defined as: [32,34]

$$q = \frac{4\pi\tilde{\mathrm{N}}}{\lambda_0}\sin\left(\frac{\phi}{2}\right) \qquad (2.11)$$

where $\tilde{N}$ is the solvent refractive index, λ_0 is the wavelength of the laser in vacuum, and ϕ is the scattering angle.

The measured quantity is the diffusion coefficient (D). The particle shape is related to this coefficient in the simple case of a spherical object, and by the application of the Stokes-Einstein relationship, relating the diffusion coefficient to the hydrodynamic diameter (D_H) of the particle, is expressed in the equation (2.12):[32]

$$D_H = \frac{k_B T}{3\pi\eta D} \qquad (2.12)$$

where D is the translational diffusion coefficient of the set of illuminated particles, k_B is Boltzmann's constant, T is the absolute temperature and η is the viscosity of the dispersing medium.

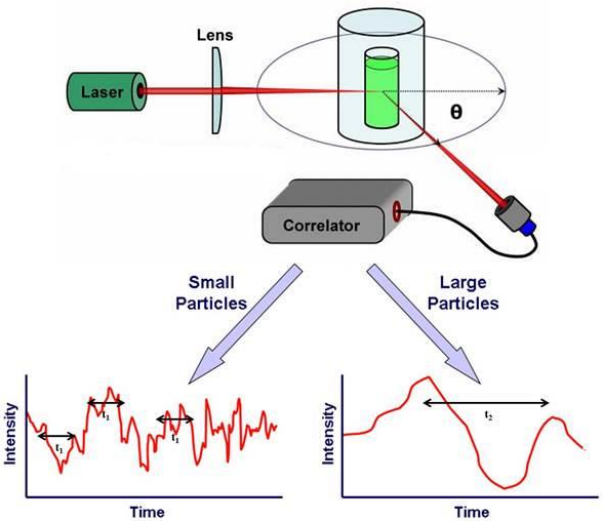

Figure 2.12 Upper panel: Scheme of DLS set-up. Lower Panels: Intensity fluctuations as a function of time. Lower Left Panel: fluctuations for small particles indicating a delay time t_1, where at a very small time, there is a strong correlation between the intensities of two signals. Lower Right Panel: fluctuations for large particles indicating a longer delay time t_2, where the correlation is reduced as a function of time.

Malvern Zetasizer Nano ZS instrument, which operates in the range from 0.3 nm to 10 μm,[33] was used to determine the hydrodynamic diameter, D_H, of nanoparticles at room temperature in water. All measurements were carried out when the light was scattered by the sample at a backscatter angle of θ= 173°.[32,33] The size distribution by intensity plot was employed in this work.

2.2.2. ATOMIC FORCE MICROSCOPY

Atomic Force Microscopy is a scanning probe technique capable of measuring nanometric surface features. It was developed by Binnig, Quale and Geber in 1986,[35] who took the design of the Scanning Tunneling Microscope (STM) and adapted it for measuring non-conductive samples. Generally, AFM works by measuring the vertical motion of a cantilever beam with ultra-small mass as it scans a surface. The cantilever has a micrometric tip attached to its end,

which is responsible for detecting the topographic morphology. The tip radii is on the order of 5 – 50 nm and the force required to move the beam is in the range between 10^{-12} to 10^{-9} N. This level of sensitivity is around the regime of interatomic forces.[36] Although the AFM was originally designed for measuring topographic images, nowadays it is possible to get information about physical properties at the nanoscale.[36] For instance, AFM-based physical techniques allow measurement of mechanical properties,[37] dielectric spectroscopy[38] and ferroelectric response[39] among others.

2.2.2.1. Amplitude Modulation Imaging

The AFM can be operated in different modes. Here we describe the amplitude modulation AFM mode,[27] which is relevant to the present work. In such mode, the cantilever is scanned through the surface as it is being vibrated at constant amplitude and at a frequency close to its resonance. In details, during an amplitude modulation imaging process, as the sample is being scanned, the AFM feedback system controls that the vibration of the cantilever occurs at a fixed amplitude value, which is kept constant as topographic features are found. In order to fulfill this requirement, a change in the vertical position of the tip with respect to the sample must occur depending on the size and shape of the surface features, and thus topography can be reconstructed (see Figure 2.13). In this thesis, two types of probes were used for the amplitude modulated experiments, setting the setpoint between 0.5 and 1 V. (i) Budget Sensors silicon AFM Probes, Tap150Al-G, with a nominal resonant frequency of 150 kHz and constant force of 5 N/m, with an aluminum reflex coating, and (ii) PPP-NLC-W probes from Nanosensors.

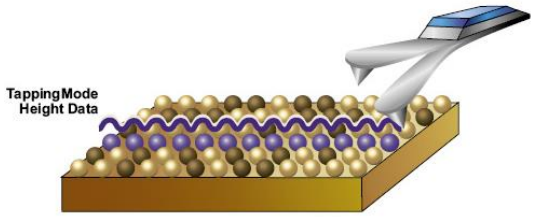

Figure 2.13 Schematic set-up of AFM Tapping Mode imaging technique.

In this thesis, AFM measurements were employed to perform topography studies on polymeric nanospheres and thin films. We have used a Multimode 8 microscope (Bruker), equipped with a Nanoscope IIIa and V controller (Bruker) in the amplitude modulation configuration (Tapping).

2.3. REFERENCES

(1) Menczel, J. D.; Prime, R. B. *Thermal Analysis of Polymers: Fundamentals and Applications*; Wiley, 2014.

(2) Gabbott, P. A Practical Introduction to Differential Scanning Calorimetry. In *Principles and Applications of Thermal Analysis*; Blackwell Publishing Ltd, 2008; pp 1–50.

(3) Azzam, R. M. A.; Bashara, N. M. *Ellipsometry and Polarized Light*; North-Holland personal library; North-Holland Pub. Co., 1977.

(4) Lai, L. H.; Allen, S. L. Mems-Based Scanning Calometer for Thermodynamic Properties of Nanostructures. *Microscale Thermophysical Engineering* **1998**, *2* (1), 11–19.

(5) Zhuravlev, E; Schick, C. Fast Scanning Power Compensated Differential Scanning Nano-Calorimeter: 1. The Device. *Thermochim. Acta* **2010**, *505* (1–2), 1–13.

(6) Zhuravlev, E.; Schick, C. Fast Scanning Power Compensated Differential Scanning Nano-Calorimeter: 2. Heat Capacity Analysis. *Thermochim. Acta* **2010**, *505* (1–2), 14–21.

(7) Mathot, V.; Pyda, M.; Pijpers, T.; Vanden Poel, G.; van de Kerkhof, E.; van Herwaarden, S.; van Herwaarden, F.; Leenaers, A. The Flash DSC 1, a Power Compensation Twin-Type, Chip-Based Fast Scanning Calorimeter (FSC): First Findings on Polymers. *Spec. Issue Interplay Nucleation Cryst. Glass Transit.* **2011**, *522* (1–2), 36–45.

(8) Schick, C. Chapter 16 - Temperature Modulated Differential Scanning Calorimetry (TMDSC) – Basics and Applications to Polymers. In *Handbook of Thermal Analysis and Calorimetry*; Stephen Z.D. Cheng, Ed.; Elsevier Science B.V., 2002; Vol. Volume 3, pp 713–810.

(9) Wunderlich, B. *Thermal Analysis of Polymeric Materials*; Springer ebook collection / Chemistry and Materials Science 2005-2008; Springer, 2005.

(10) Schawe, J. E. K.; Pogatscher, S. Part I. Material Characterization by Fast Scanning Calorimetry: Practice and Applications. In *Fast Scanning Calorimetry*; Schick, C., Mathot, V., Eds.; Springer International Publishing, 2016; pp 3–80.

(11) Minakov, A. A.; Schick, C. Ultrafast Thermal Processing and Nanocalorimetry at Heating and Cooling Rates up to 1MK⁄s. *Rev. Sci. Instrum.* **2007**, *78* (7), 073902.

(12) León-Gutierrez, E.; Garcia, G.; Lopeandía, A. F.; Fraxedas, J.; Clavaguera-Mora, M. T.; Rodríguez-Viejo, J. In Situ Nanocalorimetry of Thin Glassy Organic Films. *J. Chem. Phys.* **2008**, *129* (18), 181101.

(13) van Herwaarden, S.; Iervolino, E.; van Herwaarden, F.; Wijffels, T.; Leenaers, A.; Mathot, V. Design, Performance and Analysis of Thermal Lag of the UFS1 Twin-Calorimeter Chip for Fast Scanning Calorimetry Using the Mettler-Toledo Flash DSC 1. *Thermochim. Acta* **2011**, *522* (1), 46–52.

(14) Schawe, J. E. K. Influence of Processing Conditions on Polymer Crystallization Measured by Fast Scanning DSC. *J. Therm. Anal. Calorim.* **2014**, *116* (3), 1165–1173.

(15) Monnier, X.; Saiter, A.; Dargent, E. Vitrification of PLA by Fast Scanning Calorimetry: Towards Unique Glass above Critical Cooling Rate? *Thermochim. Acta* **2017**, *658* (Supplement C), 47–54.
(16) Tool, A. Relation between Inelastic Deformability and Thermal Expansion of Glass in Its Annealing Range. *J. Am. Ceram. Soc.* **1946**, *29* (9), 240–253.
(17) Moynihan, C. T.; Easteal, A. J.; De Bolt, M. A.; Tucker, J. Dependence of the Fictive Temperature of Glass on Cooling Rate. *J. Am. Ceram. Soc.* **1976**, *59*, 12–16.
(18) Hodge, I. M. Enthalpy Relaxation and Recovery in Amorphous Materials. *J. Non-Cryst. Solids* **1994**, *169*, 211–266.
(19) Merzlyakov, M.; Schick, C. Step Response Analysis in DSC — a Fast Way to Generate Heat Capacity Spectra. *Thermochim. Acta* **2001**, *380* (1), 5–12.
(20) Shoifet, E.; Schulz, G.; Schick, C. Temperature Modulated Differential Scanning Calorimetry – Extension to High and Low Frequencies. *Thermochimica Acta* **2015**, *603*, 227–236.
(21) Reading, M.; Hourston, D. J. *Modulated Temperature Differential Scanning Calorimetry: Theoretical and Practical Applications in Polymer Characterisation*; Springer, 2006.
(22) Weyer, S.; Merzlyakov, M.; Schick, C. Application of an Extended Tool–Narayanaswamy–Moynihan Model. *Thermochimica Acta* **2001**, *377* (1), 85–96.
(23) Stamm, M. *Polymer Surfaces and Interfaces: Characterization, Modification and Applications*; Springer ebook collection / Chemistry and Materials Science 2005-2008; Springer Berlin Heidelberg, 2008.
(24) Tompkins, H. G.; McGahan, W. A. *Spectroscopic Ellipsometry and Reflectometry: A User's Guide*; Wiley, 1999.
(25) Jenkins, F. A.; White, H. E. *Fundamentals of Optics*; International student edition; McGraw-Hill, 1976.
(26) Tompkins, H. G.; Irene, E. A. *Handbook of Ellipsometry*; Springer Berlin Heidelberg, 2005.
(27) Ellipsometry measurements https://www.jawoollam.com/resources/ellipsometry-tutorial/ellipsometry-measurements.
(28) Fukao, K.; Miyamoto, Y. Glass Transitions and Dynamics in Thin Polymer Films: Dielectric Relaxation of Thin Films of Polystyrene. *Phys. Rev. E* **2000**, *61* (2), 1743–1754.
(29) Spiece, J.; Martinez-Tong, D. E.; Sferrazza, M.; Nogales, A.; Napolitano, S. Are Polymers Glassier upon Confinement? *Soft Matter* **2015**, *11* (31), 6179–6186.
(30) Winter, W. T. Measurement of Suspended Particles by Quasi-Elastic Light Scattering, Barton E. Dahneke, Ed., Wiley, New York, 1983, 570 Pp. *J. Polym. Sci. Polym. Lett. Ed.* **1983**, *21* (12), 1020–1020.
(31) Berne, B. J.; Pecora, R. *Dynamic Light Scattering: With Applications to Chemistry, Biology, and Physics*; Dover Books on Physics Series; Dover Publications, 2000.
(32) ISO 22412:2017(En): Particle Size Analysis — Dynamic Light Scattering (DLS). February 2017.
(33) Dynamic Light Scattering: An Introduction in 30 Minutes. Malvern Instruments.

(34) Kaszuba, M.; McKnight, D.; Connah, M. T.; McNeil-Watson, F. K.; Nobbmann, U. Measuring Sub Nanometre Sizes Using Dynamic Light Scattering. *J. Nanoparticle Res.* **2008**, *10* (5), 823–829.
(35) Binnig, G.; Quate, C. F.; Gerber, C. Atomic Force Microscope. *Am. Phys. Soc.* **1986**, *56* (9), 930–933.
(36) Schönherr, H.; Vancso, G. J. *Scanning Force Microscopy of Polymers*; Springer, 2010.
(37) Dokukin, M. E.; Sokolov, I. Quantitative Mapping of the Elastic Modulus of Soft Materials with HarmoniX and PeakForce QNM AFM Modes. *Langmuir* **2012**, *28* (46), 16060–16071.
(38) Schwartz, G. A.; Riedel, C.; Arinero, R.; Tordjeman, P.; Alegría, A.; Colmenero, J. Broadband Nanodielectric Spectroscopy by Means of Amplitude Modulation Electrostatic Force Microscopy (AM-EFM). *Ultramicroscopy* **2011**, *111* (8), 1366–1369.
(39) Hu, Z.; Tian, M.; Nysten, B.; Jonas, A. M. Regular Arrays of Highly Ordered Ferroelectric Polymer Nanostructures for Non-Volatile Low-Voltage Memories. *Nat Mater* **2009**, *8* (1), 62–67.

3

VITRIFICATION AND MOLECULAR MOBILITY IN POLYSTYRENE NANOSPHERES AND IN BULK

The aim of this chapter is to address the origin of T_g suppression in confined polymer glasses. As model systems, polystyrene (PS) nanospheres were considered and their glass dynamics was investigated by means of Fast Scanning Calorimetry (FSC). The determination of the T_g was based on the concept of limiting fictive temperature (T_f) and the vitrification kinetics was taken from the total specific heat (c_p^{Tot}) step. Suppression of the T_g in comparison to bulk PS, both in terms of T_f, and temperature range of vitrification was observed. At the same time, regarding the polymer molecular mobility, in terms of relaxation time (τ), was found to be independent of the nanospheres diameter and bulk-like, in a frequency range from 1 to 150 Hz. Hence, in order to understand these results, the conceptual difference between vitrification kinetics and molecular mobility is highlighted.

3.1. INTRODUCTION

The study of confined amorphous polymers, that is, those with a reduced length scale in one or more dimensions, has become increasingly important as these systems enable numerous technologies were the miniaturization is required.[1–4] However, as mentioned in Chapter 1, if the physical properties of these systems change due to confinement, it is essential to understand such effects so as to assess their potential use in nanotechnology. As a matter of facts, due to the large area of the interface (*e.g.* polymer/external world

interface) to volume of polymer ratio, the properties of confined polymeric systems can dramatically deviate from those bulk counterparts.[5]

Recently, a plethora of investigations has paid attention to the study of glassy dynamics at the nanoscale. This activity has been stimulated by pioneering studies by Keddie *et al.*[6,7] in the early 90s, as introduced in Chapter 1. The main outcome of these studies was that the T_g of polystyrene (PS) thin films can deviate significantly from its bulk analogue. Inspired by those results, a huge number of experiments, in particular for the case of polymer glasses in different nanostructure configurations as thin films,[8–12] nanospheres[13–15] and nanocomposites,[16–18] where deviations in T_g have been observed, were performed.

These deviations in T_g are generally explained to be a result of interfacial interactions between the polymer and the interface,[19,20] which perturb the molecular mobility associated with the glass transition. Therefore, an important question arises from these results: do the observed changes in T_g due to confinement entail changes in molecular mobility? Though with some exceptions,[21] in bulk glass-forming systems a one-to-one relationship between T_g and molecular mobility is generally encountered,[22,23] however, it is worth recalling, as discussed in details in Chapter 1, that the two aspects of glass dynamics are conceptually different. Hence, there exists no reason why T_g and molecular mobility should be one-to-one related in any condition. In fact, several recent studies have provided strong indication for the presence of decoupling between T_g and molecular dynamics in polymer thin films,[24–26] nanospheres[15,27,28] and nanocomposites.[17,18,29–32] These studies basically showed the presence of a dominant component with bulk-like dynamics in combination with depressed T_g.

However, it has to be pointed out that the mentioned results entail measurement protocols where the non-linear perturbation, to determine the T_g, and the linear one, delivering the molecular mobility, are different. For

instance, in ref.[33] the molecular mobility is probed by applying a small perturbation of the dielectric polarization, whereas the T_g is obtained by capacitive dilatometry, which is essentially based on a (non-linear) perturbation of the density. Furthermore, the range of temperature relevant for the determination of the molecular mobility is often larger than that relevant for the T_g. Hence, it has been hypothesized that, upon temperature reduction, the molecular mobility would deviate from bulk behavior and speed up in ways consistent with the T_g reduction.[34]

On the debate regarding the origin of T_g reduction in confinement, it has been also proposed that accelerated molecular mobility at the free interface, is a key parameter.[35–38] The existence of a "fast" surface layer has been proved in several studies, ranging from photobleaching experiments[11] or embedding of gold nanospheres into a surface.[39] These experiments all point toward a "fast" surface layer with thickness of several nanometers.

To summarize, at present two main hypotheses have been formulated to explain T_g reduction in confinement. On one side, it is argued that at the nanoscale, T_g and molecular dynamics are decoupled. On the other side, the role of free surface to speed dynamics has been addressed to explain T_g suppression in confinement.[40]

Given all these premises, the main objective of this study is to unveil the origin of T_g reduction in confinement. To do so, we have employed fast scanning calorimetry (FSC) to study PS nanospheres with different diameters. As detailed in Chapter 2, such technique allows determining simultaneously and with the same perturbation (in this case that of the entropy) the T_g and the molecular mobility.

3.2. SAMPLES AND EXPERIMENTAL DETAILS

3.2.1. SAMPLES

3.2.1.1. Poly(styrene) (PS)

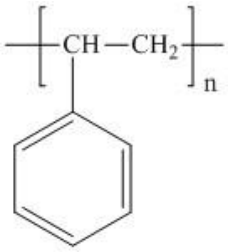

Figure 3.1 Sketch of PS repeating unit

In Figure 3.1 polystyrene (PS) repeating unit is depicted. PS is a vinyl polymer that structurally comprises a long hydrocarbon chain, with a phenyl group attached to a main chain carbon atom.[41–43] PS was purchased from Polymer Source Inc. and has the following molecular weight: M_n= 1203.6 kg/mol and M_w/M_n = 1.17. As a standard procedure before sample preparation, PS was dissolved in THF and re-precipitated in order to remove any impurity of the original material. The calorimetric T_g of the investigated PS on cooling at 10 K/min was 373 K.

3.2.1.2. Production of Polymer Nanospheres

In this section we will present how to prepare three dimensional confined polymer objects through the nanoprecipitation technique.[44–47]

PS nanoparticles were prepared following the conditions developed by Zhang *et al.*,[48] in which nanoparticles were precipitated from polymer chains in solution.[44] This rapid solvent mixing technique was denoted as Flash nanoprecipitation (FNP).[49] In our case PS was dissolved in THF and the solution was filtered with a syringe filter (pore diameter about 0.2 μm) to avoid the presence of any macroscopic polymer aggregate or dust, which

might lead to a macroscopic precipitation of the solution. Thereafter, as schematically is shown in Figure 3.2, two streams were prepared: stream 1, was a syringe containing 3 mL of PS dissolved in THF at different concentrations and stream 2 was another syringe containing 3 mL of pure water (MilliQ H_2O). Subsequently, both fluids were pressed manually from syringes at the same time, causing the two streams to merge into a mixing reservoir. Finally, the merged streams were dispersed into a 27 mL MilliQ H_2O reservoir to favor the quenching of the precipitated nanoparticles.[48]

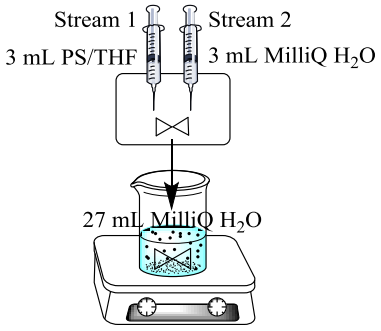

Figure 3.2 Schematic representation of the flash nanoprecipitation set-up to generate PS nanoparticles.

Afterwards, THF was evaporated from the precipitated reservoir over the course of 48 hours at room temperature in a fume hood.[48] Considering the large differences in both solvents boiling points, the evaporation of the THF will take place first compared to the water one. Table 3.1 shows the physical properties of water and THF.

Table 3.1 Physical properties of the studied solvents.[50]

Component	*Boiling Point, b.p.(ºC)*	*Density, ρ, 21 ºC (g/mL)*	*Vapor Pressure, 21 ºC (mmHg)*
Water	100	1	19
THF	66	0.889	133

We finally isolated the remaining solution of PS nanospheres/water by drying several drops in a fume hood at room temperature for 24 h. The residual water was subsequently removed under vacuum at room temperature for 24 h.

3.2.1.3. Preparation of Nanospheres for FSC experiments

For FSC measurements samples are usually placed directly on the sensor membrane and heated before the actual measurement, in order to optimize the contact between sensor and sample.[51] However, in some cases, media like oils are needed on the surface of the sensor to reduce mechanical stresses generated due to differences in the thermal expansion of the membrane and the sample.[51]

In order to place the nanospheres powder on the chip membrane and to ensure the good thermal contact, we placed a film of silicon oil between the sensor membrane and the sample. In particular, we used PDMS, purchased from Polymer Source Inc. with a low molecular weight of M_n= 800 g/mol. This polymer is completely incompatible with PS.[52] A layer of PDMS was deposited on the chip from a solution of diethyl-ether. We placed the nanospheres powder on the backside of the chip sample's membrane, where a drop of PDMS/diethyl-ether solution at 0.01% (w/w) concentration was previously deposited. This provides a thickness of PDMS of several tens nanometers. Immediately after, all the prepared chip samples were placed inside the vacuum oven at 343 K for 12 h, in order to remove any trace of solvent and to ensure the good deposition of the nanospheres on the sensor membrane.

3.2.2. DETERMINATION OF T_f AND STEP RESPONSE ANALYSIS

With regard to obtaining information on the temperature of vitrification, the determination of the fictive temperature (T_f) was employed as a metric. Its definition and the way it is obtained have been explained in detail in Chapters 1 and 2. In Figure 3.3, the used thermal protocol for the determination of T_f by Flash DSC 1 is depicted. Samples were first heated up to 473 K. Then an isothermal step of 0.1 s and a cooling ramp of 1000 K/s was applied to reach 433 K. Such fast cooling step is performed to avoid the interparticles coalescence at high temperatures when very low cooling rates are applied.[53] Samples were subsequently cooled down from 433 K at rates ranging from 0.1 to 1000 K/s until 183 K and immediately heated up to 473 K at 1000 K/s. During this heating ramp, heat flow scans were recorded and analyzed to obtain T_f according to the description developed in Chapter 2.

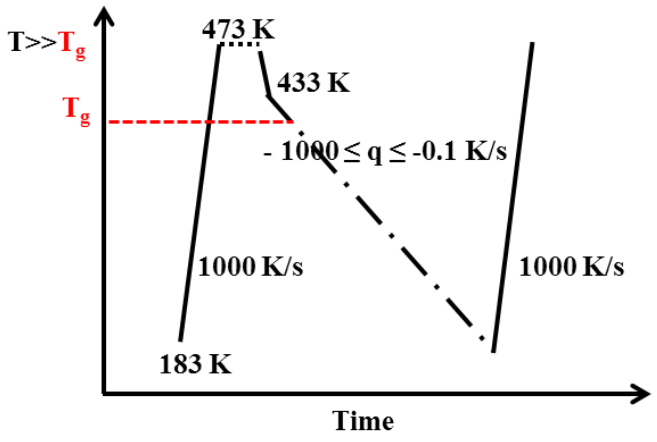

Figure 3.3 Schematization of the thermal protocol applied to PS nanospheres for the determination of T_f by Flash DSC 1.

To estimate the specific heat (c_p), the sample mass was first determined by exploiting the heat flow rate jump (ΔHF) in the range of temperature of the glass transition, as explained in detail in Chapter 2, section 2.1.1.2. The step

response analysis allows accessing the complex specific heat capacity (c_p^*) by Fourier transformation of the instantaneous heat flow and cooling rate after a temperature jump of 2 K. Such protocol also delivers the total specific heat (c_p^{Tot}), as the ratio of the average heat flow rate and the underlying cooling rate. Details regarding the step response analysis are provided in Chapter 2, section 2.1.1.3. The one and two steps protocols were found to deliver identical information regarding both linear dynamics and kinetics of vitrification.

3.3. RESULTS AND DISCUSSION

In this section we will first present the characterization of the PS nanospheres diameter. Subsequently, FSC results, in terms of glass transition and molecular mobility, on PS bulk and nanospheres with different diameters will be presented.

3.3.1. SAMPLES MORPHOLOGY

We characterized the size and shape of nanoparticles dispersion by dynamic light scattering (DLS) and atomic force microscopy (AFM). Figure 3.4 displays the DLS correlation curves and the intensity distributions of the mean diameter size of nanoparticles, obtained over the course of THF evaporation time for three different PS concentrations. A stable dispersion of surfactant-free polymer nanoparticles in water was obtained.

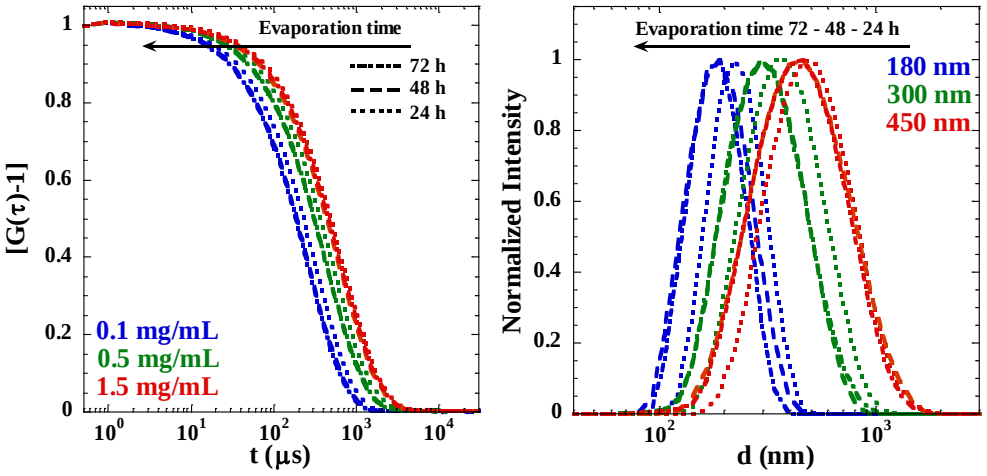

Figure 3.4 Left Panel: Normalized correlation function G(τ)-1 as a function of time for concentrations of 0.1-0.5-1.5 mg/mL PS/THF in Stream 1. Right Panel: Normalized intensity size distribution curves. Dotted lines, 24 h; dashed lines, 48 h; and dashed-dotted lines, 72 h of evaporation. Experiments were carried out at a scattering angle of 173º and a temperature of 298 K.

The precipitated PS nanoparticles suspended in an aqueous solution were collected in scintillation vials. THF was subsequently removed through air evaporation in the fume hood over the course of time. Following the protocol of ref.,[48] the air evaporation was stopped after 48 h. No size distribution differences were observed leaving the suspension in air for longer times, as shown in Figure 3.4. The values depicted in the right panel of Figure 3.4, 180 – 300 – 450 nm, are the hydrodynamic diameters (D_H) of the particles according to the maximum scattering intensity distribution of particles in water.

AFM images were obtained by depositing a drop of 10 μL of PS nanoparticles final dispersion in water onto silicon oxide wafers (SiO_x). Prior to imaging the nanoparticles topography, they were dried evaporating the drop of water at room temperature, inside a glass Petri dish covered with a lid for 12 h. All the images were taken on tapping mode with a 10 x 10 μm^2 scanning area, using

Budget Sensors silicon probes. AFM images are reported in Figure 3. **5** for all investigated systems. Observation of the AFM images indicates that spherical nanoparticles, though somewhat polydispersed particularly for the largest nanospheres, are obtained. This is evident from the discrete probability distributions of log-normal fits.

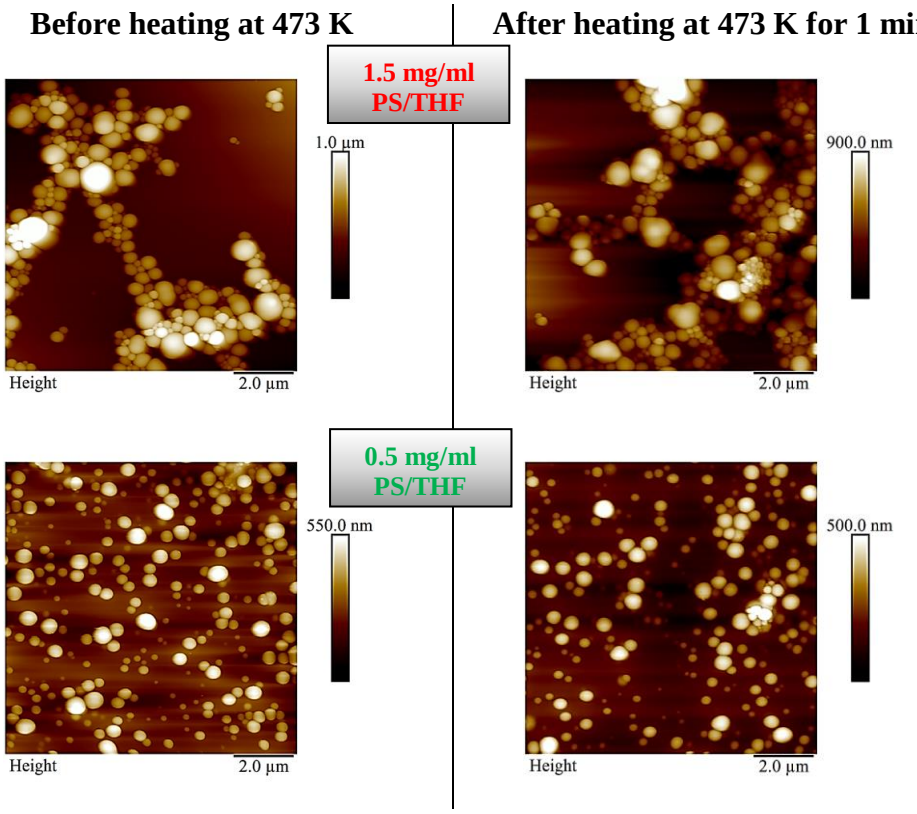

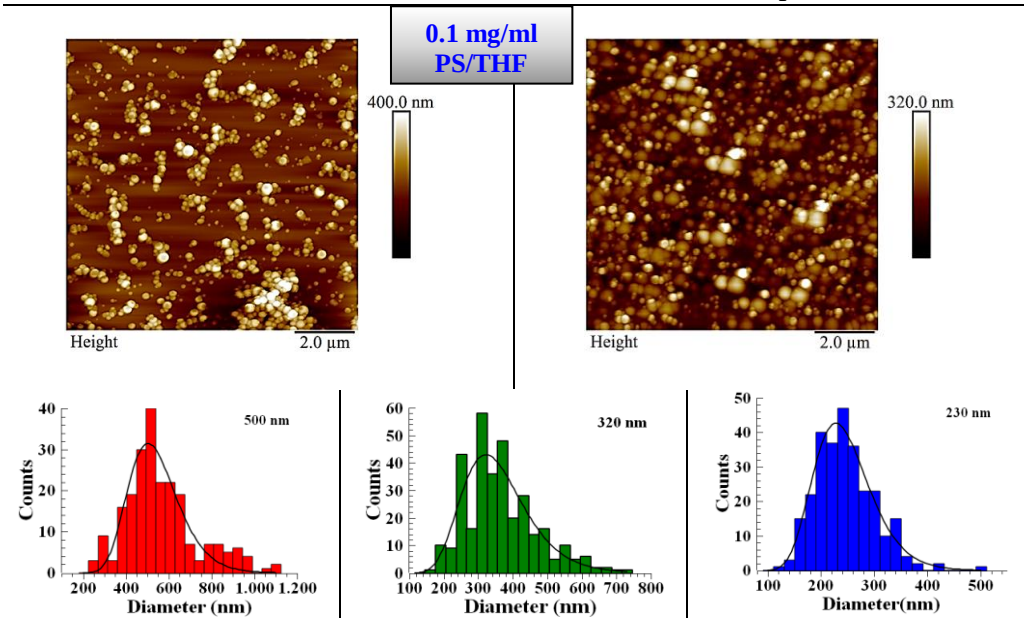

Figure 3. 5 Left Panels: AFM images PS nanospheres by the flash nanoprecipitation method[48] before heating at 473 K. Right Panels: PS nanospheres after heating at 473 K for 1 min in a vacuum oven. Histograms represent the size distribution plots. Black solid lines are log-normal fits and the reported values of the diameter correspond to the maximum of the distribution.

Figure 3. **5** indicates that the nanoparticles diameter increases with the solution concentration. From the size distribution histograms, the following nanospheres diameters depending on the initial concentration of the PS/THF solution, were obtained: 500, 320 and 230 nm. Most importantly, the images showed that the nanoparticles were neither destroyed, nor aggregated after heating the samples at 473 K for 1 min in a vacuum oven. This time is by far larger than that spent at such temperature in FSC experiments, that is, 0.1 s at 473 K.

Regarding the Flash DSC 1 measurements, a little piece of PS bulk sample was deposited on the top of the sensor membrane and subsequently submitted to a pre-melt scan at low heating rate (1 K/s) up to 473 K, in order to ensure

the thermal contact between the sensor and the samples. In the case of PS nanospheres, the isolated powder was deposited on the backside of the membrane on top of a PDMS layer.

The sample masses were calculated according to the procedure described in Chapter 2, section 2.1.1.2. All the samples were in a range of 100 – 500 ng (see Table A.1 and Figure A.1).

3.3.2. VITRIFICATION KINETICS AND MOLECULAR MOBILITY

In this section we report results on enthalpy state achieved by PS nanospheres vitrified in a cooling range of 0.1 – 1000 K/s. To do so, we determine the T_g using the concept of limiting fictive temperature T_f.[54] Apart from the T_f, we also show results on the vitrification kinetics in terms of the step of c_p^{Tot}. As introduced in Chapter 2 section 2.1.1.3, the latter is obtained from step response experiments, which also allows accessing the complex specific heat capacity (c_p^*). The c_p^* is exploited to determine the relaxation time (τ) corresponding to a frequency range from 1 to 150 Hz.

3.3.2.1. Cooling rate dependent glass transition

Figure 3.6 shows the specific heat capacity scans obtained for PS nanospheres with different diameters on heating at 1000 K/s and after cooling at the indicated rates.

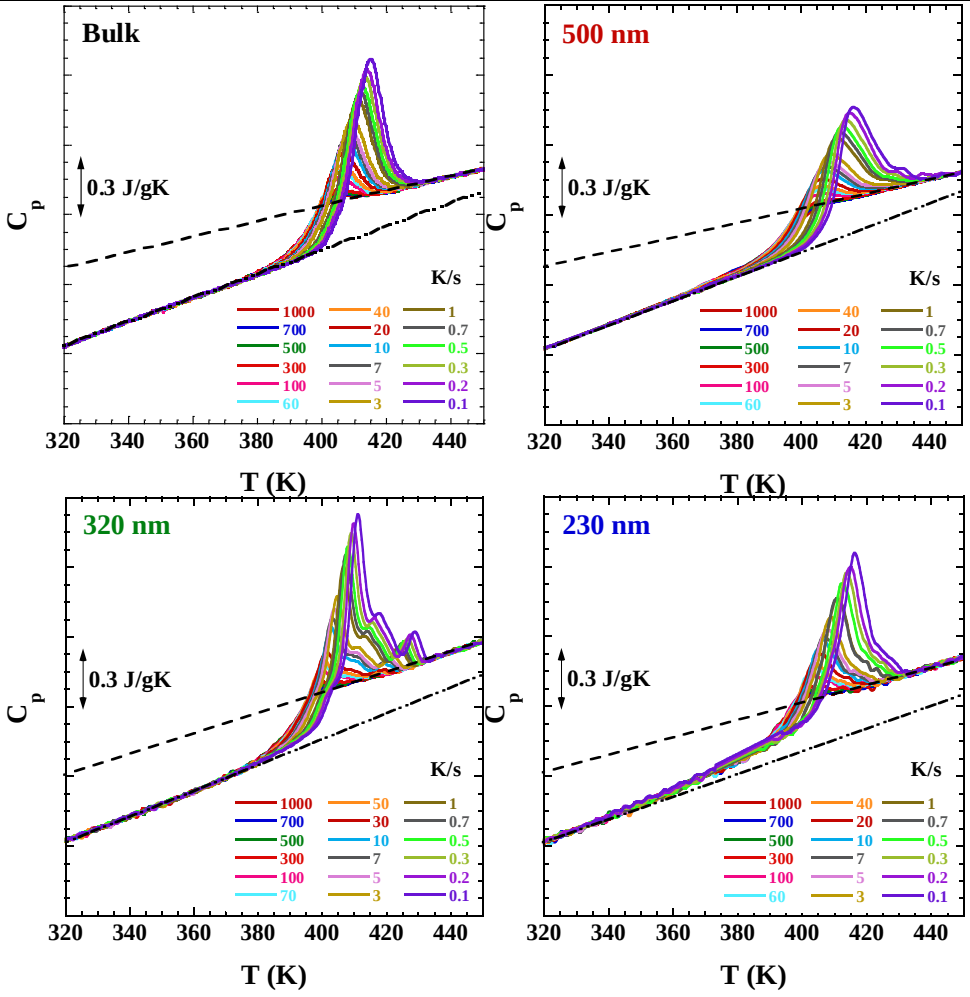

Figure 3.6 Specific heat capacity vs temperature plots on heating at 1000 K/s after cooling at the indicated rates. Dashed lines represent the specific heat of the melt (c_{pm}) and dashed dotted lines the specific heat of the glass (c_{pg}).

All curves exhibit the common feature of a main endothermic overshoot increasing in magnitude with decreasing the cooling rate.[a]

From the observation of Figure 3.6, the following qualitative differences can be highlighted: (i) the onset of devitrification progressively shifts toward lower temperatures with decreasing diameter; (ii) such shift is especially evident for nanospheres with 230 nm diameter, which at 340 K, exhibit an excess of specific heat well below the location of the main overshoot. This suggests that devitrification in the smallest nanospheres begins via a fast mechanism of equilibration before the standard mechanism responsible for the main endothermic overshoot takes over. This result is consistent with the finding of a two-step recovery of equilibrium in both bulk polymers,[56] thin PS films,[57,58] and other glasses.[59–63]

[a] It is worth pointing out that the specific heat scans of nanospheres with 320 nm diameter exhibit additional secondary overshoots at higher temperatures. Such profile has been observed as well by others, and its origin is at present unknown,[55] however, as noticed in the investigations performed by Gao *et al.*[55] the effect on T_f of considering these peaks is of the order of 1 K.

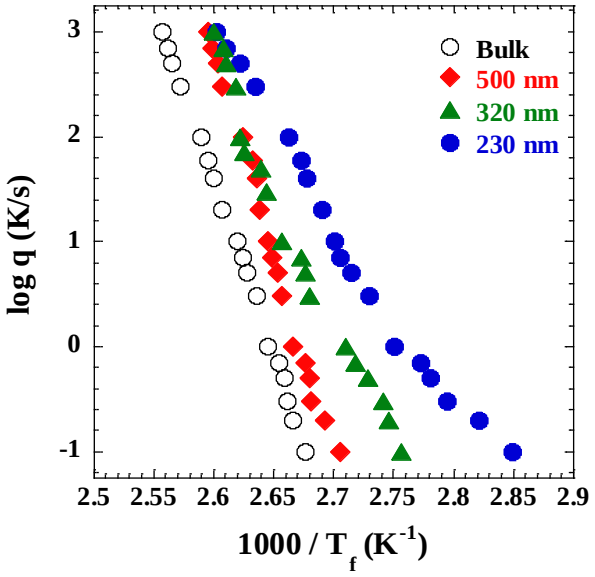

Figure 3.7 Cooling rate dependence of T_f for all investigated systems. Error bars in T_f are smaller than ± 1 K.

In Figure 3.7 the cooling rate dependence of T_f is presented. This figure shows that T_f exhibits negative deviations from bulk behavior and decreases with the nanospheres diameter. Such dependence becomes more marked with decreasing the cooling rate. This result is consistent with those obtained in thin PS films by FSC.[5,55] Furthermore, T_f values obtained on cooling at 0.1 K/s match with those obtained on PS nanospheres at a similar cooling rate by standard calorimetry in water[13] and by capacitive dilatometry in nanospheres exposed to air.[15] This means that T_g suppression is independent of whether PS nanospheres are surrounded by air, water, or PDMS thin layer as in our case.

Summarizing, our results show negative deviations of the T_f from bulk behavior and these are more pronounced for nanospheres with smaller diameter and at lower cooling rates in agreement with previous results.[34,64,65]

3.3.2.2. Step response analysis

The upper panel of Figure 3. **8** shows the temperature dependence of the normalized total specific heat capacity ($c_{\mathrm{p\,Norm}}^{\mathrm{Tot}}$). This was obtained on cooling at 20 K/s from the step-response methods, as the ratio of the baseline corrected total heat flow rate and the underlying cooling rate, see equation (2.5) in Chapter 2, section 2.1.1.3. The normalized $c_{\mathrm{p}}^{\mathrm{Tot}}$ varying between 0 and 1, was obtained through the following equation:

$$c_{\mathrm{p\,Norm}}^{\mathrm{Tot}} = \frac{\left(c_{\mathrm{p}}^{\mathrm{Tot}} - c_{\mathrm{pg}}^{\mathrm{Tot}}\right)}{\left(c_{\mathrm{pm}}^{\mathrm{Tot}} - c_{\mathrm{pg}}^{\mathrm{Tot}}\right)} \qquad (3.\ 1)$$

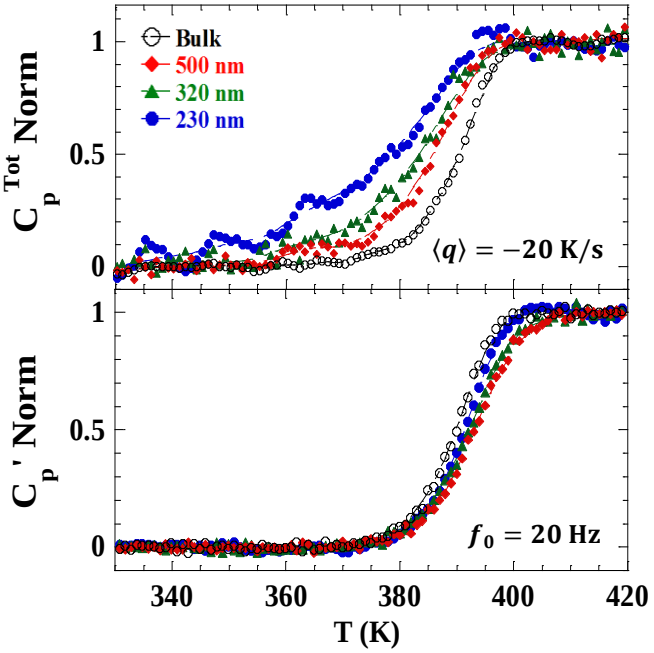

Figure 3. 8 Normalized total specific heat capacity (upper panel) and real part of the complex specific heat capacity (lower panel) at a frequency of 20 Hz as a function of temperature. Both results are obtained in the same experiment based on step-response protocol.

The $c_{\mathrm{p}}^{\mathrm{Tot}}$ consists of both linear (reversible) and non-linear (irreversible) contributions to the specific heat of the system and, thereby, provides information on how vitrification takes place. Observation of the upper panel of Figure 3. **8** indicates that decreasing the nanospheres diameter, results in a progressive lowering of the temperature range at which vitrification occurs. In other words, these results indicate a decrease of T_{g} with the nanosphere diameter. This result is generally consistent with that showing T_{f} depression with decreasing the nanospheres diameter. Furthermore, nanospheres exhibit a broadening of the vitrification range with the reduction of the diameter, in comparison to bulk PS. In the most extreme case, that is, for 230 nm diameter nanospheres, vitrification takes place in a temperature range of approximately 40 – 45 K. Altogether, these results indicate that PS nanospheres are able to maintain equilibrium at temperatures lower than bulk PS.

The step response analysis allows determining the c_{p}^{*}. This is done from the Fourier transformation of the heat flow and cooling rate after a temperature jump of 2 K and an isotherm of variable duration,[66,67] which has been explained in details in Chapter 2. The 2 K jump ensures linearity of the response, as temperature fluctuations of supercooled liquids in the glass transition region are generally larger than such value.[68,69] Figure 3. **8** (lower panel) and Figure 3.9 show the normalized real part of the complex specific heat $c'_{\mathrm{p\,Norm}}$, calculated in the same way as the normalization of the total specific heat, see equation (3. 1), as a function of temperature at a frequency of 20 Hz; and 10 and 60 Hz, respectively. The former frequency corresponds to a time scale comparable to the cooling rate employed to determine the $c_{\mathrm{p}}^{\mathrm{Tot}}$ of the upper panel in Figure 3. **8** (20 K/s). Given the linearity of the response, $c'_{\mathrm{p}}(T)$ contains information on the molecular mobility of the system.[70] Within the experimental error, as can be appreciated in the lower panel of Figure 3. **8** and Figure 3.9, all $c'_{\mathrm{p}}(T)$ curves collapse on each other, indicating that the linear responses of PS nanospheres and bulk PS are identical.

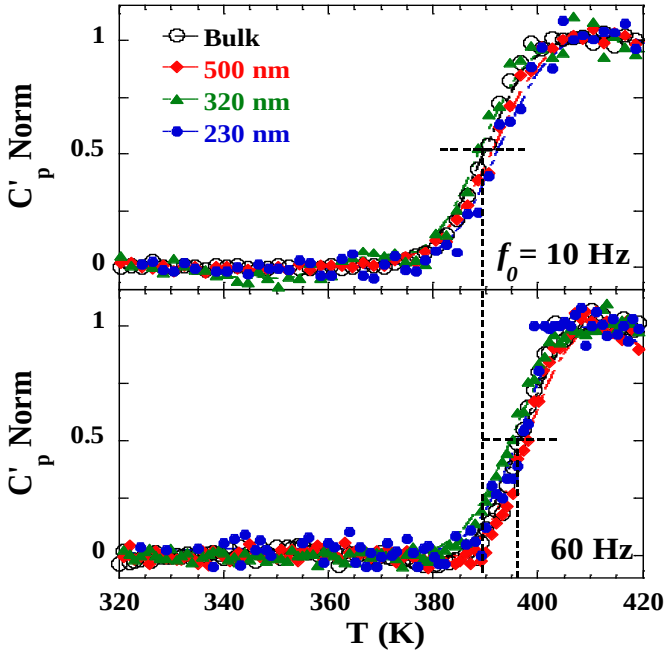

Figure 3.9 Normalized real part of the complex specific heat capacity obtained at frequency of 10 Hz (upper panel); and 60 Hz (lower panel). Dashed lines are guide lines to indicate the midpoint of the step of $c'_{\mathrm{p\,Norm}}$.

The molecular mobility for all investigated systems is summarized in Figure 3.10, where plots of the reciprocal of $\tau = 1/(2\pi f)$ as a function of the inverse of the temperature are shown. Such plot was built considering the midpoint of the step of the real part of the specific heat, as depicted in Figure 3.9. Figure 3.10 indicates that the invariance of the molecular mobility is verified in the whole investigated temperature range. Furthermore, it shows that our data generally agree with those previously reported by dielectric relaxation and heat capacity spectroscopy on both bulk PS and thin films in different configurations.[33,71,72]

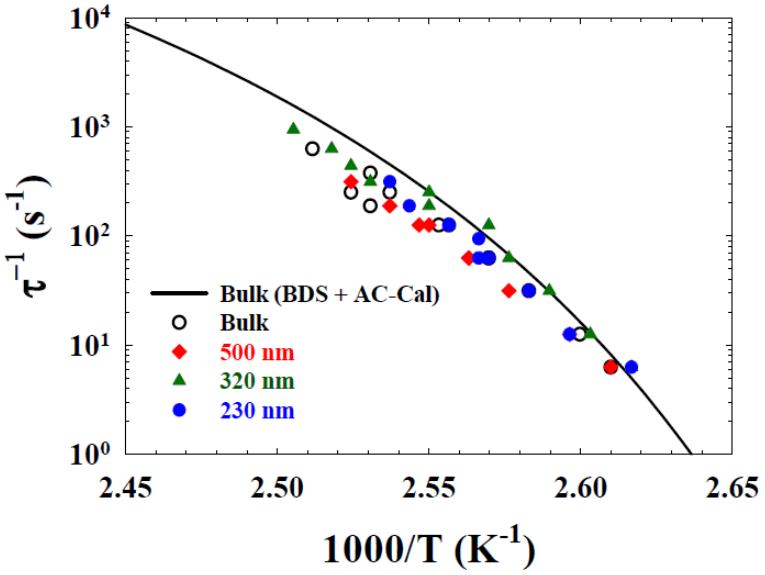

Figure 3.10 Reciprocal of the relaxation time as a function of the inverse temperature, obtained considering the midpoint of the step of the real part of the specific heat. The black solid line is built from data obtained by BDS and AC-calorimetry for bulk PS and thin films taken from ref.[32]

Summarizing, our results show that delayed vitrification on cooling from melt state in PS nanospheres is unrelated to a modification of the molecular mobility. If we compare the upper and lower panel of Figure 3. **8**, and Figure 3.6 and Figure **3.10**, an increased irreversibility of the vitrification process with confinement is shown, leading to a decoupling between molecular dynamics and glass transition. It is important to remark that this finding was achieved on samples prepared in identical conditions and in the case of Figure 3. **8**, in the same experiment. In this case, the step-response protocols allow accessing simultaneously the complex specific heat resulting from a linear perturbation, and the total specific heat, originating from a non-linear perturbation, that is, the underlying cooling ramp. Hence, the non-linear response contains contributions to the specific heat related to the irreversibility of the vitrification process.[70,73]

Apart from clarifying the non-relaxational origin of T_g suppression in confinement, our results imply that vitrification in PS nanospheres exhibit pronounced irreversibility. This is evident from the difference between $c_{p\,Norm}^{Tot}(T)$ and $c'_{p\,Norm}(T)$ displayed in Figure 3. **8**, where in bulk PS such difference is smaller implying that vitrification occurs in a sharper range. On the contrary, for the smaller nanospheres of 230 nm diameter, the transformation from supercooled liquid to glassy state covers a broad temperature range, extending well below the temperature at which $c'_{p\,Norm} = 0$.

Finally, it is worth pointing out that $c'_{p\,Norm}$ plots shown in the lower panel of Figure 3. **8** and Figure 3.9 provide no indication of the presence of a layer with enhanced mobility in proximity of the interface. However, according to the work performed by Paeng and co-workers,[10,74] the thickness of such layer was estimated to be of the order of a few nanometers. This means that for nanospheres with the lowest investigated diameter (230 nm), such layer would correspond to a portion of material too small to be detectable by our step-response analysis method. For instance, specific heat spectroscopy provides evidence for a fast component of molecular mobility for PS films with thickness smaller than 20 – 30 nm,[36] that is, at conditions of nanoscale confinement considerably more extreme than those of the present study. Despite the fact that our results do not supply any indication against the presence of that layer, they certainly provide compelling evidence that factors beyond the role of such interfacial layer must be taken into account, in order to explain T_g suppression at the nanoscale confinement.

3.4. CHAPTER SUMMARY

In this chapter, we have exploited the ability of FSC to characterize all aspects of glass dynamics. To investigate the effect of confinement, the chosen system was PS nanospheres. In the first section, we have explained how to prepare these nanospheres following the Flash nanoprecipitation technique, as well as sample preparation for the Flash DSC 1 experiments. In the second section, we

have shown how investigating glass dynamics of such nanospheres is able to provide insights on the origin of T_g suppression in polymer glasses under nanoscale confinement. In particular, we have tested whether this behavior should be attributed to (i) the presence of accelerated molecular mobility at the free interface or rather (ii) is a phenomenon that can be observed even in the presence of bulk-like molecular mobility. Our results indicate that the T_g decreases with the nanospheres diameter, whereas τ was found to be bulk-like for all investigated systems. Hence, these results provide compelling arguments, beyond what it was previously found,[14,32] in favor of the decoupling between thermal T_g and molecular mobility in glasses under nanoscale confinement.

Part of this chapter is published in *ACS Macro Lett.* **2017**; **DOI:** 10.1021/acsmacrolett.7b00484

3.5. REFERENCES

(1) Yang, X.; Loos, J.; Veenstra, S. C.; Verhees, W. J. H.; Wienk, M. M.; Kroon, J. M.; Michels, M. A. J.; Janssen, R. A. J. Nanoscale Morphology of High-Performance Polymer Solar Cells. *Nano Lett.* **2005**, *5* (4), 579–583.

(2) Noh, Y.-Y.; Zhao, N.; Caironi, M.; Sirringhaus, H. Downscaling of Self-Aligned, All-Printed Polymer Thin-Film Transistors. *Nat Nano* **2007**, *2* (12), 784–789.

(3) Cho, W. K.; Kong, B.; Choi, I. S. Highly Efficient Non-Biofouling Coating of Zwitterionic Polymers: Poly((3-(Methacryloylamino)Propyl)-Dimethyl(3-Sulfopropyl)Ammonium Hydroxide). *Langmuir* **2007**, *23* (10), 5678–5682.

(4) Yave, W.; Car, A.; Wind, J.; Peinemann, K.-V. Nanometric Thin Film Membranes Manufactured on Square Meter Scale: Ultra-Thin Films for CO2 Capture. *Nanotechnology* **2010**, *21*, 395301.

(5) Cangialosi, D.; Alegría, A.; Colmenero, J. Cooling Rate Dependent Glass Transition in Thin Polymer Films and in Bulk. In *Fast Scanning Calorimetry*; Schick, C., Mathot, V., Eds.; Springer International Publishing: Cham, 2016; pp 403–431.

(6) Keddie, J. L.; Jones, R. A. L.; Cory, R. A. Size-Dependent Depression of the Glass Transition Temperature in Polymer Films. *Europhys. Lett.* **1994**, *27*, 59–64.

(7) Keddie, J. L.; Jones, R. A. L.; Cory, R. A. Interface and Surface Effects on the Glass-Transition Temperature in Thin Polymer Films. *Faraday Discuss.* **1994**, *98* (0), 219–230.

(8) Fukao, K.; Miyamoto, Y. Glass Transitions and Dynamics in Thin Polymer Films: Dielectric Relaxation of Thin Films of Polystyrene. *Phys. Rev. E* **2000**, *61* (2), 1743–1754.

(9) Ellison, C. J.; Torkelson, J. M. The Distribution of Glass-Transition Temperatures in Nanoscopically Confined Glass Formers. *Nat. Mater.* **2003**, *2* (10), 695.

(10) Pye, J. E.; Roth, C. B. Two Simultaneous Mechanisms Causing Glass Transition Temperature Reductions in High Molecular Weight Freestanding Polymer Films as Measured by Transmission Ellipsometry. *Phys. Rev. Lett.* **2011**, *107* (23), 235701.

(11) Paeng, K.; Swallen, S. F.; Ediger, M. D. Direct Measurement of Molecular Motion in Freestanding Polystyrene Thin Films. *J. Am. Chem. Soc.* **2011**, *133* (22), 8444–8447.

(12) Kim, S.; Torkelson, J. M. Distribution of Glass Transition Temperatures in Free-Standing, Nanoconfined Polystyrene Films: A Test of de Gennes' Sliding Motion Mechanism. *Macromolecules* **2011**, *44* (11), 4546–4553.

(13) Zhang, C.; Guo, Y.; Priestley, R. D. Glass Transition Temperature of Polymer Nanoparticles under Soft and Hard Confinement. *Macromolecules* **2011**, *44*, 4001–4006.

(14) Zhang, C.; Guo, Y.; Shepard, K. B.; Priestley, R. D. Fragility of an Isochorically Confined Polymer Glass. *J. Phys. Chem. Lett.* **2013**, *4* (3), 431–436.

(15) Zhang, C.; Boucher, V. M.; Cangialosi, D.; Priestley, R. D. Mobility and Glass Transition Temperature of Polymer Nanospheres. *Polymer* **2013**, *54* (1), 230–235.

(16) Amanuel, S.; Gaudette, A. N.; Sternstein, S. S. Enthalpic Relaxation of Silica–polyvinyl Acetate Nanocomposites. *J. Polym. Sci. Part B Polym. Phys.* **2008**, *46* (24), 2733–2740.

(17) Boucher, V. M.; Cangialosi, D.; Alegría, A.; Colmenero, J. Enthalpy Recovery of PMMA/Silica Nanocomposites. *Macromolecules* **2010**, *43* (18), 7594–7603.
(18) Boucher, V. M.; Cangialosi, D.; Alegría, A.; Colmenero, J.; Pastoriza-Santos, I.; Liz-Marzan, L. M. Physical Aging of Polystyrene/Gold Nanocomposites and Its Relation to the Calorimetric Tg Depression. *Soft Matter* **2011**, *7* (7), 3607–3620.
(19) Park, C. H.; Kim, J. H.; Ree, M.; Sohn, B.-H.; Jung, J. C.; Zin, W.-C. Thickness and Composition Dependence of the Glass Transition Temperature in Thin Random Copolymer Films. *Polymer* **2004**, *45* (13), 4507–4513.
(20) Priestley, R. D.; Mundra, M. K.; Barnett, N. J.; Broadbelt, L. J.; Torkelson, J. M. Effects of Nanoscale Confinement and Interfaces on the Glass Transition Temperatures of a Series of Poly(n-Methacrylate)Films. *Aust. J. Chem.* **2007**, *60* (10), 765–771.
(21) Robertson, C. .; Santangelo, P. .; Roland, C. . Comparison of Glass Formation Kinetics and Segmental Relaxation in Polymers. *J. Non-Cryst. Solids* **2000**, *275* (3), 153–159.
(22) Wang, L.-M.; Velikov, V.; Angell, C. A. Direct Determination of Kinetic Fragility Indices of Glassforming Liquids by Differential Scanning Calorimetry: Kinetic versus Thermodynamic Fragilities. *J. Chem. Phys.* **2002**, *117* (22), 10184–10192.
(23) Schawe, J. E. K. Vitrification in a Wide Cooling Rate Range: The Relations between Cooling Rate, Relaxation Time, Transition Width, and Fragility. *J. Chem. Phys.* **2014**, *141* (18), 184905.
(24) Kremer, F.; Tress, M.; Mapesa, E. U. Glassy Dynamics and Glass Transition in Nanometric Layers and Films: A Silver Lining on the Horizon. *J. Non-Cryst. Solids* **2015**, *407*, 277–283.
(25) Napolitano, S.; Glynos, E.; Tito, N. B. Glass Transition of Polymers in Bulk, Confined Geometries, and near Interfaces. *Rep. Prog. Phys.* **2017**, *80* (3), 036602.
(26) Chowdhury, M.; Priestley, R. D. Discrete Mobility on the Surface of Glasses. *Proc. Natl. Acad. Sci.* **2017**, *114* (19), 4854–4856.
(27) Priestley, R. D.; Cangialosi, D.; Napolitano, S. On the Equivalence between the Thermodynamic and Dynamic Measurements of the Glass Transition in Confined Polymers. *J. Non-Cryst. Solids* **2015**, *407*, 288–295.
(28) Cangialosi, D.; Alegría, A.; Colmenero, J. Effect of Nanostructure on the Thermal Glass Transition and Physical Aging in Polymer Materials. *Prog. Polym. Sci.* **2016**, *54–55* (Supplement C), 128–147.
(29) Boucher, V. M.; Cangialosi, D.; Alegría, A.; Colmenero, J.; González-Irun, J.; Liz-Marzan, L. M. Accelerated Physical Aging in PMMA/Silica Nanocomposites. *Soft Matter* **2010**, *6* (14), 3306–3317.
(30) Boucher, V. M.; Cangialosi, D.; Alegrìa, A.; Colmenero, J.; González-Irun, J.; Liz-Marzan, L. M. Physical Aging in PMMA/Silica Nanocomposites: Enthalpy and Dielectric Relaxation. *J. Non-Cryst. Solids* **2011**, *357* (2), 605–609.
(31) Cangialosi, D.; Boucher, V. M.; Alegría, A.; Colmenero, J. Enhanced Physical Aging of Polymer Nanocomposites: The Key Role of the Area to Volume Ratio. *Polymer* **2012**, *53* (6), 1362–1372.
(32) Ramakrishnan, V.; Harsiny, S.; Goossens, J. G. P.; Hoeks, T. L.; Peters, G. W. M. Physical Aging in Polycarbonate Nanocomposites Containing Grafted Nanosilica

Particles: A Comparison between Enthalpy and Yield Stress Evolution. *J. Polym. Sci. Part B: Polym. Phys.* **2016**, *54* (20), 2069–2081.
(33) Boucher, V. M.; Cangialosi, D.; Yin, H.; Schönhals, A.; Alegría, A.; Colmenero, J. T g Depression and Invariant Segmental Dynamics in Polystyrene Thin Films. *Soft Matter* **2012**, *8* (19), 5119–5122.
(34) Glor, E. C.; Fakhraai, Z. Facilitation of Interfacial Dynamics in Entangled Polymer Films. *J. Chem. Phys.* **2014**, *141* (19), 194505.
(35) Fakhraai, Z.; Forrest, J. A. Measuring the Surface Dynamics of Glassy Polymers. *Science* **2008**, *319*, 600–604.
(36) Yin, H.; Madkour, S.; Schönhals, A. Unambiguous Evidence for a Highly Mobile Surface Layer in Ultrathin Polymer Films by Specific Heat Spectroscopy on Blends. *Macromolecules* **2015**, *48* (14), 4936–4941.
(37) Madkour, S.; Yin, H.; Füllbrandt, M.; Schönhals, A. Calorimetric Evidence for a Mobile Surface Layer in Ultrathin Polymeric Films: Poly(2-Vinyl Pyridine). *Soft Matter* **2015**, *11* (40), 7942–7952.
(38) Zhang, Y.; Fakhraai, Z. Decoupling of Surface Diffusion and Relaxation Dynamics of Molecular Glasses. *Proc. Natl. Acad. Sci. U. S. A.* **2017**, *114* (19), 4915–4919.
(39) Qi, D.; Daley, C. R.; Chai, Y.; Forrest, J. A. Molecular Weight Dependence of near Surface Dynamical Mechanical Properties of Polymers. *Soft Matter* **2013**, *9* (37), 8958–8964.
(40) Ediger, M. D.; Forrest, J. A. Dynamics near Free Surfaces and the Glass Transition in Thin Polymer Films: A View to the Future. *Macromolecules* **2014**, *47*, 471–478.
(41) Wypych, G. *Handbook of Polymers*; Elsevier Science, 2016.
(42) Barón, M.; Hellwich, K.-H.; Hess, M.; Horie, K.; Jenkins, A. D.; Jones, R. G.; Kahovec, J.; Kratochvíl, P.; Metanomski, W. V.; Mormann, W.; et al. Glossary of Class Names of Polymers Based on Chemical Structure and Molecular Architecture (IUPAC Recommendations 2009). *Pure Appl. Chem.* **2009**, *81* (6), 1131–1186.
(43) Mark, J. E. *Polymer Data Handbook*; Oxford University Press, 1999.
(44) Fessi, H.; Puisieux, F.; Devissaguet, J. P.; Ammoury, N.; Benita, S. Nanocapsule Formation by Interfacial Polymer Deposition Following Solvent Displacement. *Int. J. Pharm.* **1989**, *55* (1), R1–R4.
(45) Horn, D.; Rieger, J. Organic Nanoparticles in the Aqueous Phase—Theory, Experiment, and Use. *Angew. Chem. Int. Ed.* **2001**, *40* (23), 4330–4361.
(46) Aubry, J.; Ganachaud, F.; Cohen Addad, J.-P.; Cabane, B. Nanoprecipitation of Polymethylmethacrylate by Solvent Shifting:1. Boundaries. *Langmuir* **2009**, *25* (4), 1970–1979.
(47) Cheng, J. C.; Vigil, R. D.; Fox, R. O. A Competitive Aggregation Model for Flash NanoPrecipitation. *J. Colloid Interface Sci.* **2010**, *351* (2), 330–342.
(48) Zhang, C.; Pansare, V. J.; Prud'homme, R. K.; Priestley, R. D. Flash Nanoprecipitation of Polystyrene Nanoparticles. *Soft Matter* **2011**, *8* (1), 86–93.
(49) Johnson, B. K.; Prud'homme, R. K. Chemical Processing and Micromixing in Confined Impinging Jets. *AIChE J.* **2003**, *49* (9), 2264–2282.
(50) Smallwood, I. *Handbook of Organic Solvent Properties*; Elsevier Science, 2012.

(51) Schawe, J. E. K.; Pogatscher, S. Part I. Material Characterization by Fast Scanning Calorimetry: Practice and Applications. In *Fast Scanning Calorimetry*; Schick, C., Mathot, V., Eds.; Springer International Publishing, 2016; pp 3–80.
(52) Coppée, S.; Gabriele, S.; Jonas, A. M.; Jestin, J.; Damman, P. Influence of Chain Interdiffusion between Immiscible Polymers on Dewetting Dynamics. *Soft Matter* **2011**, *7* (21), 9951–9955.
(53) Whitlow, S. J.; Wool, R. P. Diffusion of Polymers at Interfaces: A Secondary Ion Mass Spectroscopy Study. *Macromolecules* **1991**, *24* (22), 5926–5938.
(54) Tool, A. Relation between Inelastic Deformability and Thermal Expansion of Glass in Its Annealing Range. *J. Am. Ceram. Soc.* **1946**, *29* (9), 240–253.
(55) Gao, S.; Koh, Y. P.; Simon, S. L. Calorimetric Glass Transition of Single Polystyrene Ultrathin Films. *Macromolecules* **2013**, *46* (2), 562–570.
(56) Daniele Cangialosi, V. M. B.; Angel Alegría, J. C. Direct Evidence of Two Equilibration Mechanisms in Glassy Polymers. *Phys. Rev. Lett.* **2013**, *111*, 095701.
(57) Boucher, V. M.; Cangialosi, D.; Alegria, A.; Colmenero, J. Reaching the Ideal Glass Transition by Aging Polymer Films. *Phys. Chem. Chem. Phys.* **2017**, *19* (2), 961–965.
(58) Boucher, V. M.; Cangialosi, D.; Alegría, A.; Colmenero, J. Complex Nonequilibrium Dynamics of Stacked Polystyrene Films Deep in the Glassy State. *J. Chem. Phys.* **2017**, *146* (20), 203312.
(59) Miller, R. S.; MacPhail, R. A. Ultraslow Nonequilibrium Dynamics in Supercooled Glycerol by Stimulated Brillouin Gain Spectroscopy. *J. Chem. Phys.* **1997**, *106* (8), 3393–3401.
(60) Louzguine-Luzgin, D. V.; Seki, I.; Yamamoto, T.; Kawaji, H.; Suryanarayana, C.; Inoue, A. Double-Stage Glass Transition in a Metallic Glass. *Phys. Rev. B* **2010**, *81* (14), 144202.
(61) Golovchak, R.; Kozdras, A.; Balitska, V.; Shpotyuk, O. Step-Wise Kinetics of Natural Physical Ageing in Arsenic Selenide Glasses. *J. Phys.: Condens. Matter* **2012**, *24*, 505106.
(62) Wang, C.; Hu, L.; Wei, C.; Tong, X.; Zhou, C.; Sun, Q.; Hui, X.; Yue, Y. Sub-Tg Relaxation Patterns in Cu-Based Metallic Glasses Far from Equilibrium. *J. Chem. Phys.* **2014**, *141* (16), 164507.
(63) Gallino, I.; Cangialosi, D.; Evenson, Z.; Schmitt, L.; Hechler, S.; Stolpe, M.; Ruta, B. Hierarchical Aging Pathways and Reversible Fragile-to-Strong Transition upon Annealing of a Metallic Glass Former. *Acta Mater.* **2018**, *144* (Supplement C), 400–410.
(64) Boucher, V. M.; Cangialosi, D.; Alegría, A.; Colmenero, J. Enthalpy Recovery in Nanometer to Micrometer Thick Polystyrene Films. *Macromolecules* **2012**, *45* (12), 5296–5306.
(65) Koh, Y. P.; Simon, S. L. Structural Relaxation of Stacked Ultrathin Polystyrene Films. *J. Polym. Sci. Part B Polym. Phys.* **2008**, *46* (24), 2741–2753.
(66) Merzlyakov, M.; Schick, C. Step Response Analysis in DSC — a Fast Way to Generate Heat Capacity Spectra. *Thermochim. Acta* **2001**, *380* (1), 5–12.

(67) Shoifet, E.; Schulz, G.; Schick, C. Temperature Modulated Differential Scanning Calorimetry – Extension to High and Low Frequencies. *Thermochimica Acta* **2015**, *603*, 227–236.
(68) Hempel, E.; Hempel, G.; Hensel, A.; Schick, C.; Donth, E. Characteristic Length of Dynamic Glass Transition near Tg for a Wide Assortment of Glass-Forming Substances. *J. Phys. Chem. B* **2000**, *104* (11), 2460–2466.
(69) Chua, Y. Z.; Zorn, R.; Holderer, O.; Schmelzer, J. W. P.; Schick, C.; Donth, E. Temperature Fluctuations and the Thermodynamic Determination of the Cooperativity Length in Glass Forming Liquids. *J. Chem. Phys.* **2017**, *146* (10), 104501.
(70) Reading, M.; Hourston, D. J. *Modulated Temperature Differential Scanning Calorimetry: Theoretical and Practical Applications in Polymer Characterisation*; Springer, 2006.
(71) Huth, H.; Minakov, A. A.; Schick, C. Differential AC-Chip Calorimeter for Glass Transition Measurements in Ultrathin Films. *J. Polym. Sci. Part B Polym. Phys.* **2006**, *44* (20), 2996–3005.
(72) Tress, M.; Erber, M.; Mapesa, E. U.; Huth, H.; Müller, J.; Serghei, A.; Schick, C.; Eichhorn, K.-J.; Voit, B.; Kremer, F. Glassy Dynamics and Glass Transition in Nanometric Thin Layers of Polystyrene. *Macromolecules* **2010**, *43* (23), 9937–9944.
(73) Schmelzer, J. W. P.; Gutzow, I. S.; Schmelzer, J. W. P.; Gutzow, I. S.; Mazurin, O. V.; Priven, A. I.; Todorova, S. V.; Petroff, B. P. Generic Theory of Vitrification of Glass-Forming Melts. In *Glasses and the Glass Transition*; Wiley-VCH Verlag GmbH & Co. KGaA, 2011; pp 91–164.
(74) Paeng, K.; Richert, R.; Ediger, M. D. Molecular Mobility in Supported Thin Films of Polystyrene, Poly(Methyl Methacrylate), and Poly(2-Vinyl Pyridine) Probed by Dye Reorientation. *Soft Matter* **2012**, *8* (3), 819–826.

4

STRUCTURAL RECOVERY IN POLYSTYRENE NANOSPHERES AND IN BULK

In the previous chapter, the way vitrification takes place and its connection to molecular mobility on polystyrene (PS) nanospheres has been shown. It has been demonstrated how vitrification is delayed when cooling, with respect to the bulk. This fact provided indications on the ability of PS nanospheres to maintain equilibrium more efficiently. The aim of this chapter is to extend these results to the physical aging regime, investigating how equilibrium is recovered in the glassy state. In this context, we have considered the same 3-D confinement system as the one employed in the previous Chapter 3, that is, PS nanospheres. We have investigated how enthalpy is recovered in the glassy state by means of Fast Scanning Calorimetry (FSC). The main outcome of this chapter is that, in line with the T_g suppression, an accelerated enthalpy recovery toward equilibrium with confinement is found. This result well agrees with previous findings on other confined polymer glasses with weak interactions polymer-substrate. Importantly, the time evolution of enthalpy exhibits two mechanisms of equilibration as the one observed in bulk glasses, though on considerably larger time scales.

4.1. INTRODUCTION

The behavior of glass-forming materials at the nanoscale has been an active area of research for the past twenty years, including the effect of confinement on the glass transition temperature and on the dynamics in the glassy state.[1–4] As introduced in Chapter 1, the main consequence of the kinetic nature of the

glass transition is that glasses are non-equilibrium systems and they always experience a slow evolution of their thermodynamic state toward equilibrium, by a loss of the excess in the thermodynamic properties such as volume, enthalpy and entropy.[5] This phenomenon is known as structural recovery[6] or physical aging.[5,7–9] The study of such phenomenon is of great fundamental interest, because it can deliver information of utmost importance of the dynamics and thermodynamics of glass-forming systems below T_g.[9–11]

Recent studies in bulk polymeric [12–14] and other kind of glasses[15–21] have shown that, when a glass-forming system is aged at very long times and considerably below T_g, equilibrium recovery takes place via two or more mechanisms until achieving the thermodynamic state of the extrapolated liquid line. Furthermore, each mechanism of equilibration shows different behavior: (i) the slow one exhibits the standard Vogel-Fulcher-Tammann (VFT) behavior with pronounced temperature dependence, typical of glass dynamics,[13] whereas (ii) the fast mechanism displays a much milder temperature dependence.[13,21,22] Given the long time scales required to observed these multiple steps in bulk polymers,[12,13,23] other kinetic pathways able to accelerate equilibrium recovery are needed. On that account, numerous experimental studies have shown how polymers confined at the nanoscale are able to approach equilibrium in shorter time scales.[4,9,24] Such characteristic of accelerated equilibrium recovery has already been observed in polymeric[25–27] and non-polymeric thin films,[28] nanocomposites[9,29] and nanospheres.[30–34] Generally, such acceleration and its associated T_g depression, is associated to weak interactions of the polymer with its surrounding medium.[35] Furthermore, in analogy with bulk glasses, studies in PS films have shown that when aging is carried out considerably below T_g, equilibrium recovery takes place through different mechanisms.[36,37]

In this chapter, employing PS nanospheres, we have investigated the effect of 3-D confinement on the physical aging behavior following the enthalpy recovery by FSC.[38] These systems have already shown in the previous chapter

to exhibit T_g suppression similar to PS nanospheres suspended in water[30] or surrounded by atmospheric gas.[33] Apart from the acceleration of physical aging, this study also shows the presence of two equilibration mechanisms in terms of the fictive temperature (T_f). These findings are analogous to those obtained in 1-D confinement systems (*i.e.* thin films).[36,37]

4.2. SAMPLES AND EXPERIMENTAL DETAILS

4.2.1. SAMPLES

The studied polystyrene nanospheres and bulk samples are identical to those used in Chapter 3 following the same production and characterization techniques.

4.2.2. PHYSICAL AGING MEASUREMENTS

Fast Scanning Calorimetry was performed by means of the Mettler Toledo Flash DSC 1 equipment, described in details in Chapter 2. FSC experiments are performed to determine the amount of recovered enthalpy by conducting (i) isochronal and (ii) isothermal experiments. In both cases, the thermal histories were erased by holding the sample at 473 K for 0.1 s and subsequently quenching at 183 K prior to the annealing protocol. This protocol was based on holding the sample at a specific aging temperature (T_a) during a certain time (t_a). Afterwards, the aged scan was collected by reheating the sample from 183 K to 473 K at 1000 K/s. Second scans were run immediately after a new quench at 1000 K/s in order to obtain the unaged reference. The employed thermal protocol is outlined in Figure 4.1.

For the isochronal experiments, an aging time of 60 min and aging temperatures ranging from T_g + 5 K until 248 K were considered. For the isothermal experiments, aging times varying between 0.1 and 10^5 s at temperatures ranging from T_g to T_g – ~80 K were performed. The thermodynamic state achieved after aging at the given conditions was

characterized by using the concept of the fictive temperature, introduced in detail in Chapter 2.

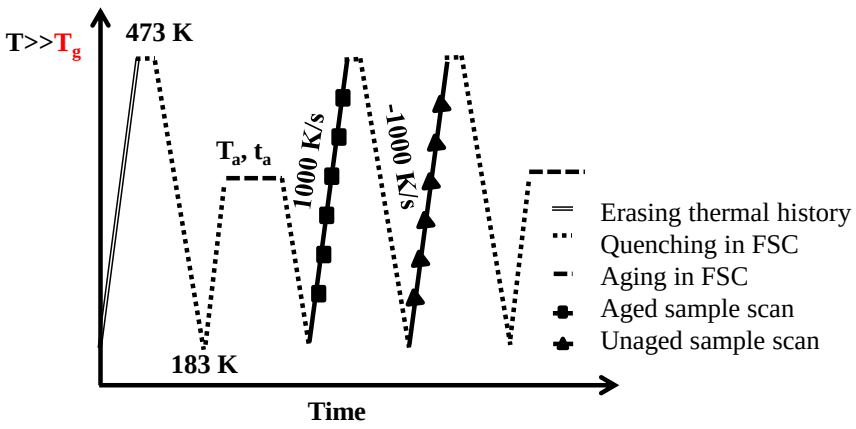

Figure 4.1 Schematization of the thermal protocol procedure employed to determine the amount of recovered enthalpy after aging for a given time (t_a) at a given temperature (T_a).

4.3. RESULTS AND DISCUSSION

In this section we will present the physical aging of PS nanospheres and bulk samples after a given annealing time and temperature. Firstly, isochronal enthalpy recovery experiments, where the aging time is fixed and the temperature is varied, will be shown. Secondly, isothermal enthalpy recovery experiments, where the aging temperature is kept fixed while time is varied, will be presented. Finally, both results will be discussed.

4.3.1. ISOCHRONAL AGING

The heat flow rate of the samples, aged for 60 min in excess (ΔHF) to the reference unaged samples over a wide range of aging temperatures is shown in Figure 4.2. Irrespective of the investigated systems, when aging at temperatures close to T_g, all the excess heat flow rate scans exhibit pronounced endothermic overshoots at temperatures above ~ 400 K. This is the typical signature of physical aging in calorimetry.[38] When the aging is performed at low temperatures, progressively farther from T_g, the endothermic overshoot decreases in intensity, becomes broader and shifts to lower temperatures. However, while such overshoot tends to disappear for bulk PS, its presence is clearly visible even at the lowest aging temperatures for PS nanospheres, as can be observed in the inset of Figure 4.2 for 230 nm diameter.

Data shown in Figure 4.2 allow determining the aging temperature dependence of the T_f achieved after 60 min annealing. An overview of T_f as a function of aging temperature from T_g + 5 K down to 248 K for all investigated systems, is provided in Figure 4.3. At high aging temperatures, the onset of non-equilibrium effects shifts to lower temperature with decreasing the spheres diameter. This results well agrees with the T_f suppression, shown in Chapter 3.

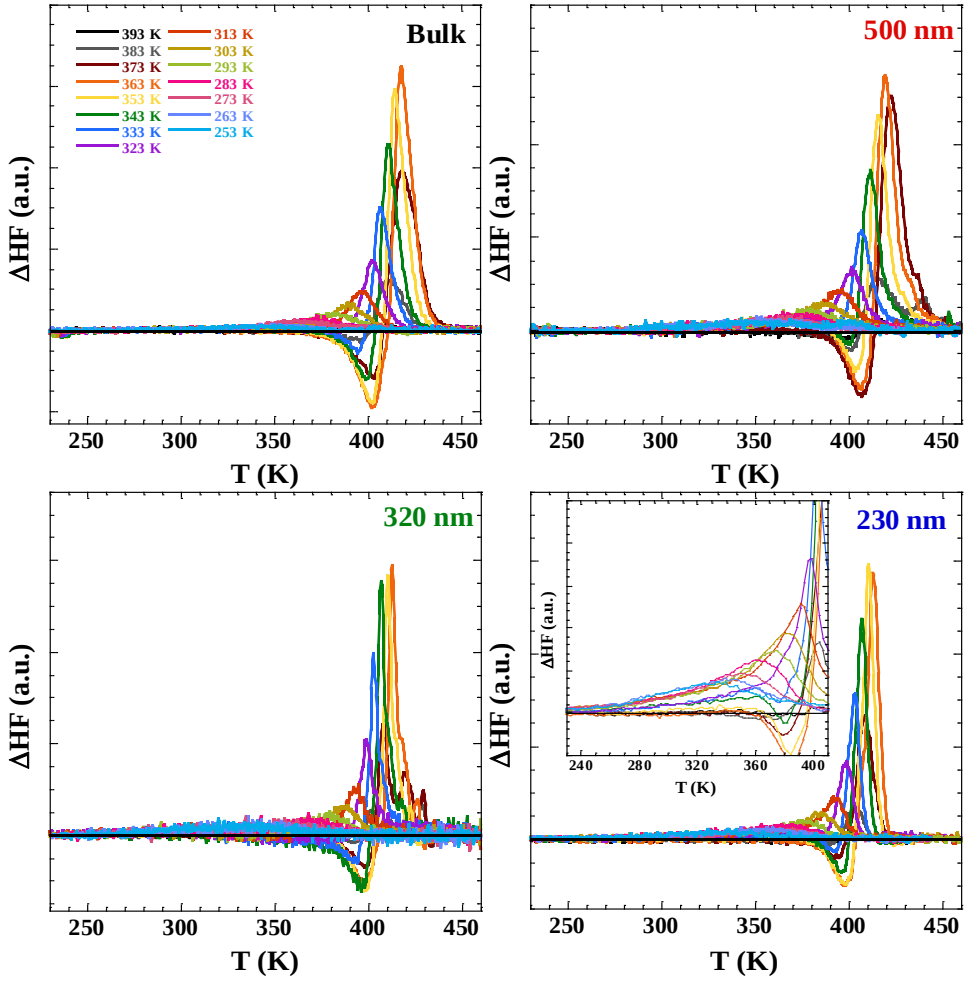

Figure 4.2 Heat flow rate in excess to the unaged reference for samples aged for 60 min at the indicated temperatures obtained at a heating rate of 1000 K/s for: bulk (upper left panel); and PS nanospheres with diameter 500 nm (upper right panel), 320 nm (lower left panel) and 230 nm (lower right panel). The inset for the 230 nm PS nanospheres is a magnification of the low temperature part of the main panel.

As can be noticed in Figure 4.3, bulk PS and 500 nm diameter nanospheres follow the standard behavior observed in this kind of experiments consisting of a minimum in T_f. However, in 500 nm nanospheres such minimum is

located at lower temperatures than in bulk. This behavior results from the role of two competing effects: (i) the temperature variation of the driving force for physical aging, and (ii) that of the molecular mobility. The driving force for physical aging (*i.e.* the distance from equilibrium) increases with decreasing temperature. This effect induces the initial decrease of T_f with decreasing aging temperature. On the other hand, the reduction of the temperature involves a slow-down of the molecular mobility, which results in an increase of the T_f reached after 60 min of aging.

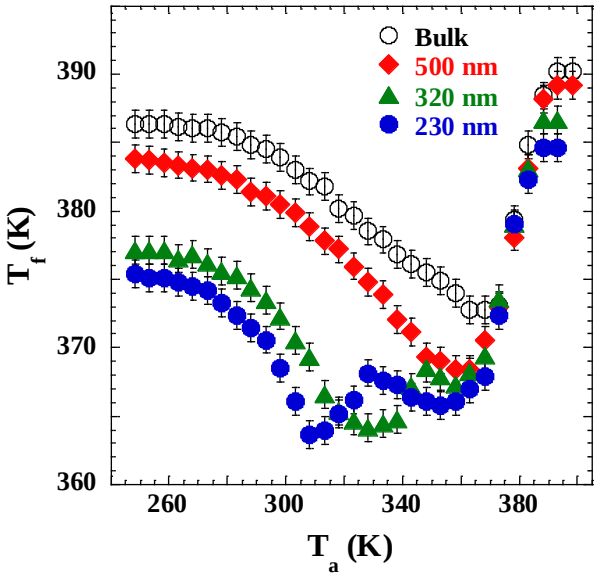

Figure 4.3 Aging temperature dependence of the fictive temperature (T_f) achieved after aging for 60 min all the investigated systems. Error bars in T_f are ± 1 K.

Given the general picture of physical aging, we note that a non-monotonous dependence of the T_f on the aging temperature for 320 and 230 nm PS nanospheres is observed. Apart from the minimum in T_f at temperatures close to T_g, the presence of an additional minimum at lower temperatures is also observed. This result points toward the existence of different mechanisms of

equilibration. This outcome will be further unveiled in the next section with the analysis of the isothermal results.

4.3.2. ISOTHERMAL AGING

Figure 4.4, as a showcase, displays the specific heat in excess to the unaged reference of 230 nm PS nanospheres after aging at 343 K for different times. As a general feature, aging in such conditions results in a progressive development of an endothermic overshoot. The resulting aging time dependence of T_f, in terms of the distance from the equilibrium, that is, the aging temperature (T_a) is displayed in the bottom right panel of Figure 4.5. As can be observed in this figure, the time evolution of T_f exhibits a complex behavior with an initial decay to a plateau during the first ~100 s. This plateau corresponds to a T_f value larger than T_a, indicating that the thermodynamic state of the glass at such plateau belongs to a higher enthalpy state than that of the extrapolated supercooled liquid line. However, on further annealing, the system continues evolving to the final thermodynamic state, following a second decay between 10^4 and 10^5 s. An important observation is that, in the time interval of the plateau in T_f, that is, at isoenthalpic conditions, specific heat temperature scans exhibit pronounced evolution, as can be observed in Figure 4.4. The initial broad low temperature endothermic peak, shifts to higher temperatures and becomes increasingly narrower.

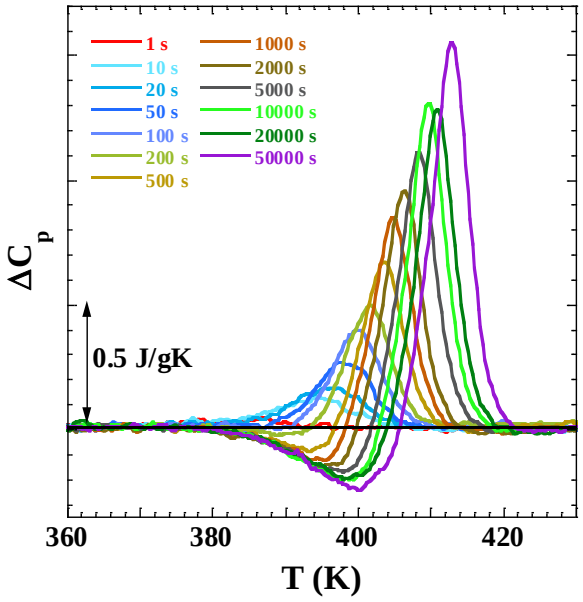

Figure 4.4 Specific heat in excess to the unaged reference sample of PS nanospheres with 230 nm of diameter obtained at a heating rate of 1000 K/s and aged at the indicated aging times, at a temperature of 343 K.

An overview of the aging times dependence of T_f for all investigated systems over a wide range of aging temperatures, is presented in Figure 4.5. Diagonal arrows indicate the onset of equilibration time (τ_{eq}), determined by the intersection of the drawn dashed lines fitted linearly to the data at the time interval corresponding to the plateau, and that of maximum slope of the fictive temperature change.

In the explored aging time scales from 0.1 to 10^5 s, bulk PS exhibits the standard behavior with a monotonous decay toward equilibrium, being consistent with the recent investigations on the enthalpy recovery of bulk PS performed by FSC.[40,41] As mentioned in the Introduction, for bulk glasses much larger aging time scales to observe the non-monotonous decay of the thermodynamic state toward equilibrium are required.[12,13]

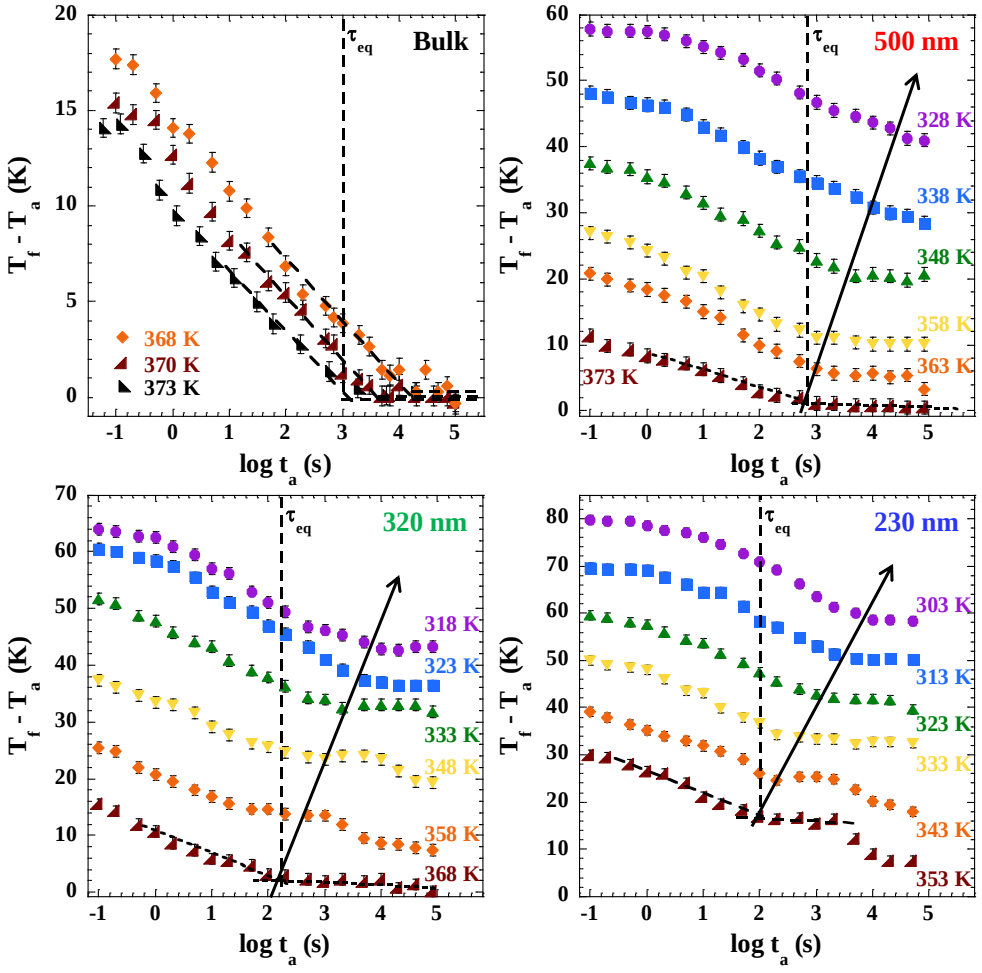

Figure 4.5 Aging time evolution of the fictive temperature T_f, shown as its difference with T_a for: bulk PS (upper left panel); and PS nannospheres with diameter 500 nm (upper right panel), 320 nm (lower left panel) and 230 nm (lower right panel). Error bars in T_f are ± 1 K.

Regarding the behavior of PS nanospheres, inspecting Figure 4.5, it is noticed that in the proximity of T_g a single decay to $T_f \sim T_a$ is observed. However, when the system is aged at lower temperatures, a relatively fast decay until a plateau with $T_f > T_a$ is observed. In some cases, the onset of a second decay is detected. This is the case of nanospheres with 230 and 320 nm diameters aged

between 343 and 358 K. At the lowest investigated aging temperatures, for instance, in the case of nanospheres with 230 nm diameter aged at 303 K, the first plateau in T_f differs from the final ultimate thermodynamic state ($T_f = T_a$) by as much as 60 K. This implies that the system lays on an intermediate plateau after prolonged aging at such low temperature.

Altogether, both physical aging data in isochronal and isothermal conditions reveal the presence of two mechanisms of equilibrium recovery. These results are consistent with those obtained in PS thin films.[36,37] Furthermore, the existence of two temperatures of vitrification was previously shown by Pye *et al.*[42] They investigated the temperature dependence of the film thickness by ellipsometry in freestanding PS films. Experiments at low cooling rates (< 1 K/min) aiming to characterize the temperature dependent specific volume of several bulk polymers, revealed the presence of different steps in the coefficient of thermal expansion, beyond the main one at the T_g of the polymer.[43] More recently, experiments by ellipsometry on thick PS films aged for several months at room temperature, showed the presence of two temperature ranges of devitrification.[44] The presence of multiple steps to recover equilibrium is also consistent with equilibrium recovery data of bulk polymers,[12,13] chalcogenide[18,20] and metallic glasses.[21] Furthermore, in the latter kind of glasses, also two mechanisms of vitrification have been identified by calorimetry employing cooling rates of the order of 1 to 20 K/min.[17,45,46]

To get insights on the nature of the mechanisms involved in the physical aging, data from Figure 4.5 were used to analyze the kinetics of the equilibrium recovery. Such kinetics was parametrized by means of the equilibration time (τ_{eq}). This was quantified from the intersection of the linear fits (Figure 4.5 dashed lines) at the time interval corresponding to the plateau in T_f. Its dependence on the temperature and the nanospheres diameter and bulk sample, is shown in Figure 4.6. This figure also includes τ_{eq} data taken

from the study reported in ref.[13] on the long-term aging bulk PS (closed and opened squares).

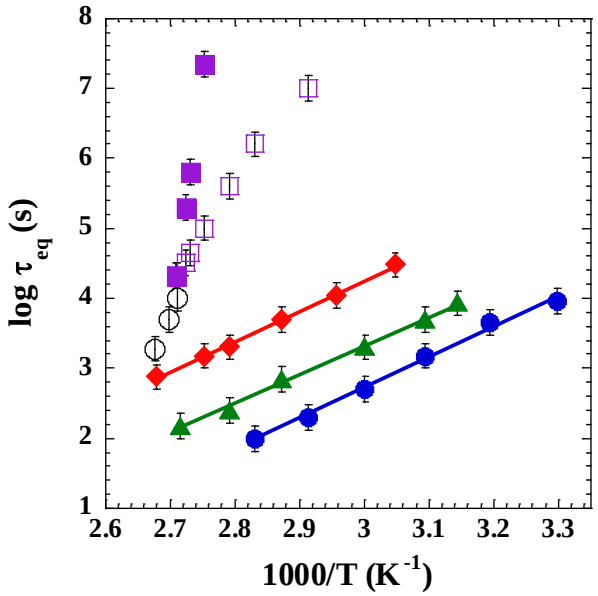

Figure 4.6 Time to reach equilibrium as a function of the inverse temperature for all investigated systems. Symbols: Bulk PS (black open circles); PS nanospheres of 500 nm (red filled diamonds), 320 nm (green filled triangles) and 230 nm (blue filled circles). Solid lines indicate the linear Arrhenius fit for each system. Purple filled and opened squares correspond to the equilibration time of bulk PS obtained by standard DSC taken from ref.[13]

Regarding bulk PS data shown in Figure 4.6, there is a good agreement between data obtained from ref.[13] and the ones obtained in the present work from the upper left panel of Figure 4.5. The main difference between these two sets of data arises from the employed cooling rates. The squares were obtained from enthalpy recovery experiments after cooling in a conventional DSC at 20 K/min, whereas the ones obtained in this work were carried out by FSC at 1000 K/s. Thus, these results indicate that the time scale to reach equilibrium is independent of the cooling rate employed before physical aging. Summarizing both results of τ_{eq} data on bulk PS, it can be appreciated that the

presence of a slow mechanism of equilibration (see opened circles and closed squares) is compatible with the Vogel-Fulcher-Tammann (VFT) behavior with a large activation energy. This can be associated with the so-called α process. Furthermore, a second mechanism of recovery is observed (opened squares) with activation energy gradually decreasing with temperature.

Concerning to PS nanospheres, our results and their analysis in terms of the kinetics of equilibrium recovery, indicate that a common mechanism drives the initial part of equilibrium recovery with Arrhenius temperature dependence. The continuous lines in Figure 4.6 are the fits of experimental τ_{eq} values to the Arrhenius law (4.1):

$$\tau_{eq} = \tau_0 \exp\left(\frac{E_a}{k_B T}\right) \qquad (4.1)$$

where τ_0 is the pre-exponential factor, E_a is the activation energy of the process and k_B is the Boltzman constant.

A common value of E_a= 80 ± 3 kJ/mol, which is considerably smaller than that associated to α process, is found for all PS nanopsheres. This value is considerably larger than the obtained in 30 nm PS thin films by standard DSC (E_a= 31 ± 3 kJ/mol).[36] However, the latter value was acquired at temperatures as low as T_g – 75 K and, at higher temperature, a tendency toward an increase in the activation energy was evident. This activation energy values are considerably smaller than that of the β relaxation process found for PS by means of dielectric or mechanical spectroscopy (E_a= 160 ± 3 kJ/mol).[46] Thus, its origin must be attributed to other molecular motions.

The finding of common activation energy but different time scales for the fast equilibration mechanism, points toward the existence of an identical process of molecular motion for all nanospheres. Hence, two different scenarios can be hypothesized: (i) such molecular motion, while exhibiting the same

temperature dependence, is more rapid in nanospheres with smaller diameter or (ii) such motion is identical for nanospheres with any investigated diameter, but factors exclusively related to the size are responsible for the shift in the time scale. According to the findings shown in Chapter 3, it is possible to discriminate between the two scenarios. In such chapter, we have observed that PS nanospheres exhibited negative deviations of the T_g but identical (bulk-like) molecular mobility,[47] in line with previous results obtained in polymer thin films[48–50] and nanocomposites[28,51,52] with weak interaction polymer/interface. Hence, these results, while suggesting more efficient equilibration of different confined glasses, show that this is not related to the accelerated molecular mobility and rather originate from size arguments.[53] Within this context, recent efforts have shown that the key factor determining the enhanced efficiency to stay in equilibrium or to recover it from the glassy state is the amount of free interfacial area,[2,34,54–57] unslaved by an underlying adsorbing layer.[58]

Regarding the role of the kind of confinement on glass dynamics, our results demonstrate that the physical aging behaviour is affected by the dimensionality of confinement in a qualitative manner. However, it is worth of remark that, on further reducing the diameter of nanospheres (*e.g.* ~ 20 nm) positive deviations from bulk T_g can be found. This was shown by Mi *et al.*[60] and Martinez-Tong *et al.*[61,62] Given the fact that, in thin films with weak interactions with the substrate generally exhibit negative T_g deviations from bulk behavior even for very thin layers, this result implies that the analogy of 1-D vs 3-D confinement found in this and previous works,[30,63,64] may be invalid at extremely small length scales.

4.4. CHAPTER SUMMARY

In this chapter, we have employed PS nanospheres and bulk PS to provide insights on the way polymer glasses subjected to different level of confinement recover equilibrium below T_g. This was done by performing isochronal annealing experiments over a wide range of aging temperatures. Our results show a non-monotonous temperature behavior for 320 and 230 nm diameter nanospheres. Furthermore, we have complemented these experiments with isothermal aging experiments with aging times ranging from 0.1 to 10^5 s at $T_a < T_g$. In line with the non-monotonous behavior observed in the isochronal conditions at shorter time scales, isothermal experiments show complex evolution of the enthalpy toward equilibrium. In this context, we have shown that in PS nanospheres: (i) equilibrium recovery proceeds faster than in bulk; and (ii) the accelerated equilibrium recovery allows the detection of two mechanisms of equilibration from the glassy state in the employed time scale range. The former result is discussed in the context of the universality of the way polymer glasses (subjected to weak interactions with the interface) in different kinds of geometrical confinement recover equilibrium. Regarding the presence of two mechanisms of equilibration, our results are consistent with other studies on bulk and confined polymers, as well as, other kinds of glasses.

Part of this chapter is published in *Macromolecules* **2018**; **DOI:** 10.1021/acsmacromol.8b00502

4.5. REFERENCES

(1) Ediger, M. D.; Forrest, J. A. Dynamics near Free Surfaces and the Glass Transition in Thin Polymer Films: A View to the Future. *Macromolecules* **2014**, *47*, 471–478.

(2) Priestley, R. D.; Cangialosi, D.; Napolitano, S. On the Equivalence between the Thermodynamic and Dynamic Measurements of the Glass Transition in Confined Polymers. *J. Non-Cryst. Solids* **2015**, *407*, 288–295.

(3) Kremer, F.; Tress, M.; Mapesa, E. U. Glassy Dynamics and Glass Transition in Nanometric Layers and Films: A Silver Lining on the Horizon. *J. Non-Cryst. Solids* **2015**, *407*, 277–283.

(4) Cangialosi, D.; Alegría, A.; Colmenero, J. Effect of Nanostructure on the Thermal Glass Transition and Physical Aging in Polymer Materials. *Prog. Polym. Sci.* **2016**, *54–55* (Supplement C), 128–147.

(5) Struik, L. C. E. Physical Aging in Plastics and Other Glassy Materials. *Polym. Eng. Sci.* **1977**, *17* (3), 165–173.

(6) Kovacs, A. J. Transition vitreuse dans les polymères amorphes. Etude phénoménologique. In *Fortschritte Der Hochpolymeren-Forschung*; Advances in Polymer Science; Springer, Berlin, Heidelberg, 1964; pp 394–507.

(7) Hutchinson, J. M. Physical Aging of Polymers. *Prog. Polym. Sci.* **1995**, *20* (4), 703–760.

(8) McKenna, G. B. Physical Aging in Glasses and Composites. In *Long-Term Durability of Polymeric Matrix Composites*; Springer, Boston, MA, 2012; pp 237–309.

(9) Cangialosi, D.; Boucher, V. M.; Alegría, A.; Colmenero, J. Physical Aging in Polymers and Polymer Nanocomposites: Recent Results and Open Questions. *Soft Matter* **2013**, *9* (36), 8619–8630.

(10) Cangialosi, D. Dynamics and Thermodynamics of Polymer Glasses. *J. Phys. Condens. Matter* **2014**, *26* (15), 153101.

(11) McKenna, G. B.; Simon, S. L. 50th Anniversary Perspective: Challenges in the Dynamics and Kinetics of Glass-Forming Polymers. *Macromolecules* **2017**, *50* (17), 6333–6361.

(12) Wimberger-Friedl, R.; de Bruin, J. G. The Very Long-Term Volume Recovery of Polycarbonate: Is Self-Retardation Finite? *Macromolecules* **1996**, *29* (14), 4992–4997.

(13) Daniele Cangialosi, V. M. B.; Angel Alegría, J. C. Direct Evidence of Two Equilibration Mechanisms in Glassy Polymers. *Phys. Rev. Lett.* **2013**, *111*, 095701.

(14) Righetti, M. C.; Gazzano, M.; Delpouve, N.; Saiter, A. Contribution of the Rigid Amorphous Fraction to Physical Ageing of Semi-Crystalline PLLA. *Polymer* **2017**, *125*, 241–253.

(15) Chen, H. S.; Inoue, A.; Masumoto, T. Two-Stage Enthalpy Relaxation Behavior of (Fe0.5Ni0.5)83P17 and (Fe0.5Ni0.5)83B17 Amorphous Alloys upon Annealing. *J. Mater. Sci.* **1985**, *20* (7), 2417–2438.

(16) Miller, R. S.; MacPhail, R. A. Ultraslow Nonequilibrium Dynamics in Supercooled Glycerol by Stimulated Brillouin Gain Spectroscopy. *J. Chem. Phys.* **1997**, *106* (8), 3393–3401.

(17) Louzguine-Luzgin, D. V.; Seki, I.; Yamamoto, T.; Kawaji, H.; Suryanarayana, C.; Inoue, A. Double-Stage Glass Transition in a Metallic Glass. *Phys. Rev. B* **2010**, *81* (14), 144202.
(18) Golovchak, R.; Kozdras, A.; Balitska, V.; Shpotyuk, O. Step-Wise Kinetics of Natural Physical Ageing in Arsenic Selenide Glasses. *J. Phys. Condens. Matter* **2012**, *24* (50), 505106.
(19) Wang, C.; Hu, L.; Wei, C.; Tong, X.; Zhou, C.; Sun, Q.; Hui, X.; Yue, Y. Sub-Tg Relaxation Patterns in Cu-Based Metallic Glasses Far from Equilibrium. *J. Chem. Phys.* **2014**, *141* (16), 164507.
(20) Golovchak, R.; Kozdras, A.; Shpotyuk, O.; Balitska, V. Crossover between Cooperative and Fractal Relaxation in Complex Glass-Formers. *J. Phys. Condens. Matter* **2016**, *28* (35), 355101.
(21) Gallino, I.; Cangialosi, D.; Evenson, Z.; Schmitt, L.; Hechler, S.; Stolpe, M.; Ruta, B. Hierarchical Aging Pathways and Reversible Fragile-to-Strong Transition upon Annealing of a Metallic Glass Former. *Acta Mater.* **2018**, *144* (Supplement C), 400–410.
(22) Boucher, V. M.; Cangialosi, D.; Alegría, A.; Colmenero, J. Enthalpy Recovery of Glassy Polymers: Dramatic Deviations from the Extrapolated Liquidlike Behavior. *Macromolecules* **2011**, *44* (20), 8333–8342.
(23) Robertson, C. G.; Wilkes, G. L. Long-Term Volume Relaxation of Bisphenol A Polycarbonate and Atactic Polystyrene. *Macromolecules* **2000**, *33* (11), 3954–3955.
(24) Priestley, R. D. Physical Aging of Confined Glasses. *Soft Matter* **2009**, *5* (5), 919–926.
(25) Keddie, J. L.; Jones, R. A. L.; Cory, R. A. Size-Dependent Depression of the Glass Transition Temperature in Polymer Films. *Europhys. Lett.* **1994**, *27*, 59–64.
(26) Forrest, J. A.; Dalnoki-Veress, K. The Glass Transition in Thin Polymer Films. *Adv. Colloid Interface Sci.* **2001**, *94* (1), 167–195.
(27) Ahrenberg, M.; Chua, Y. Z.; Whitaker, K. R.; Huth, H.; Ediger, M. D.; Schick, C. In Situ Investigation of Vapor-Deposited Glasses of Toluene and Ethylbenzene via Alternating Current Chip-Nanocalorimetry. *J. Chem. Phys.* **2013**, *138* (2), 024501.
(28) Sepúlveda, A.; Leon-Gutierrez, E.; Gonzalez-Silveira, M.; Rodríguez-Tinoco, C.; Clavaguera-Mora, M. T.; Rodríguez-Viejo, J. Accelerated Aging in Ultrathin Films of a Molecular Glass Former. *Phys. Rev. Lett.* **2011**, *107* (2), 025901.
(29) Ramakrishnan, V.; Harsiny, S.; Goossens, J. G. P.; Hoeks, T. L.; Peters, G. W. M. Physical Aging in Polycarbonate Nanocomposites Containing Grafted Nanosilica Particles: A Comparison between Enthalpy and Yield Stress Evolution. *J. Polym. Sci. Part B Polym. Phys.* **2016**, *54* (20), 2069–2081.
(30) Zhang, C.; Guo, Y.; Priestley, R. D. Glass Transition Temperature of Polymer Nanoparticles under Soft and Hard Confinement. *Macromolecules* **2011**, *44* (10), 4001–4006.
(31) Guo, Y.; Zhang, C.; Lai, C.; Priestley, R. D.; D'Acunzi, M.; Fytas, G. Structural Relaxation of Polymer Nanospheres under Soft and Hard Confinement: Isobaric versus Isochoric Conditions. *ACS Nano* **2011**, *5* (7), 5365–5373.
(32) Zhang, C.; Guo, Y.; Shepard, K. B.; Priestley, R. D. Fragility of an Isochorically Confined Polymer Glass. *J. Phys. Chem. Lett.* **2013**, *4* (3), 431–436.

(33) Zhang, C.; Boucher, V. M.; Cangialosi, D.; Priestley, R. D. Mobility and Glass Transition Temperature of Polymer Nanospheres. *Polymer* **2013**, *54* (1), 230–235.
(34) Feng, S.; Li, Z.; Liu, R.; Mai, B.; Wu, Q.; Liang, G.; Gao, H.; Zhu, F. Glass Transition of Polystyrene Nanospheres under Different Confined Environments in Aqueous Dispersions. *Soft Matter* **2013**, *9* (18), 4614–4620.
(35) Napolitano, S.; Glynos, E.; Tito, N. B. Glass Transition of Polymers in Bulk, Confined Geometries, and near Interfaces. *Rep. Prog. Phys.* **2017**, *80* (3), 036602.
(36) Boucher, V. M.; Cangialosi, D.; Alegria, A.; Colmenero, J. Reaching the Ideal Glass Transition by Aging Polymer Films. *Phys. Chem. Chem. Phys.* **2017**, *19* (2), 961–965.
(37) Boucher, V. M.; Cangialosi, D.; Alegría, A.; Colmenero, J. Complex Nonequilibrium Dynamics of Stacked Polystyrene Films Deep in the Glassy State. *J. Chem. Phys.* **2017**, *146* (20), 203312.
(38) *Fast Scanning Calorimetry*; Schick, C., Mathot, V., Eds.; Springer International Publishing, 2016.
(39) Hodge, I. M. Enthalpy Relaxation and Recovery in Amorphous Materials. *J. Non-Cryst. Solids* **1994**, *169* (3), 211–266.
(40) Lopez, E.; Simon, S. L. Signatures of Structural Recovery in Polystyrene by Nanocalorimetry. *Macromolecules* **2016**, *49* (6), 2365–2374.
(41) Koh, Y. P.; Gao, S.; Simon, S. L. Structural Recovery of a Single Polystyrene Thin Film Using Flash DSC at Low Aging Temperatures. *Polymer* **2016**, *96*, 182–187.
(42) Pye, J. E.; Roth, C. B. Two Simultaneous Mechanisms Causing Glass Transition Temperature Reductions in High Molecular Weight Freestanding Polymer Films as Measured by Transmission Ellipsometry. *Phys. Rev. Lett.* **2011**, *107* (23), 235701.
(43) Greiner, R.; Schwarzl, F. R. Thermal Contraction and Volume Relaxation of Amorphous Polymers. *Rheol. Acta* **1984**, *23* (4), 378–395.
(44) Pradipkanti, L.; Chowdhury, M.; Satapathy, D. K. Stratification and Two Glass-like Thermal Transitions in Aged Polymer Films. *Phys. Chem. Chem. Phys.* **2017**, *19* (43), 29263–29270.
(45) Louzguine-Luzgin, D. V.; Seki, I.; Ketov, S. V.; Louzguina-Luzgina, L. V.; Polkin, V. I.; Chen, N.; Fecht, H.; Vasiliev, A. N.; Kawaji, H. Glass-Transition Process in an Au-Based Metallic Glass. *J. Non-Cryst. Solids* **2015**, *419*, 12–15.
(46) Song, L.; Xu, W.; Huo, J.; Wang, J.-Q.; Wang, X.; Li, R. Two-Step Relaxations in Metallic Glasses during Isothermal Annealing. *Intermetallics* **2018**, *93*, 101–105.
(47) McCrum, N. G.; Read, B. E.; Williams, G. *Anelastic and Dïelectric Effects in Polymeric Solids*; John Wiley, 1967.
(48) Perez-de-Eulate, N. G.; Di Lisio, V.; Cangialosi, D. Glass Transition and Molecular Dynamics in Polystyrene Nanospheres by Fast Scanning Calorimetry. *ACS Macro Lett.* **2017**, *6* (8), 859–863.
(49) Boucher, V. M.; Cangialosi, D.; Yin, H.; Schönhals, A.; Alegría, A.; Colmenero, J. T g Depression and Invariant Segmental Dynamics in Polystyrene Thin Films. *Soft Matter* **2012**, *8* (19), 5119–5122.
(50) Yin, H.; Cangialosi, D.; Schönhals, A. Glass Transition and Segmental Dynamics in Thin Supported Polystyrene Films: The Role of Molecular Weight and Annealing. *Thermochim. Acta* **2013**, *566* (Supplement C), 186–192.

(51) Luo, S.; Chen, Y.; Sha, Y.; Xue, G.; Zhuravlev, E.; Schick, C.; Wang, X.; Zhou, D.; Li, L. Molecular Weight and Interfacial Effect on the Kinetic Stabilization of Ultrathin Polystyrene Films. *Polymer* **2018**, *134*, 204–210.
(52) Boucher, V. M.; Cangialosi, D.; Alegría, A.; Colmenero, J.; Pastoriza-Santos, I.; Liz-Marzan, L. M. Physical Aging of Polystyrene/Gold Nanocomposites and Its Relation to the Calorimetric Tg Depression. *Soft Matter* **2011**, *7* (7), 3607–3620.
(53) Cangialosi, D.; Boucher, V. M.; Alegría, A.; Colmenero, J. Enhanced Physical Aging of Polymer Nanocomposites: The Key Role of the Area to Volume Ratio. *Polymer* **2012**, *53* (6), 1362–1372.
(54) Cangialosi, D.; Alegría, A.; Colmenero, J. Cooling Rate Dependent Glass Transition in Thin Polymer Films and in Bulk. In *Fast Scanning Calorimetry*; Schick, C., Mathot, V., Eds.; Springer International Publishing: Cham, 2016; pp 403–431.
(55) Napolitano, S.; Rotella, C.; Wübbenhorst, M. Can Thickness and Interfacial Interactions Univocally Determine the Behavior of Polymers Confined at the Nanoscale? *ACS Macro Lett.* **2012**, *1* (10), 1189–1193.
(56) Glynos, E.; Frieberg, B.; Chremos, A.; Sakellariou, G.; Gidley, D. W.; Green, P. F. Vitrification of Thin Polymer Films: From Linear Chain to Soft Colloid-like Behavior. *Macromolecules* **2015**, *48* (7), 2305–2312.
(57) Burroughs, M. J.; Napolitano, S.; Cangialosi, D.; Priestley, R. D. Direct Measurement of Glass Transition Temperature in Exposed and Buried Adsorbed Polymer Nanolayers. *Macromolecules* **2016**, *49*, 4647–4655.
(58) Sun, S.; Xu, H.; Han, J.; Zhu, Y.; Zuo, B.; Wang, X.; Zhang, W. The Architecture of the Adsorbed Layer at the Substrate Interface Determines the Glass Transition of Supported Ultrathin Polystyrene Films. *Soft Matter* **2016**, *12*, 8348–8358.
(59) Perez-de-Eulate, N. G.; Sferrazza, M.; Cangialosi, D.; Napolitano, S. Irreversible Adsorption Erases the Free Surface Effect on the Tg of Supported Films of Poly(4-Tert-Butylstyrene). *ACS Macro Lett.* **2017**, *6* (4), 354–358.
(60) Mi, Y.; Xue, G.; Wang, X. Glass Transition of Nano-Sized Single Chain Globules. *Polymer* **2002**, *43* (25), 6701–6705.
(61) Martínez-Tong, D. E.; Soccio, M.; Sanz, A.; García, C.; Ezquerra, T. A.; Nogales, A. Chain Arrangement and Glass Transition Temperature Variations in Polymer Nanoparticles under 3D-Confinement. *Macromolecules* **2013**, *46* (11), 4698–4705.
(62) Martínez-Tong, D. E.; Cui, J.; Soccio, M.; García, C.; Ezquerra, T. A.; Nogales, A. Does the Glass Transition of Polymers Change Upon 3D Confinement? *Macromol. Chem. Phys.* **2014**, *215* (17), 1620–1624.
(63) Sharp, J. S.; Forrest, J. A. Free Surfaces Cause Reductions in the Glass Transition Temperature of Thin Polystyrene Films. *Phys. Rev. Lett.* **2003**, *91* (23), 235701.
(64) Bäumchen, O.; McGraw, J. D.; Forrest, J. A.; Dalnoki-Veress, K. Reduced Glass Transition Temperatures in Thin Polymer Films: Surface Effect or Artifact? *Phys. Rev. Lett.* **2012**, *109* (5), 055701.

5

VERY LONG-TERM PHYSICAL AGING OF GLASSY POLYMERS

In the previous chapters of this thesis we have shown how 3-D confinement allows (i) delaying vitrification when cooling down from the melt and (ii) accelerating equilibrium recovery in the glassy state. Such general enhancement of non-equilibrium dynamics provides a route, entailing the employment of reduced aging time scale, to study glass dynamics deep in the glassy state and; as a result, the presence of multiple mechanisms of equilibrium recovery has been unveiled. The question is, whether such phenomenology is confinement specific or rather is general feature of glasses. The aim of this chapter is to study the kinetics of equilibrium recovery of bulk polymer glasses well below the glass transition temperature (T_g). In these conditions, investigations are rather scarce due to the long time scales required for reaching thermodynamic equilibrium. Given this fact, long-term physical aging of polymers deep in the glassy state is much less understood rather than the short-term one close to T_g. In this chapter, the thermodynamic state attained after about 30 years aging at room temperature of glassy poly(arylate), poly(carbonate) and poly(sulfone), by differential scanning calorimetry (DSC) is investigated. These results were complemented with extensive DSC studies on these polymers aged in the same conditions of temperature, for time scales ranging from minutes to months. The main outcome of this investigation is that these polymers attain an intermediate plateau in the enthalpy with a partial recovery. This is indicative of the presence of multiple mechanisms of equilibrium recovery, in analogy with confined polymer glasses. The presence of a relatively fast mechanism of

equilibrium recovery, results in the observation of the onset of devitrification well below T_g. These results generally agree with those showed in Chapter 4 for PS nanospheres. Furthermore, the analogy with other kind of glass-forming systems is highlighted pointing toward the universality of such behavior.

5.1. INTRODUCTION

In recent years, understanding of physical aging on a variety of glass-forming liquids such as metallic glasses,[1] small organic glasses,[2] chalcogenide glasses[3] or polymer glasses,[4–6] has been subject of active research.

The classic description of physical aging is based on a monotonous evolution of the thermodynamic state toward equilibrium,[7] on a time scale connected to the so-called α relaxation, with strong temperature dependence often described by the Vogel-Fulcher-Tammann (VFT) equation.[8–10] Hence, within such description, only one molecular mechanism and its associated time scale are considered in different theoretical approaches.[11–15] However, recent studies in the physical aging regime over long time scales and significantly below T_g, provided evidence for the existence of multiple mechanisms of equilibration including polymers,[16–21] low molecular weight glass formers,[22,23] chalcogenides[24,25] and metallic glasses,[26,27] where the recovery of equilibrium was found to proceed in two or more steps, being the slowest of such steps dependent on the aging temperature in ways analogous to VFT behavior. In contrast, the temperature dependence of the fast mechanism of equilibrium recovery was found to exhibit low activation energy, amenable to the Arrhenius law description.[19,21,27]

In this context, as shown in Chapter 4 for PS nanospheres and in thin films in refs.,[20,21] it has to be pointed out that the observation of different equilibrium recovery steps requires shorter time scales than in bulk glasses. In the latter systems the same observation needs larger time scales always larger than several weeks[19,27] or even years.[16,17,24]

In summary the presence of multiple equilibration mechanisms, constitute an important issue in order to understand the dynamics and thermodynamics of glass-forming systems. Thus, the main objective of this study is to shed light on how polymer glasses recover thermodynamic equilibrium well below T_g. To this aim, we employ DSC to unveil how several polymer glasses aged over about 30 years well below their respective T_g, devitrify when heated to the melt state. Furthermore, we complement these data with additional DSC experiments on the same polymers, aged for times ranging from minutes to several months in conditions of temperature essentially equal to those of samples aged for 30 years. Our results indicate that, devitrification of these samples proceeds via two distinct mechanisms. Apart from the slow one, responsible for the devitrification in proximity of the polymers' T_g, a fast mechanism is also detected. The fact that the aging is conducted far below T_g, implies that, differently from glasses aged in proximity of T_g,[19] devitrification takes places in a temperature range considerably below to that associated to the glass transition; and recovery of equilibrium proceeds to a plateau with thermodynamic state exhibiting an enthalpy much larger than that of the extrapolated supercooled liquid.

5.2. SAMPLES AND EXPERIMENTAL DETAILS

Aromatic amorphous bulk polymers, that is, poly(arylate) (PAr), poly(carbonate) (PC) and poly(sulfone) (PSU) with high thermal, oxidative and hydrolytic stability were aged for times ranging from minutes to several months basically in the same conditions to those of samples aged for ~ 30 years. The T_g values obtained by DSC on cooling at 20 K/min considering the mid-point of the step in the specific heat and the specific heat step (Δc_p) at T_g are summarized in Table 5.1. Prior to their use, all the polymers were stored in a dry atmosphere during about 30 years (10^9 s).

Table 5.1 T_g and specific heat step at T_g for all investigated polymers. Data extracted from Figure A.3.

Materials	T_g *(K)*	$\Delta c_p (T_g)$*(J/gK)*
PAr	463	0.225
PC	423	0.23
PSU	459	0.225

5.2.1. SAMPLES

5.2.1.1. Poly(arylate) – (PAr)

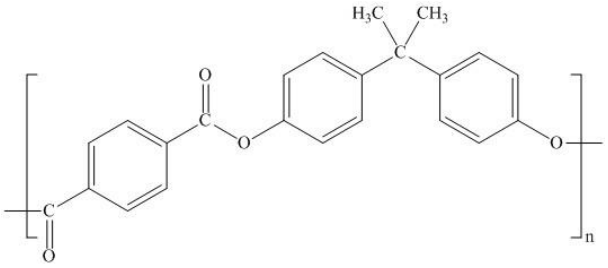

Figure 5.1 Sketch of the PAr repeating unit

Poly(arylate) abbreviated as PAr, comes from a family of aromatic polyesters.[28] It is derived from a dicarboxylic acid with a phenolic compound and the repeating unit consists of ester groups (-CO-O-) and aromatic rings as schematically shown in Figure 5.1. PAr (Ardel-D100) was purchased from Union Carbide (M_n = 22700 g/mol; M_w/M_n = 1.27) characterized by Size Exclusion Chromatography (SEC), see Figure A.2.

5.2.1.2. Poly(carbonate) – (PC)

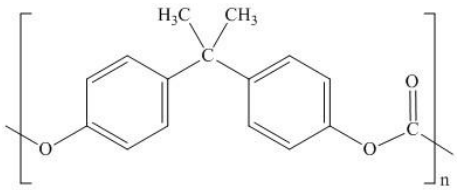

Figure 5.2 Sketch of the PC repeating unit

Poly(bisphenol-A-carbonate) abbreviated as PC, is a thermoplastic polymer which contains linkages of (-O-CO-O-) in the backbone[29] as shown in Figure 5.2. PC was purchased from Bayer, Makrolon 2800 (M_n = 23600 g/mol; M_w/M_n = 1.22), characterized by Size Exclusion Chromatography (SEC), see Figure A.2.

5.2.1.3. Poly(sulfone) – (PSU)

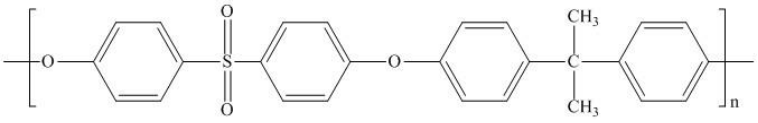

Figure 5.3 Sketch of the PSU repeating unit

Poly(sulfone) abbreviated as PSU, is a high thermal, oxidative and hydrolytic stable thermoplastic polymer. It is formed by polycondensation of bisphenol-A and bis(4-chlorophenyl) sulfone,[28] as shown in Figure 5.3. PSU (Udel-P1700) was purchased from Union Carbide (M_n = 57000 g/mol; M_w/M_n = 1.28) characterized by Size Exclusion Chromatography (SEC), see Figure A.2.

5.2.2. PHYSICAL AGING

Specific heat measurements of bulk polymers were performed by DSC-Q2000, where helium flow was warranted during all the thermal cycles. Samples aged for about 30 years were first cooled to 183 K and heated at 10 K/min while recording specific heat data to a temperature considerably above the polymer T_g. This was 523 K for PSU and PAr and 473 K for PC. In such a way, the samples' thermodynamic state after ~ 30 years aging was assessed, and the previous thermal history erased. All samples were subsequently cooled at 20 K/min to 183 K and immediately heated to room temperature (296 K) for aging times between 2 min and 60 days. After annealing, samples were again cooled to 183 K and heated to above T_g at 10 K/min for specific heat data collection. Figure 5.4 shows the scheme of the applied thermal procedure employed in the study of the physical aging.

For aging times shorter than one week, aging was carried out inside the DSC, whereas vacuum ovens were employed for larger times. The temperature in the oven was monitored continuously by a thermometer placed beside the samples. For the sake of reproducibility, at least three samples were employed for each aging time.

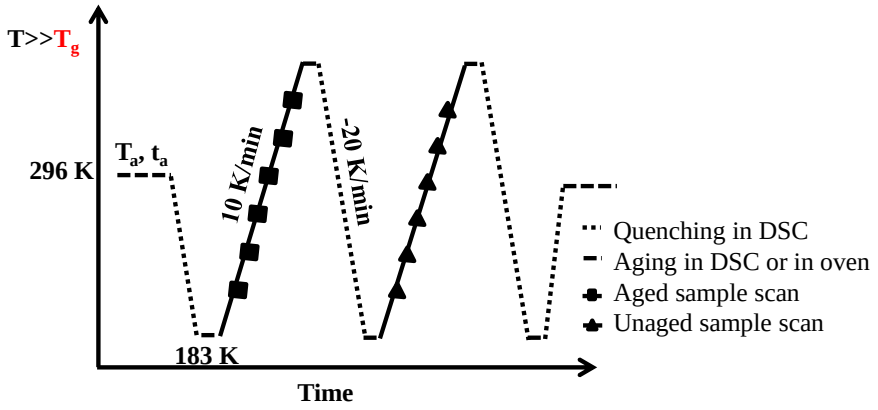

Figure 5.4 Schematization of the thermal protocol applied to bulk amorphous polymers (PSU, PAr and PC) for the determination of the recovered enthalpy. T_a and t_a are the aging temperature and time, respectively.

Likewise the results presented in the previous Chapter 4, the thermodynamic state of the aged systems was analysed in terms of the fictive temperature (T_f) using the Moynihan's equation:[30] $\int_{T_f}^{T\gg T_g}(c_{pm}-c_{pg})dT=\int_{T\ll T_g}^{T\gg T_g}(c_p-c_{pg})dT$, where $c_{pm}(T)$ and $c_{pg}(T)$ are the specific heat of the melt and the glass samples respectively.

5.3. RESULTS AND DISCUSSION

The calorimetric signature of devitrification of a glass with a given thermodynamic state generally consists of two components:[31] (i) the variation from the specific heat of the glass to that of the melt, that is, the reversing part of the specific heat and (ii) the contribution resulting from the irreversibility, in the thermodynamic sense of the glass transition. The latter component results in the presence of an overshoot whose magnitude depends on the thermodynamic state of the glass. For glasses aged over relatively short times close to T_g, such overshoot is generally located in proximity of the step in the specific heat capacity underlying the devitrification of the glass.

Figure 5.5 from a) to c) shows the specific heat scans at 10 K/min for all investigated polymers aged at room temperature at the indicated aging times. The step in the specific heat capacity (c_p) in proximity of the polymer T_g is essentially unaffected by aging. In this case, the main signature of enthalpy recovery during physical aging is the development of a broad endothermic overshoot in the range of the glassy state, whose onset is located far below T_g. Furthermore, panels from d) to f) of Figure 5.5 display the specific heat capacity of the aged sample in excess to the unaged reference (Δc_p). As can be observed, this endothermic overshoot systematically increases its magnitude with increasing aging time. The result based on the development of an endothermic overshoot well below T_g is analogous to that shown in Chapter 4 for polystyrene nanospheres, for thin polymer films[20,21] and for a plastic crystal aged for 7 years.[22] Such endothermic overshoot may also bear some relation to the so-called "pre-peak" or "second glass transition", which is well documented in different glasses such as polymers,[32,33] glassy water[34] and metallic glasses,[26,35] obtained after a variety of thermo-mechanical histories.

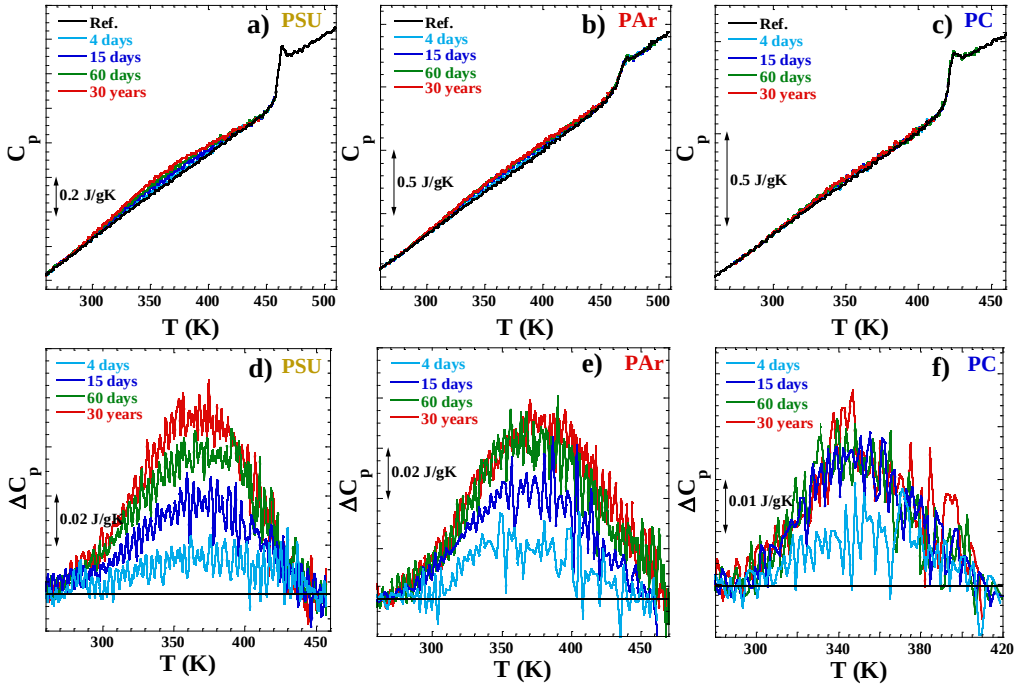

Figure 5.5 Upper Panels: Specific heat scans for samples aged at the indicated times at room temperature (296 K) and the unaged references. Lower Panels: The corresponding specific heats in excess to the unaged reference in the temperature range where the endothermic overshoot underlying enthalpy recovery is visible.

Data shown in Figure 5.5 were analyzed to evaluate the aging time evolution of T_f, obtained by integrating the specific heat capacity curves in accordance with the Moynihan method. The obtained results, that is, the evolution of T_f during structural recovery as a function of aging time, are shown in Figure 5.6 for all investigated polymer glasses. Data are plotted in terms of the departure from equilibrium, $T_f - T_a$ (T_a= 296 K). As a general observation, all the polymers that were aged at room temperature exhibit a monotonous decrease to a plateau after a time scale between 10^6 and 10^7 s. This means that the thermodynamic state of these glasses reached at T_a = 296 K evolves in the first few months and remains essentially unaltered until a time scale of about 30 years. In all cases, the T_f achieved at the plateau deviates from the aging

temperature by more than 100 K, implying that only a portion of the total recoverable enthalpy is actually recovered at the plateau.

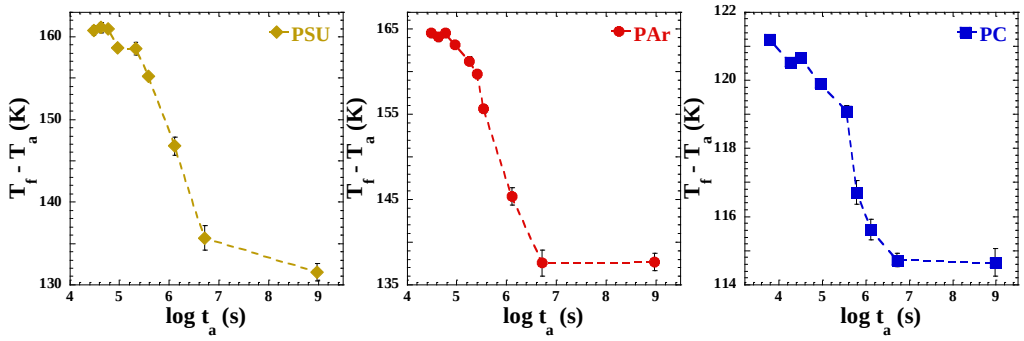

Figure 5.6 Evolution of fictive temperature T_f, during the storage at 296 K. Dashed lines are guides for the eye.

The most relevant result in the context of the present study is the presence of (at least) two mechanisms of equilibrium recovery. Figure 5.7 displays qualitatively the temperature dependence of the enthalpy of the investigated polymer glasses on the base of experimentally found behavior of the specific heat scans (see Figure 5.5). In particular, Figure 5.7 shows the existence of an intermediate equilibrium, corresponding to partial equilibrium recovery. This first plateau is in line with the aging time evolution of $T_f - T_a$, displayed in Figure 5.6, which indicates that the partial recovery of equilibrium is reached after about 10^7 s. Thus, this implies that, if in the case of the present study time scales longer than 30 years were employed, further decrease of enthalpy would likely be observed via the slow mechanism of equilibration until the complete equilibrium recovery.

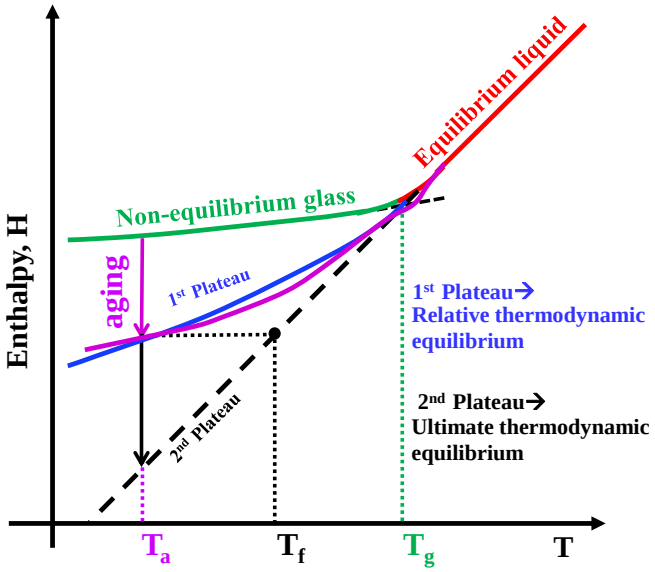

Figure 5.7 Schematic representation of the thermodynamic equilibria accessible upon aging a glass obtained from the equilibrium liquid. 1st plateau (blue solid line) represents the long-term aging state and 2nd plateau (black dashed line) represents the thermodynamic equilibrium of the supercooled liquid line. The way enthalpy is recovered (purple line) on heating from a state corresponding to the relative thermodynamic equilibrium with partial recovery, is also shown.

Given the fact that the time scale involved to reach the intermediate plateau is much shorter than that of the final one, heating above the aging temperature will result in an increase of the enthalpy. In other words, the initial step of devitrification takes place with an increase of the enthalpy toward the intermediate plateau. Furthermore, the broadening of the low temperature overshoot, longer than 100 K, can be understood if a low activation of the fast mechanism of equilibrium recovery is considered. Low values of the activation energy were found for the fast mechanism in bulk amorphous polymers,[19] thin films,[21] and in Chapter 4 for PS nanospheres. In this sense, Figure 5.6 shows how the presence of the fast mechanism of equilibrium recovery results in a T_f decrease as large as 30 K for PSU and PAr, while only

of 10 K for PC. In all cases, the decrease in T_f is significant and is observed far below T_g, that is, at temperatures where the slow mechanism of equilibration is expected to reach geological time scales given its large activation energy. Thus, our results indicate that in contrast with the conventional view of physical aging, massive decrease of the enthalpy toward equilibrium can be observed even at conditions at which the α relaxation is expected to be "frozen".

Finally, it is worth to point out that in order to observe experimentally detectable physical aging effects in bulk polymer glasses, in terms of excess in the specific heat capacity and T_f depression, several days are required as displayed in Figure 5.5 and Figure 5.6, respectively. However, as also discussed in Chapter 4, confined polymers exhibiting large amount of free interface,[36–38] essentially exhibit the same phenomenology but on shorter time scales.[20,21]. This allowed to access energy states with T_f corresponding to glasses with vanishing excess entropy;[20] a fact that was interpreted as a signature of the existence of the so-called "ideal" glass transition, long ago theorized by Gibbs and DiMarzio.[39]

5.4. CHAPTER SUMMARY

This study takes inspiration from recent findings showing the existence of multiple mechanisms of equilibrium recovery in different kinds of glasses. To achieve further insights on this issue, we have investigated the thermodynamic state of polymer glasses aged for about 30 years by DSC. These results were complemented with a wide range of additional results on the same polymers, aged from minutes to several months. Our results indicate that, the studied polymers age via a fast mechanism of equilibrium recovery. This conclusion has been reached after the following observations: (i) devitrification on heating begins at temperatures far below T_g, in a range where the mechanism associated to the α relaxation is expected to exhibit geological relaxation times and (ii) the plateaus in the enthalpy revoery exhibit T_f(s) vastly different from

the imposed T_a, indicating that such states correspond to a relative equilibrium. Altogether these results show how glasses with low energy could be accessed by exploiting the fast mechanism of equilibrium recovery. In this sense, it is important to highlight that the employment of confined polymer glasses with large amount of free interface, can provide a route to access low energy states in time scales shorter than the times required for bulk homologues.

Part of this chapter is published in *Phys. Chem. Chem. Phys.* **2018**; **DOI:** 10.1039/C8CP01940A. Communication

5.5. REFERENCES

(1) Ruta, B.; Pineda, E.; Evenson, Z. Relaxation Processes and Physical Aging in Metallic Glasses. *J. Phys. Condens. Matter* **2017**, *29* (50), 503002.

(2) Swallen, S. F.; Kearns, K. L.; Mapes, M. K.; Kim, Y. S.; McMahon, R. J.; Ediger, M. D.; Wu, T.; Yu, L.; Satija, S. Organic Glasses with Exceptional Thermodynamic and Kinetic Stability. *Science* **2007**, *315* (5810), 353–356.

(3) Golovchak, R.; Shpotyuk, O.; Kozdras, A.; Vlček, M.; Bureau, B.; Kovalskiy, A.; Jain, H. Long-Term Physical Ageing in As–Se Glasses with Short Chalcogen Chains. *J. Phys. Condens. Matter* **2008**, *20* (24), 245101.

(4) Hutchinson, J. M. Physical Aging of Polymers. *Prog. Polym. Sci.* **1995**, *20* (4), 703–760.

(5) Cangialosi, D.; Boucher, V. M.; Alegría, A.; Colmenero, J. Physical Aging in Polymers and Polymer Nanocomposites: Recent Results and Open Questions. *Soft Matter* **2013**, *9* (36), 8619–8630.

(6) Cangialosi, D. Dynamics and Thermodynamics of Polymer Glasses. *J. Phys. Condens. Matter* **2014**, *26* (15), 153101.

(7) Kovacs, A. J. Transition Vitreuse Dans Les Polymères Amorphes. Étude Phénoménologique. *Fortschr. Hochpolym. Forsch.* **1964**, *3*, 394− 507.

(8) Vogel, H. *Phys Zeit* **1921**, *22*, 645–646.

(9) Fulcher, G. S. *J. Am. Ceram. Soc.* **1925**, *8* (6), 339–355.

(10) Tammann, G.; Hesse, W. *Z. Für Anorg. Allg. Chem.* **1926**, *156* (1), 245–257.

(11) Narayanaswamy, O. S. A Model of Structural Relaxation in Glass. *J. Am. Ceram. Soc.* **1971**, *54* (10), 491–498.

(12) Moynihan, C. T.; Macedo, P. B.; Montrose, C. J.; Montrose, C. J.; Gupta, P. K.; DeBolt, M. A.; Dill, J. F.; Dom, B. E.; Drake, P. W.; Easteal, A. J.; et al. Structural Relaxation in Vitreous Materials. *Ann. N. Y. Acad. Sci.* **1976**, *279* (1), 15–35.

(13) Kovacs A. J.; Aklonis J. J.; Hutchinson J. M.; Ramos A. R. Isobaric Volume and Enthalpy Recovery of Glasses. II. A Transparent Multiparameter Theory. *J. Polym. Sci. Polym. Phys. Ed.* **1979**, *17* (7), 1097–1162.

(14) Tropin, T. V.; Schmelzer, J. W.; Aksenov, V. L. Modern Aspects of the Kinetic Theory of Glass Transition. *Phys.-Uspekhi* **2016**, *59* (1), 42.

(15) Grassia, L.; Koh, Y. P.; Rosa, M.; Simon, S. L. Complete Set of Enthalpy Recovery Data Using Flash DSC: Experiment and Modeling. *Macromolecules* **2018**, *51* (4), 1549–1558.

(16) Wimberger-Friedl, R.; de Bruin, J. G. The Very Long-Term Volume Recovery of Polycarbonate: Is Self-Retardation Finite? *Macromolecules* **1996**, *29* (14), 4992–4997.

(17) Robertson, C. G.; Wilkes, G. L. Long-Term Volume Relaxation of Bisphenol A Polycarbonate and Atactic Polystyrene. *Macromolecules* **2000**, *33* (11), 3954–3955.

(18) Pye, J. E.; Roth, C. B. Two Simultaneous Mechanisms Causing Glass Transition Temperature Reductions in High Molecular Weight Freestanding Polymer Films as Measured by Transmission Ellipsometry. *Phys. Rev. Lett.* **2011**, *107* (23), 235701.

(19) Daniele Cangialosi, V. M. B.; Angel Alegría, J. C. Direct Evidence of Two Equilibration Mechanisms in Glassy Polymers. *Phys. Rev. Lett.* **2013**, *111*, 095701.
(20) Boucher, V. M.; Cangialosi, D.; Alegria, A.; Colmenero, J. Reaching the Ideal Glass Transition by Aging Polymer Films. *Phys. Chem. Chem. Phys.* **2017**, *19* (2), 961–965.
(21) Boucher, V. M.; Cangialosi, D.; Alegría, A.; Colmenero, J. Complex Nonequilibrium Dynamics of Stacked Polystyrene Films Deep in the Glassy State. *J. Chem. Phys.* **2017**, *146* (20), 203312.
(22) Fan, J.; Cooper, E. I.; Angell, C. A. Glasses with Strong Calorimetric .Beta.-Glass Transitions and the Relation to the Protein Glass Transition Problem. *J. Phys. Chem.* **1994**, *98* (37), 9345–9349.
(23) Miller, R. S.; MacPhail, R. A. Ultraslow Nonequilibrium Dynamics in Supercooled Glycerol by Stimulated Brillouin Gain Spectroscopy. *J. Chem. Phys.* **1997**, *106* (8), 3393–3401.
(24) Golovchak, R.; Kozdras, A.; Balitska, V.; Shpotyuk, O. Step-Wise Kinetics of Natural Physical Ageing in Arsenic Selenide Glasses. *J. Phys. Condens. Matter* **2012**, *24* (50), 505106.
(25) Golovchak, R.; Kozdras, A.; Shpotyuk, O.; Balitska, V. Crossover between Cooperative and Fractal Relaxation in Complex Glass-Formers. *J. Phys. Condens. Matter* **2016**, *28* (35), 355101.
(26) Louzguine-Luzgin, D. V.; Seki, I.; Yamamoto, T.; Kawaji, H.; Suryanarayana, C.; Inoue, A. Double-Stage Glass Transition in a Metallic Glass. *Phys. Rev. B* **2010**, *81* (14), 144202.
(27) Gallino, I.; Cangialosi, D.; Evenson, Z.; Schmitt, L.; Hechler, S.; Stolpe, M.; Ruta, B. Hierarchical Aging Pathways and Reversible Fragile-to-Strong Transition upon Annealing of a Metallic Glass Former. *Acta Mater.* **2018**, *144* (Supplement C), 400–410.
(28) Wypych, G. *Handbook of Polymers*; Elsevier Science, 2016.
(29) Barón, M.; Hellwich, K.-H.; Hess, M.; Horie, K.; Jenkins, A. D.; Jones, R. G.; Kahovec, J.; Kratochvíl, P.; Metanomski, W. V.; Mormann, W.; et al. Glossary of Class Names of Polymers Based on Chemical Structure and Molecular Architecture (IUPAC Recommendations 2009). *Pure Appl. Chem.* **2009**, *81* (6), 1131–1186.
(30) Moynihan, C. T.; Easteal, A. J.; De Bolt, M. A.; Tucker, J. Dependence of the Fictive Temperature of Glass on Cooling Rate. *J. Am. Ceram. Soc.* **1976**, *59*, 12–16.
(31) Reading, M.; Hourston, D. J. *Modulated Temperature Differential Scanning Calorimetry: Theoretical and Practical Applications in Polymer Characterisation*; Springer, 2006.
(32) Hodge, I. M.; Berens, A. R. Effects of Annealing and Prior History on Enthalpy Relaxation in Glassy Polymers. 2. Mathematical Modeling. *Macromolecules* **1982**, *15* (3), 762–770.
(33) Johari, G. P. Comment on "Water's Second Glass Transition, K. Amann-Winkel, C. Gainaru, P. H. Handle, M. Seidl, H. Nelson, R. Böhmer, and T. Loerting, Proc. Natl. Acad. Sci. (U.S.) 110 (2013) 17720.", and the Sub-Tg Features of Pressure-Densified Glasses. *Thermochim. Acta* **2015**, *617*, 208–218.

(34) Amann-Winkel, K.; Gainaru, C.; Handle, P. H.; Seidl, M.; Nelson, H.; Böhmer, R.; Loerting, T. Water's Second Glass Transition. *Proc. Natl. Acad. Sci. U. S. A.* **2013**, *110* (44), 17720–17725.
(35) Chen, H. S.; Inoue, A.; Masumoto, T. Two-Stage Enthalpy Relaxation Behavior of (Fe0.5Ni0.5)83P17 and (Fe0.5Ni0.5)83B17 Amorphous Alloys upon Annealing. *J. Mater. Sci.* **1985**, *20* (7), 2417–2438.
(36) Napolitano, S.; Rotella, C.; Wübbenhorst, M. Can Thickness and Interfacial Interactions Univocally Determine the Behavior of Polymers Confined at the Nanoscale? *ACS Macro Lett.* **2012**, *1* (10), 1189–1193.
(37) Burroughs, M. J.; Napolitano, S.; Cangialosi, D.; Priestley, R. D. Direct Measurement of Glass Transition Temperature in Exposed and Buried Adsorbed Polymer Nanolayers. *Macromolecules* **2016**, *49*, 4647–4655.
(38) Perez-de-Eulate, N. G.; Sferrazza, M.; Cangialosi, D.; Napolitano, S. Irreversible Adsorption Erases the Free Surface Effect on the Tg of Supported Films of Poly(4-Tert-Butylstyrene). *ACS Macro Lett.* **2017**, *6* (4), 354–358.
(39) Gibbs, J. H.; DiMarzio, E. A. Nature of the Glass Transition and the Glassy State. *J. Chem. Phys.* **1958**, *28* (3), 373–383.

6

TUNING CONFINEMENT EFFECTS ON POLY(TERT-BUTYLSTYRENE) THIN FILMS

In the previous chapters, non-equilibrium has been studied in confined and bulk polymers below T_g. However, it is worth pointing out that non-equilibrium phenomena can also be relevant in the melt state of confined polymers, overall when they are supported on a substrate. In this chapter, we study these phenomena for polymer thin films supported on non-repulsive interfaces. Prolonged annealing in $T>>T_g$ allows modifying properties, as a result of polymer irreversible adsorption on the interface. Here, we show that the irreversible adsorbed layer can perturb and eventually erase the reduction in T_g. To verify this claim, we have determined the thickness and annealing time dependence of T_g for thin films of poly(4-tert-butyl styrene) (PTBS) with one free surface. Our results show that the shift in T_g and the manifestation of the free surface get reduced upon annealing in the liquid state, following the kinetics of irreversible adsorption.

6.1 INTRODUCTION

The discovery of Keddie *et al.*[1] that the glass transition temperature can deviate significantly from the bulk to nanoconfined polymer glass-formers, opened a new aspect of glassy behavior that continues to provide challenges for fundamental understanding.[2] Most of the work performed on nanoconfined polymers has been conducted on supported films, where layers thinner than 100 nm thickness (h) are deposited onto flat substrates, thus having one free surface.[3]

For supported thin polymer films, deviations in T_g with confinement could be interpreted to be a result of interfacial interactions between the polymer and the interface,[4,5] as introduced in Chapter 1. Thus, tuning the interfacial interactions between the substrate and the polymer, allows modifying the value of the T_g[6,7] of nanoconfined systems. Furthermore, reducing the thickness of the film, which corresponds to the inverse of the surface/volume ratio, enhances the deviation from bulk behavior, supporting the idea that confinement effects on T_g have an interfacial nature.[6] Several studies have moreover demonstrated a correlation between the number of chains irreversibly adsorbed on the supporting substrate and perturbation in T_g,[6,8] viscosity,[9] thermal expansion,[10] segmental dynamics,[11] crystallization,[12,13] dewetting,[14] and maximum water uptake.[15]

Focusing on the glass transition,[1,4,16,17] for supported films of polystyrene, which is the most widely investigated system, a T_g reduction is commonly observed for films thinner than 40 nm. In the case of PS, a drop by 10 K is reported for films as thin as 20 nm.[1] These results are commonly explained by the role of the free surface. However, the reduction in T_g is not only observed in supported or freestanding films, but also in capped films, where the chains at both interfaces are in direct contact with non-attractive solid mediums,[18–20] although at smaller extents compared to the above mentioned geometries. To explain these observations, the role of irreversible adsorption of a polymer onto the supporting interface must be recalled.

Irreversible polymer adsorption may already take place during solvent evaporation in dilute polymer solutions.[21] Subsequently, polymer adsorption can be enhanced by annealing well above T_g. The formation rate of that irreversible adsorbed layer at the interface between a solid substrate and a polymer melt, is generally described as a process of chain pinning via a first order reaction mechanism, which slows down at large surface coverage.[6,22,23] A competition between two driving mechanisms has been shown to drive polymer adsorption. The first mechanism is active at short annealing times,

when crowding at the available pinning sites on the interface is weak.[21] The second mechanism takes place when pinning new chains can only occur through the formation of loops, due to the scarcity of available sites. As a result of this limitation, the adsorption rate becomes logarithmic in time until the saturation of the adsorbed layer.[22]

Based on previous works,[6,22,24–26] the reduction of the T_g in thin films can be correlated to an excess in interfacial free volume[27] located either at the polymer/solid interface or at the free surface.[3,28–30] For the former case, such deviations from bulk T_g can be varied by modifying the degree of adsorption of polymer films onto the supporting interface.[7,31]

In this thesis, we successfully demonstrate that irreversible adsorption can also perturb, and eventually erase, the reduction in T_g imposed by the presence of a free surface. To verify this claim, we have determined the thickness and annealing time dependence of the T_g on thin film of poly(4-tert-butylstyrene) with one free surface. The selection of PTBS has been done since this polymer exhibits the largest depression in T_g upon confinement at the nanoscale level, for supported polymer films.[32] Our results show that the shift in T_g and the manifestation of the free surface get reduced upon annealing in the liquid state, following the kinetics of irreversible adsorption.

6.2 SAMPLES AND EXPERIMENTAL DETAILS

6.2.1. SAMPLES

6.2.1.1. Poly(4-tert-butylstyrene) (PTBS)

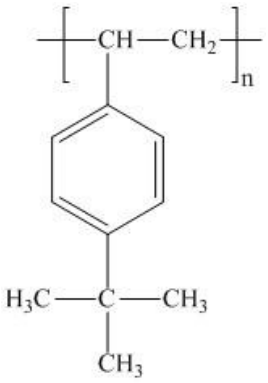

Figure 6.1 Sketch of the PTBS repeating unit

The poly(4-tert-butylstyrene) (PTBS), is a vinyl polymer, which differs from the repeat unit structure of PS by the addition of a tert-butyl group to the 4-carbon on the phenyl ring. PTBS repeating unit is depicted Figure 6.1. The polymer was purchased from Polymer Source Inc. and used as received (M_n = 70000 g/mol; M_w/M_n = 1.07) according to the manufacturer and used for the preparation of thin films. PTBS was dissolved at various concentrations in toluene (> 99.9% purity) purchased from Sigma-Aldrich.

6.2.1.2. Preparation of polymer thin films

Polymer thin films are bi-dimensional structures which can be prepared by physical vapor deposition,[33] laser ablation,[34] pulsed laser deposition,[35] matrix assisted pulsed evaporation[36] and spin coating.[37] All of these techniques allow the fabrication of thin films with the desired thickness. In this section we have used the spin coating technique, also known as spin casting, where a polymer solution is poured on top of a substrate. Afterwards, the substrate is spun at a certain speed for a specified time. During the spinning the polymer solvent

quickly evaporates and thin films are obtained. The final thickness and homogeneity of the film depend on the following factors: (i) the speed of rotation, (ii) the acceleration, (iii) the spinning time and (iv) the polymer concentration.[38]

Preparation of thin films

All the thin films were obtained through the WS-650-23 Spin Coater. Figure 6.2 shows the protocol followed for achieving different film thicknesses.

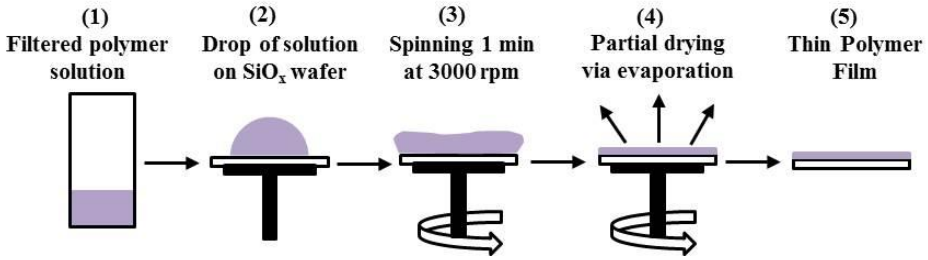

Figure 6.2 Spin coating scheme protocol

1. Firstly, a polymer solution in toluene is prepared in 15 mL disposable glass bottle. Afterwards, such solution is dissolved by means of a vortex mixer and filtered through a syringe into a new glass bottle.
2. A 2”-wide silicon wafer is deposited on top of the coating machine, where a drop of polymeric solution is poured on the top of the substrate with a complete covering.
3. Immediately after pouring the drop, rotation must be started. In this work, we have used a rotation speed of 3000 rpm for 1 minute and an acceleration of 3000 m/s^2.
4. It is important to start the rotation immediately after pouring the drop, in order to avoid early solvent evaporation, because it would result in

an increase of the solution viscosity, forming instabilities and leading to a non-homogenous film.[39–41]

5. Once the programmed specification is completed, a polymer thin film supported on a silicon wafer is formed.

To study the impact of thickness and thermal annealing on the T_g a series of samples with thickness ranging from 25 to 265 ± 1 nm were prepared. The 2" wide wafers were spin-coated with solutions of different concentrations and underwent a pre-annealing treatment of T_g^{bulk} + 5 K, which is larger than the $T_{boiling}$ of the solvent, for 1 min in order to ensure structural relaxation. Afterwards, the wafers were successfully cut in pieces and annealed at 453 K on a hot plate for different times ranging from 0 to 12 h, without any oxidation (see Figure A.4).

Preparation of adsorbed layers

To determine the formation of adsorbed layer and its kinetics, a 2"-wide silicon wafer was spin-coated with a ~200 ± 1 nm PTBS thick film, which was prepared from a 5 w/w % solution in toluene. The wafer was successively cut into smaller pieces, which were annealed for different times from 25 min to 32 hours at a fixed temperature T_{ANN} = 453 K (T_g^{bulk} + 50 K) on a hot plate. After annealing, films were soaked into toluene, that is, the same good solvent used for spin-coating, during 40 min following the Guiselin's experiment[42] and drained at room temperature for 10 min. Figure 6.3 displays the schematic protocol of this experiment.

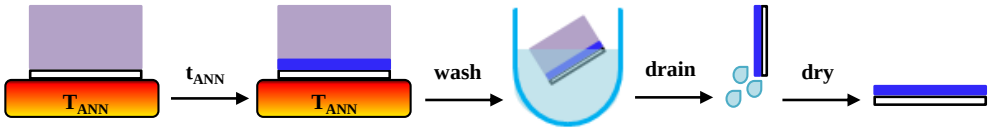

Figure 6.3 Schematic protocol of Guiselin's experiment.[22,42] Films (purple) anneal at T_{ANN}= 453 K for t_{ANN} from 25 min to 32 h to form the adsorbed layer (blue). Films were washed in toluene to get rid of the non-adsorbed layers.

Afterwards, the thickness of the adsorbed layer was determined via spectroscopic ellipsometry, as detailed in Chapter 2. The spectroscopic angle Ψ and Δ were fitted using a Cauchy model,[43] see Appedix section A.3.1, where the system was modeled considering multilayers: air/PTBS/SiO_x/Si (substrate). To reduce the number of fitting parameters, the thickness of the native oxide layer (SiO_x) was determined before spin-coating the polymer layer and kept fixed while fitting to the above mentioned multilayer model.

6.2.2. SPECTROSCOPIC ELLIPSOMETRY

Many prior studies have investigated thermal behavior of polymer films such as T_g and/or thermal expansion coefficient (α) using ellipsometry.[10,44–48] Specifically in our case, the thermal protocol used for the determination of thin films thermal T_g was achieved by using an external temperature controller and heating samples from 298 to 433 K at 2 K/min while acquiring the ellipsometric angles, as shown in Figure 6.4.

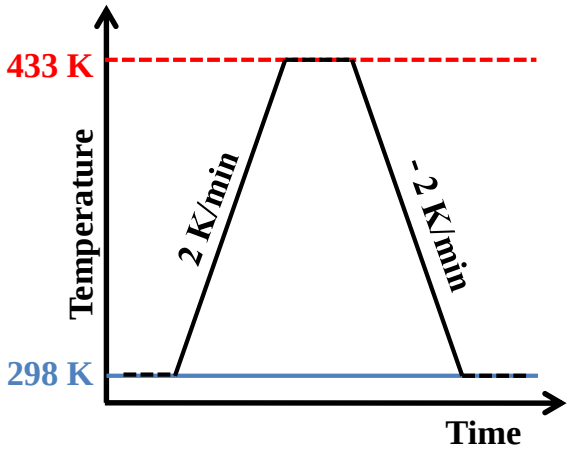

Figure 6.4 Schematization of the thermal protocol applied to PTBS thin films for the determination of thermal T_g by spectroscopic ellipsometry.

Linear fits of the $\Psi(T)$ data to glass and melt regimes were pursued by moving inwards the corresponding function in order to insure the best linear regression, as specified in Chapter 2 section 2.1.2.1.

6.3 RESULTS AND DISCUSSION

In this section, we will present the different results obtained via ellipsometry. In particular, thermal scans of the thin films used to study the impact of thickness and thermal annealing on the T_g will be presented. Furthermore, we will show results on the kinetics of formation of an adsorbed layer in the employed annealing conditions to determine the T_g.

6.3.1. FORMATION OF THE ADSORBED LAYER

To determine the kinetics of adsorption we have followed the procedure explained in section 6.2.1.2, and for a selected number of samples we also determined the thickness of the adsorbed layer by Atomic Force Microscopy (AFM). We used sharp tweezers to scrape the polymer layer from the silicon wafer. The film thickness was quantified as the height-step between the polymer and the substrate, as depicted in the left panel of Figure 6.5. A good agreement between the thickness values obtained via the two independent methods validates our model, as shown in the right panel of Figure 6.5.

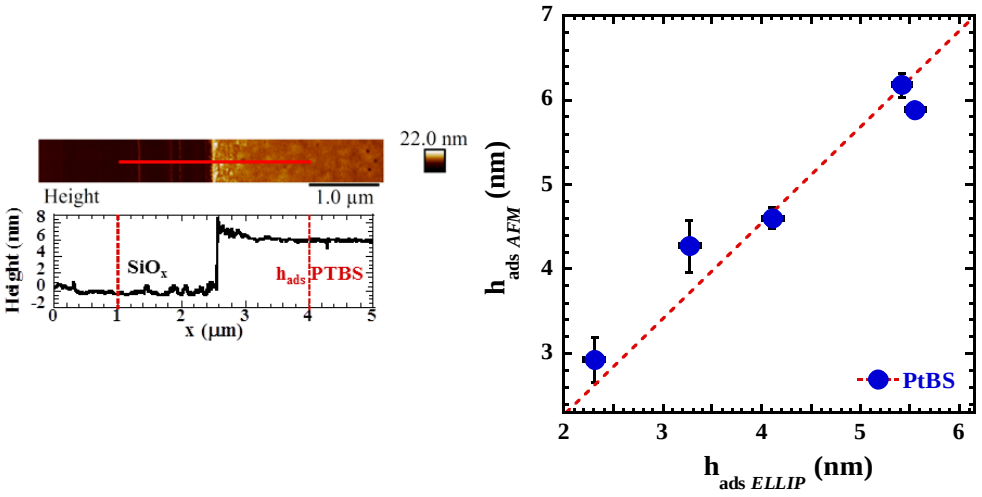

Figure 6.5 Left panel: AFM image of a scratched film with a thickness of 6 ± 1 nm after annealing 16 h at 453 K. Right panel: Comparison between the thicknesses of adsorbed layers determined by AFM (h_{adsAFM}) and ellipsometry ($h_{adsELLIP}$).

We remark that the thickness of the layers here determined, corresponds to the sum of the two sets of adsorbed chains populations indicated by Koga and coworkers,[49,50] where the assigned "flattened chains" constitute the inner higher density region of the adsorbed layers and the "loosely adsorbed polymer chains" the outer bulk-like density region.

6.3.2. IMPACT OF THICKNESS AND THERMAL ANNEALING ON Tg

Figure 6.6 shows the PTBS film thicknesses as a function of weight percent solution concentration, measured by spectroscopic ellipsometry. As can be observed, the film thickness increases in a non-linear way with the polymer concentration.

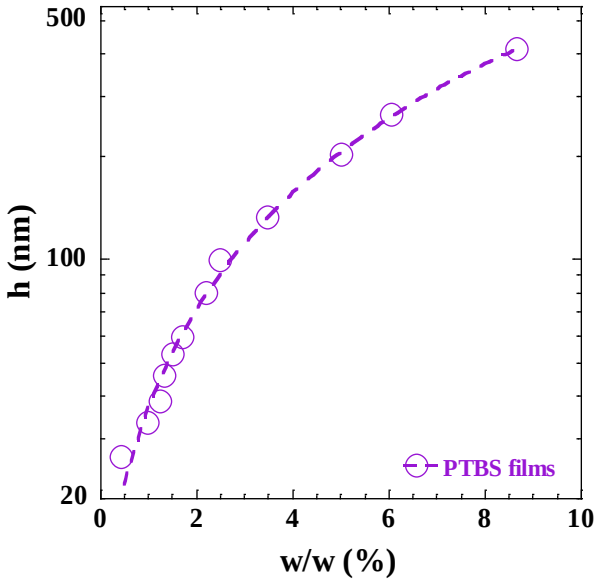

Figure 6.6 PTBS film thicknesses (*h*) as a function of weight percent concentration in toluene (w/w %). Dashed line is a third order polynomial fit for eye guiding.

As a preliminary characterization, PTBS T_g^{bulk} was determined by conventional DSC. Furthermore, spectroscopic ellipsometry was employed to measure the T_g of the thickest film. Figure 6.7 displays the specific heat scan of bulk PTBS, obtained on cooling at 10 K/min (left panel) and the temperature dependence of the thickness of a film with nominal thickness of 410 ± 1 nm (right panel). In both cases, the PTBS T_g^{bulk} is found around 404 ± 3 K.

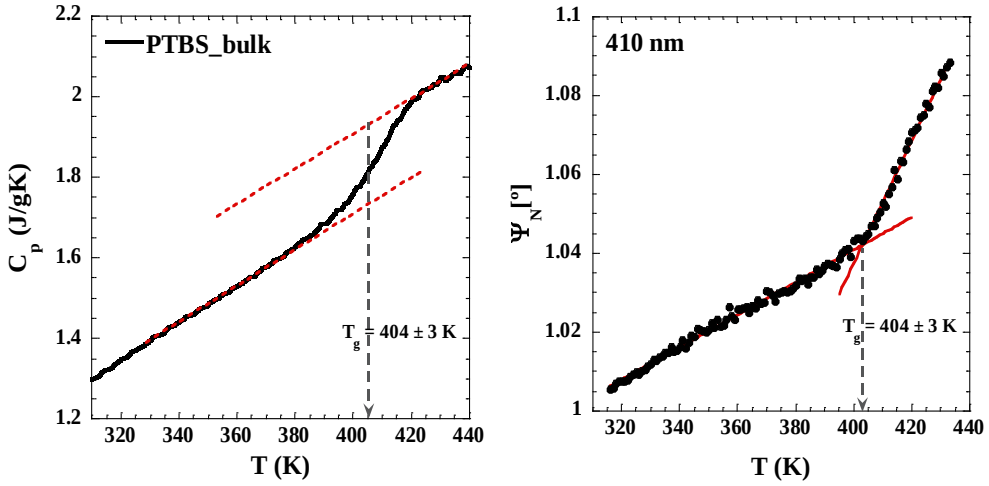

Figure 6.7 Left Panel: Heat capacity as a function of temperature for bulk PTBS cooled at 10 K/min. The temperature of the midpoint of the specific heat step was taken as the T_g value. The dashed red lines are the extrapolated melt and glass specific heats. Right Panel: Normalized ellipsometric angle Ψ taking as reference temperature 300 K as a function of temperature for a 410 nm PTBS thick film heated at 2 K/min. The crossover between melt and glass lines (red solid lines) was taken as the T_g value.

Previous investigations,[32] by temperature dependent fluorescence spectroscopy, showed deviations from bulk T_g already visible at thicknesses larger than 100 nm, and as large as 40 K lower than T_g^{bulk} for 25 nm thick films . Our results on PTBS are in perfect agreement with those results, as seen in Figure 6.8.

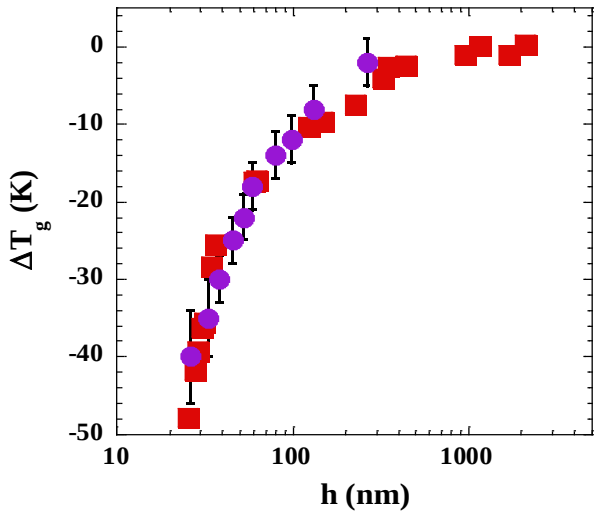

Figure 6.8 T_g for bulk and films of PTBS of different thickness prior to annealing at 453 K. Purple circles refer to measurements of the T_g as obtained via ellipsometry, while red squares are literature data from Ellison *et al.*[32] on pyrene doped PTBS films, investigated by temperature dependent fluorescence spectroscopy.

The effect of annealing for the investigated films in the melt state (T = 453 K) is presented in Figure 6.9, where the temperature dependence of the ellipsometric angle (Ψ) of films with thickness 265 and 25 nm, is presented. As can be observed, the T_g, taken as the kink in the temperature dependence of Ψ, significantly shifts to higher temperatures after annealing.

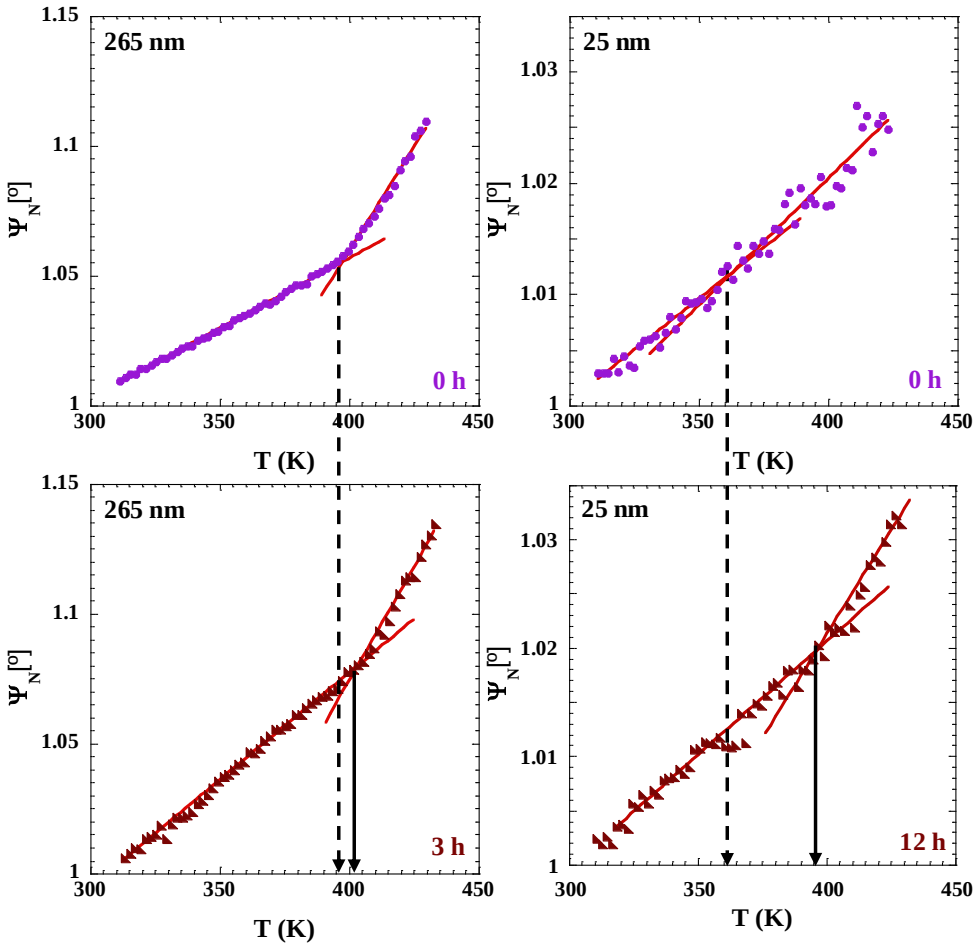

Figure 6.9 Comparison of the temperature dependence of the ellipsometric angle Ψ (at a wavelength of 600 nm, incidence angle of 70°) for films with thicknesses of 265 nm (left panels) and 25 nm (right panels) before and after annealing at 453 K.

A global picture of the effect of annealing on the thickness dependence of T_g is provided in Figure 6.10 for all investigated thicknesses and different annealing times.

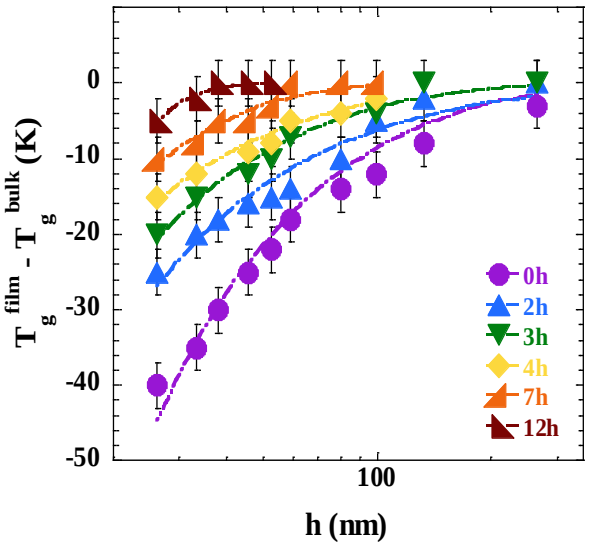

Figure 6.10 Shift in T_g as a function of film thickness and annealing time at 453 K. Dashed and dotted lines respectively represent the best fit to Eq. (6.1) with constant values of R_s (= 486 K) while keeping ξ_0 free, and constant values of ξ_0 (= 8.2 nm) while keeping R_s free.

Regardless of the thickness, the drop in T_g progressively decreases with annealing time. However, while films thicker than 40 nm exhibit complete recovery of the bulk value within moderate annealing times, for thinner films a reduction in T_g persists even after annealing for 12 h. At this point, it is important to check the integrity of the thinnest films after long annealing times. In particular, the possibility that such films dewet, as reported for other ultra-thin films,[51–53] must be discarded. Thus, we employed AFM to characterize the morphology of the thinnest investigated film (25 ± 1 nm). In particular, the integrity and uniformity of such film at the longest annealing times of 7 and 12 h were verified. The roughness of the film was analyzed considering the R_a parameter, which is the arithmetic average of the absolute

values of the surface height deviations measured from the mean plane. As observed in Figure 6.11, no indication of any kind of dewetting can be observed. As a matter of facts, in both cases the roughness of the sample was $R_a(t_{ANN}= 7\ h)= 0.48$ nm and $R_a(t_{ANN}= 12\ h)= 0.49$ nm, respectively.

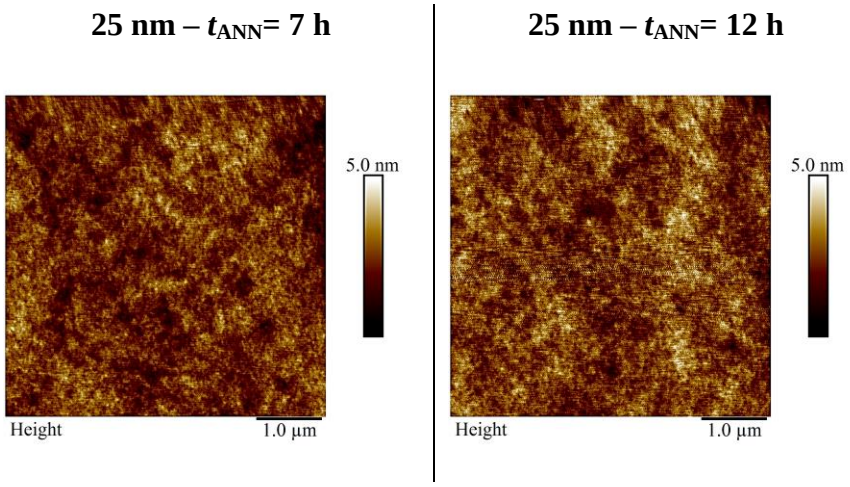

Figure 6.11 AFM height images of PTBS 25 ± 1 nm thin film: after 7 hours (left panel) and 12 hours (right panel) of annealing at 453 K.

To describe the effect of annealing on the thickness dependence of the T_g in PTBS thin films, we have employed a recent model presented by Forrest and Dalnoki-Veress:[54]

$$\frac{T_g(h) - T_g^{bulk}}{R_s - T_g^{bulk}} = \frac{1}{1 - \exp(h/2\xi_0)} \qquad (6.1)$$

The model allows rationalizing the shift in T_g with respect to the free surface via R_s, the so-called rheological temperature at the free interface. This parameter indicates the temperature at which a bulk melt system would exhibit the same mobility of the free surface, and ξ_0, the length scale associated with perturbation of the glass transition temperature. Though in its original form,

this model relies on a length scale of altered segmental mobility (ξ_0) responsible for T_g deviations, the same formalism can be maintained via different physical frameworks. For instance, as detailed in Chapter 3, experimental results[7,26,55] and theoretical approaches[25] showed that T_g deviations can be also related to the a perturbation in the amount of free interface not requiring alteration of the molecular mobility.[30,55,56] In accordance with these premises, fits in Figure 6.10 are calculated based on equation (6.1). We considered two equivalent approaches consisting of keeping, for each data set at constant annealing time, the values of ξ_0 or R_s constant, while allowing the variation of the other parameters. In analogy to previous work,[54] a reduction in T_g can be parametrized by imposing $R_s - T_g^{bulk} > 0$, which corresponds to a rheological temperature of the free surface higher than bulk T_g. We have furthermore considered values of $\xi_0 > 3.7$ nm, which is considerably larger than those found for PS, given the intrinsic difference in the extension of the liquid-like layer at the free surface for the two polymers, around 6 nm for the PS versus 10 nm for the PTBS.[57]

Given these premises, the amount of irreversible adsorbed layer was measured via ellipsometry on time scales ranging from 25 min to 32 h at 453 K for all investigated films.[6,22,23] Figure 6.12 shows how the annealing reduces in a similar manner the difference $R_s - T_g^{bulk}$ and the absolute value of ξ_0. This evidence implies that holding for a long time thin films above T_g significantly reduces, and for $h > 40$ nm totally inhibits, the confinement effects imposed by the free surface. At constant film thickness, the time evolution of $R_s - T_g^{bulk}$ and ξ_0 follows the same trend as $T_g(h) - T_g^{bulk}$.

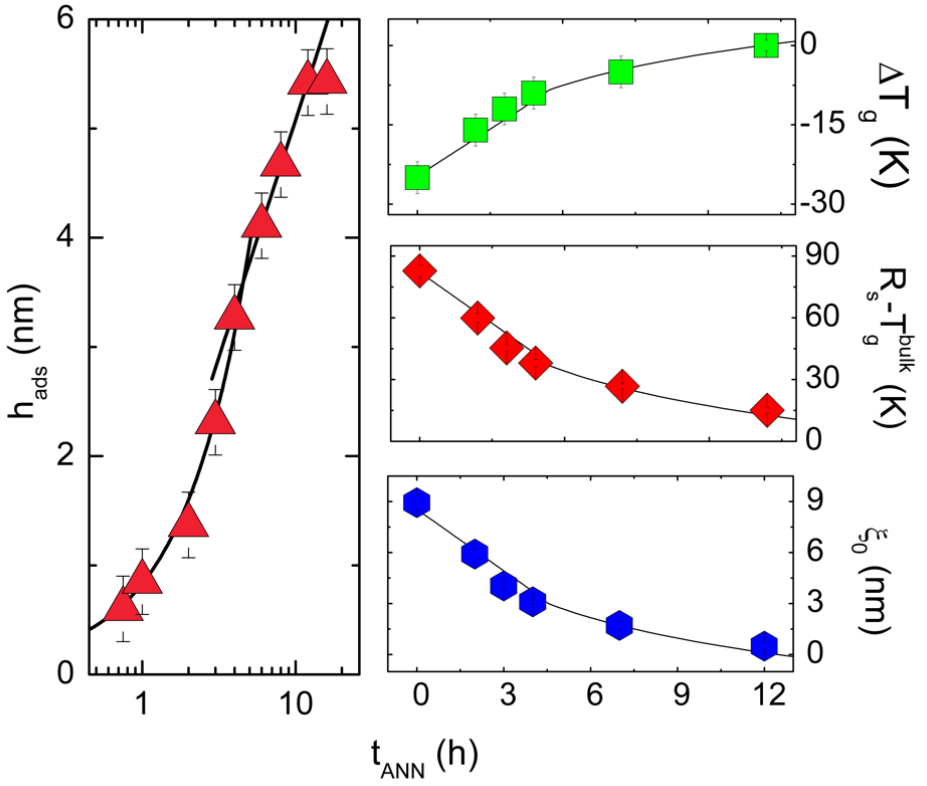

Figure 6.12 Left panel: Kinetics of irreversible adsorption for PTBS on SiO_2, solid lines are fit to the model proposed by Housmans *et al.*,[22] including a linear growth rate at short annealing times evolving in a logarithmic growth of the adsorbed amount at longer times. Right panel: Time evolution of the shift in T_g for 45 nm thick films (upper), the difference between the rheological temperature and bulk T_g (middle), and length scale of the extension of the free surface – (lower). The solid lines in the right panels are not fit to these data but traces of the kinetics of adsorption, adequately normalized between the values assumed by the plotted quantities during annealing.

For annealing protocols shorter than 5 h, these confinement effects linearly vanish with t_{ANN}, as shown in Figure 6.12. At longer annealing times, the recovery of bulk behavior slows down, becoming logarithmic, according to the analytical description of the kinetics of irreversible adsorption.[22]

In line with recent work, we speculated on a possible correlation between adsorbed amount and T_g shift proposed by Napolitano *et al.*[6] for PS films capped in aluminum layers. This relation, connecting structure and dynamics of polymer melts in the proximity of solid interfaces, has been validated by a large number of independent experimental investigations. Glynos *et al.*,[58] for example, verified that the link between shift in T_g and adsorbed amount is valid also in the case of star-shaped polymers, holding independently from molecular weight or functionality of the arms. Validity of the relation for exposed adsorbed layers is strongly supported by Burroughs *et al.*,[26] while Sun *et al.*[59] confirmed the exactness of this trend also for spin-coated films.

We have compared the time evolution of $\Delta T_g(t_{ANN})$, the time dependent deviation from bulk T_g upon annealing, with the kinetics of the irreversible adsorption within the same experimental conditions (see Figure 6.12). Excellent agreement between this independent data set validates our claims. This result implies that irreversible adsorption at the polymer/substrate interface limits or totally erases the impact of the free surface on the thermal T_g.

Evidence of the enslaving of the free surface to the behavior of molecules in direct contact with adsorbing interfaces, is not limited to the glass transition of polymeric thin films. Koga *et al.*[9] observed a neat reduction in tracer diffusivity of gold nanoparticles on the surface of 50 nm PS thick films annealed for time long enough to form stable adsorbed layers. These results indicate that the reduction in viscosity commonly observed at the free surface[60,61] (a 2-3 nm layer) can be suppressed or even reverted by adsorption of chains on far away interfaces. In this case, the presence of a 6 nm adsorbed layer at the supporting interfaces was able to turn the upper layer into an ultraviscous slab, with flow properties reduced in comparison to the bulk. Further work by Foster and coworkers[62] showed that the impact of adsorbing layer on the free surface extends up to 6-7 R_g in case of linear chains of PS, and even more, *e.g.* 14 R_g, for cyclic polymers.

Capponi *et al.*[63] observed a similar trend for the structural dynamics of glycerol, a low-molecular weight glass former. Enhanced mobility at the free surface was finally suppressed when this layer came into contact with the adsorbing interface. The molecular mechanisms behind the suppression of the free surface effect are not yet clear. Our experimental evidence shows that this process is relevant, and challenges the current picture on the glass transition in confinement.

Based on recent work,[64] we speculate that adsorption onto the supporting substrate, increases the barrier of diffusion of free volume holes at the free surface.[25,26,30] The upper layer in contact with air is often oversimplified as an infinite reservoir of free volume, which ensures a negative shift in the T_g of thin films. This conjecture might not be valid in proximity of irreversible adsorbed layers, whose impact on the vitrification of adjacent layers extends far beyond the volume occupied by monomers belonging to chains pinning into the substrate.[11] In this condition the free surface would lose its athermal liquid-like behavior and glassify together with the rest of the film, at bulk T_g.

6.4 CHAPTER SUMMARY

In this chapter we have used spectroscopic ellipsometry to explore non-equilibrium dynamics well above T_g of supported thin films based on PTBS. In particular, the kinetics of irreversible adsorption on the substrate was investigated. In the first section, we have explained how to prepare the confined polymeric thin films and the polymeric adsorbed layers onto a non-repulsive substrate. In the second section, we have investigated the impact of prolonged annealing in the liquid state on the T_g of thin films, resulting in a recovery of bulk behavior in almost all the confined levels. Furthermore, we provided insights on how the kinetics of the irreversible adsorbed layer affects the T_g in polymer thin films. Our experimental results demonstrate that, the recovery of bulk behavior and the manifestation of the free surface are correlated to the kinetics of irreversible adsorption of chains on the supporting substrate.

Part of this chapter is published in *ACS Macro Letters* **2017**; **DOI:** 10.1021/acsmacrolett.7b00129

6.5 REFERENCES

(1) Keddie, J. L.; Jones, R. A. L.; Cory, R. A. Size-Dependent Depression of the Glass Transition Temperature in Polymer Films. *Europhys. Lett.* **1994**, *27*, 59–64.
(2) Ediger, M. D.; Forrest, J. A. Dynamics near Free Surfaces and the Glass Transition in Thin Polymer Films: A View to the Future. *Macromolecules* **2014**, *47*, 471–478.
(3) Forrest, J. A.; Dalnoki-Veress, K. The Glass Transition in Thin Polymer Films. *Adv. Colloid Interface Sci.* **2001**, *94*, 167–195.
(4) Keddie, J. L.; Jones, R. A. L.; Cory, R. A. Interface and Surface Effects on the Glass-Transition Temperature in Thin Polymer Films. *Faraday Discuss.* **1994**, *98* (0), 219–230.

(5) Park, C. H.; Kim, J. H.; Ree, M.; Sohn, B.-H.; Jung, J. C.; Zin, W.-C. Thickness and Composition Dependence of the Glass Transition Temperature in Thin Random Copolymer Films. *Polymer* **2004**, *45* (13), 4507–4513.
(6) Napolitano, S.; Wübbenhorst, M. The Lifetime of the Deviations from Bulk Behaviour in Polymers Confined at the Nanoscale. *Nat. Commun.* **2011**, *2*, 260.
(7) Napolitano, S.; Rotella, C.; Wübbenhorst, M. Can Thickness and Interfacial Interactions Univocally Determine the Behavior of Polymers Confined at the Nanoscale? *ACS Macro Lett.* **2012**, *1* (10), 1189–1193.
(8) Panagopoulou, A.; Napolitano, S. Irreversible Adsorption Governs the Equilibration of Thin Polymer Films. *Phys. Rev. Lett.* **2017**, *119* (9), 097801.
(9) Koga, T.; Jiang, N.; Gin, P.; Endoh, M. K.; Narayanan, S.; Lurio, L. B.; Sinha, S. K. Impact of an Irreversibly Adsorbed Layer on Local Viscosity of Nanoconfined Polymer Melts. *Phys. Rev. Lett.* **2011**, *107*, 225901–225905.
(10) Braatz, M.-L.; Infantas, L.; Sferrazza, M.; Napolitano, S. Unexpected Impact of Irreversible Adsorption on Thermal Expansion: Adsorbed Layers Are Not That Dead. *J. Chem. Phys.* **2017**, *146*, 203304–203307.
(11) Carrillo, J.-M. Y.; Cheng, S.; Kumar, R.; Goswami, M.; Sokolov, A. P.; Sumpter, B. G. Untangling the Effects of Chain Rigidity on the Structure and Dynamics of Strongly Adsorbed Polymer Melts. *Macromolecules* **2015**, *48*, 4207–4219.
(12) Spiece, J.; Martinez-Tong, D. E.; Sferrazza, M.; Nogales, A.; Napolitano, S. Are Polymers Glassier upon Confinement? *Soft Matter* **2015**, *11* (31), 6179–6186.
(13) Jeong, H.; Napolitano, S.; Arnold, C. B.; Priestley, R. D. Irreversible Adsorption Controls Crystallization in Vapor-Deposited Polymer Thin Films. *J. Phys. Chem. Lett.* **2017**, *8* (1), 229–234.
(14) Jiang, N.; Sendogdular, L.; Di, X.; Sen, M.; Gin, P.; Endoh, M. K.; Koga, T.; Akgun, B.; Dimitriou, M.; Satija, S. Effect of CO2 on a Mobility Gradient of Polymer Chains near an Impenetrable Solid. *Macromolecules* **2015**, *48*, 1795–1803.
(15) Nguyen, H. K.; Labardi, M.; Lucchesi, M.; Rolla, P.; Prevosto, D. Plasticization in Ultrathin Polymer Films: The Role of Supporting Substrate and Annealing. *Macromolecules* **2013**, *46*, 555–561.
(16) Forrest, J. A.; Dalnoki-Veress, K.; Stevens, J. R.; Dutcher, J. R. Effect of Free Surfaces on the Glass Transition Temperature of Thin Polymer Films. *Phys. Rev. Lett.* **1996**, *77*, 2002–2005.
(17) Zhang, C.; Guo, Y.; Priestley, R. D. Glass Transition Temperature of Polymer Nanoparticles under Soft and Hard Confinement. *Macromolecules* **2011**, *44*, 4001–4006.
(18) Fukao, K.; Koizumi, H. Glassy Dynamics in Thin Films of Polystyrene. *Phys. Rev. E* **2008**, *77* (2), 021503.
(19) Boucher, V. M.; Cangialosi, D.; Yin, H.; Schönhals, A.; Alegría, A.; Colmenero, J. T g Depression and Invariant Segmental Dynamics in Polystyrene Thin Films. *Soft Matter* **2012**, *8* (19), 5119–5122.
(20) Napolitano, S.; Capponi, S.; Vanroy, B. Glassy Dynamics of Soft Matter under 1D Confinement: How Irreversible Adsorption Affects Molecular Packing, Mobility Gradients and Orientational Polarization in Thin Films. *Eur. Phys. J. E* **2013**, *36* (6), 61.

(21) O'Shaughnessy, B.; Vavylonis, D. Irreversibility and Polymer Adsorption. *Phys. Rev. Lett.* **2003**, *90* (5), 056103.
(22) Housmans, C.; Sferrazza, M.; Napolitano, S. Kinetics of Irreversible Chain Adsorption. *Macromolecules* **2014**, *47*, 3390–3393.
(23) Nieto Simavilla David; Panagopoulou Anna; Napolitano Simone. Characterization of Adsorbed Polymer Layers: Preparation, Determination of the Adsorbed Amount and Investigation of the Kinetics of Irreversible Adsorption. *Macromol. Chem. Phys.* **2017**, *219* (3), 1700303.
(24) Zhao, J.; Granick, S. How Polymer Surface Diffusion Depends on Surface Coverage. *Macromolecules* **2007**, *40*, 1243–1247.
(25) Napolitano, S.; Cangialosi, D. Interfacial Free Volume and Vitrification: Reduction in Tg in Proximity of an Adsorbing Interface Explained by the Free Volume Holes Diffusion Model. *Macromolecules* **2013**, *46*, 8051–8053.
(26) Burroughs, M. J.; Napolitano, S.; Cangialosi, D.; Priestley, R. D. Direct Measurement of Glass Transition Temperature in Exposed and Buried Adsorbed Polymer Nanolayers. *Macromolecules* **2016**, *49*, 4647–4655.
(27) White, R. P.; Lipson, J. E. G. Polymer Free Volume and Its Connection to the Glass Transition. *Macromolecules* **2016**, *49*, 3987–4007.
(28) Ellison, C. J.; Torkelson, J. M. The Distribution of Glass-Transition Temperatures in Nanoscopically Confined Glass Formers. *Nat. Mater.* **2003**, *2* (10), 695.
(29) Sharp, J. S.; Teichroeb, J. H.; Forrest, J. A. The Properties of Free Polymer Surfaces and Their Influence on the Glass Transition Temperature of Thin Polystyrene Films. *Eur. Phys. J. E* **2004**, *15*, 473–487.
(30) Cangialosi, D.; Alegría, A.; Colmenero, J. Effect of Nanostructure on the Thermal Glass Transition and Physical Aging in Polymer Materials. *Prog. Polym. Sci.* **2016**, *54–55* (Supplement C), 128–147.
(31) Yin, H.; Cangialosi, D.; Schönhals, A. Glass Transition and Segmental Dynamics in Thin Supported Polystyrene Films: The Role of Molecular Weight and Annealing. *Thermochim. Acta* **2013**, *566* (Supplement C), 186–192.
(32) Ellison, C. J.; Mundra, M. K.; Torkelson, J. M. Impacts of Polystyrene Molecular Weight and Modification to the Repeat Unit Structure on the Glass Transition−Nanoconfinement Effect and the Cooperativity Length Scale. *Macromolecules* **2005**, *38*, 1767–1778.
(33) Usui, H. Preparation of Polymer Thin Films by Physical Vapor Deposition. In *Functional Polymer Films*; Wiley-VCH Verlag GmbH & Co. KGaA, 2011; pp 287–318.
(34) Blanchet, G. B.; Fincher, C. R.; Jackson, C. L.; Shah, S. I.; Gardner, K. H. Laser Ablation and the Production of Polymer Films. *Science* **1993**, *262* (5134), 719–721.
(35) Eason, R. *Pulsed Laser Deposition of Thin Films: Applications-Led Growth of Functional Materials*; Wiley, 2007.
(36) Piqué, A.; McGill, R. A.; Chrisey, D. B.; Leonhardt, D.; Mslna, T. E.; Spargo, B. J.; Callahan, J. H.; Vachet, R. W.; Chung, R.; Bucaro, M. A. Growth of Organic Thin Films by the Matrix Assisted Pulsed Laser Evaporation (MAPLE) Technique. *Thin Solid Films* **1999**, *355*, 536–541.

(37) Lawrence, C. J. The Mechanics of Spin Coating of Polymer Films. *Phys. Fluids* **1988**, *31* (10), 2786–2795.
(38) Schubert, D. W.; Dunkel, T. Spin Coating from a Molecular Point of View: Its Concentration Regimes, Influence of Molar Mass and Distribution. *Mater. Res. Innov.* **2003**, *7* (5), 314–321.
(39) Skrobis, K. J.; Denton, D. D.; Skrobis, A. V. Effect of Early Solvent Evaporation on the Mechanism of the Spin-coating of Polymeric Solutions. *Polym. Eng. Amp Sci.* **1990**, *30* (3), 193–196.
(40) Strawhecker, K. E.; Kumar, S. K.; Douglas, J. F.; Karim, A. The Critical Role of Solvent Evaporation on the Roughness of Spin-Cast Polymer Films. *Macromolecules* **2001**, *34* (14), 4669–4672.
(41) Schaefer, C.; Michels, J. J.; van der Schoot, P. Structuring of Thin-Film Polymer Mixtures upon Solvent Evaporation. *Macromolecules* **2016**, *49* (18), 6858–6870.
(42) O. Guiselin. Irreversible Adsorption of a Concentrated Polymer Solution. *Europhys. Lett.* **1991**, *17* (3), 225–230.
(43) Jenkins, F. A.; White, H. E. *Fundamentals of Optics*; International student edition; McGraw-Hill, 1976.
(44) Kawana, S.; Jones, R. A. L. Character of the Glass Transition in Thin Supported Polymer Films. *Phys. Rev. E* **2001**, *63* (2), 021501.
(45) Singh, L.; Ludovice, P. J.; Henderson, C. L. Influence of Molecular Weight and Film Thickness on the Glass Transition Temperature and Coefficient of Thermal Expansion of Supported Ultrathin Polymer Films. *Thin Solid Films* **2004**, *449* (1), 231–241.
(46) Campbell, C. G.; Vogt, B. D. Examination of the Influence of Cooperative Segmental Dynamics on the Glass Transition and Coefficient of Thermal Expansion in Thin Films Probed Using Poly(n-Alkyl Methacrylate)S. *Polymer* **2007**, *48* (24), 7169–7175.
(47) Lan, T.; Torkelson, J. M. Fragility-Confinement Effects: Apparent Universality as a Function of Scaled Thickness in Films of Freely Deposited, Linear Polymer and Its Absence in Densely Grafted Brushes. *Macromolecules* **2016**, *49* (4), 1331–1343.
(48) Zhang, L.; Elupula, R.; Grayson, S. M.; Torkelson, J. M. Suppression of the Fragility-Confinement Effect via Low Molecular Weight Cyclic or Ring Polymer Topology. *Macromolecules* **2017**, *50* (3), 1147–1154.
(49) Gin, P.; Naisheng, J.; Liang, C.; Taniguchi, T.; Bulent, A.; K. Satija, S.; K. Endoh, M.; Koga, T. Revealed Architectures of Adsorbed Polymer Chains at Solid-Polymer Melt Interfaces. *Phys. Rev. Lett.* **2012**, *109*, 265501–265505.
(50) Jiang, N.; Shang, J.; Di, X.; Endoh, M. K.; Koga, T. Formation Mechanism of High-Density, Flattened Polymer Nanolayers Adsorbed on Planar Solids. *Macromolecules* **2014**, *47* (8), 2682–2689.
(51) Reiter, G. Dewetting of Thin Polymer Films. *Phys. Rev. Lett.* **1992**, *68* (1), 75–78.
(52) Reiter, G. Dewetting of Highly Elastic Thin Polymer Films. *Phys. Rev. Lett.* **2001**, *87* (18), 186101.
(53) Damman, P.; Gabriele, S.; Coppée, S.; Desprez, S.; Villers, D.; Vilmin, T.; Raphaël, E.; Hamieh, M.; Akhrass, S. A.; Reiter, G. Relaxation of Residual Stress and Reentanglement of Polymers in Spin-Coated Films. *Phys. Rev. Lett.* **2007**, *99* (3), 036101.

(54) Forrest, J. A.; Dalnoki-Veress, K. When Does a Glass Transition Temperature Not Signify a Glass Transition? *ACS Macro Lett.* **2014**, *3* (4), 310–314.
(55) Perez-de-Eulate, N. G.; Di Lisio, V.; Cangialosi, D. Glass Transition and Molecular Dynamics in Polystyrene Nanospheres by Fast Scanning Calorimetry. *ACS Macro Lett.* **2017**, *6* (8), 859–863.
(56) Priestley, R. D.; Cangialosi, D.; Napolitano, S. On the Equivalence between the Thermodynamic and Dynamic Measurements of the Glass Transition in Confined Polymers. *J. Non-Cryst. Solids* **2015**, *407*, 288–295.
(57) Paeng, K.; Ediger, M. D. Molecular Motion in Free-Standing Thin Films of Poly(Methyl Methacrylate), Poly(4-Tert-Butylstyrene), Poly(α-Methylstyrene), and Poly(2-Vinylpyridine). *Macromolecules* **2011**, *44*, 7034–7042.
(58) Glynos, E.; Frieberg, B.; Chremos, A.; Sakellariou, G.; Gidley, D. W.; Green, P. F. Vitrification of Thin Polymer Films: From Linear Chain to Soft Colloid-like Behavior. *Macromolecules* **2015**, *48*, 2305–2312.
(59) Sun, S.; Xu, H.; Han, J.; Zhu, Y.; Zuo, B.; Wang, X.; Zhang, W. The Architecture of the Adsorbed Layer at the Substrate Interface Determines the Glass Transition of Supported Ultrathin Polystyrene Films. *Soft Matter* **2016**, *12*, 8348–8358.
(60) Yang, Z.; Fujii, Y.; Lee, F. K.; Lam, C.-H.; Tsui, O. K. C. Glass Transition Dynamics and Surface Layer Mobility in Unentangled Polystyrene Films. *Science* **2010**, *328*, 1676–1679.
(61) Chai, Y.; Salez, T.; McGraw, J. D.; Benzaquen, M.; Dalnoki-Veress, K.; Raphaël, E.; Forrest, J. A. A Direct Quantitative Measure of Surface Mobility in a Glassy Polymer. *Science* **2014**, *343*, 994.
(62) He, Q.; Narayanan, S.; Wu, D. T.; Foster, M. D. Confinement Effects with Molten Thin Cyclic Polystyrene Films. *ACS Macro Lett.* **2016**, *5*, 999–1003.
(63) Capponi, S.; Napolitano, S.; Behrnd, N. R.; Couderc, G.; Hulliger, J.; Wübbenhorst, M. Structural Relaxation in Nanometer Thin Layers of Glycerol. *J. Phys. Chem. C* **2010**, *114*, 16696–16699.
(64) Tito, N. B.; Lipson, J. E. G.; Milner, S. T. Lattice Model of Mobility at Interfaces: Free Surfaces, Substrates, and Bilayers. *Soft Matter* **2013**, *9*, 9403–9413.

7

CONCLUSIONS

The general purpose of this thesis has been to reach a deep understanding of the thermodynamic processes that influence the glass transition in amorphous materials based on polymers. The science of the glassy state is still being a field of continuous research, where numerous theories try to explain the origin of molecular mobility and the connection with the phenomenon known as the glass transition. With this aim, we have presented a detailed study of different aspects of the glass transition in confined polymeric glasses by combining calorimetric techniques, from conventional to Fast Scanning Calorimetry (FSC), and other thermal and optical analysis.

Throughout the different chapters, polymer glasses confined in one and three dimensions (*i.e.* thin films and nanospheres) have been produced in order to study their physical properties from a fundamental point of view.

Firstly, it is important to mention that there has been an intense research activity focused on the distinctive seal of glassy materials: the transition from liquid to glass or vitrification. It is believed that the vitrification and the molecular mobility are manifestations of the same phenomenon. Our calorimetric results in polystyrene (PS) nanospheres have allowed us to obtain information about both, glass transition temperature (T_g) and molecular mobility, in terms of the fictive temperature (T_f) and the characteristic relaxation time (τ), respectively. These experiments have revealed a decoupling between these two aspects of the glass dynamics in samples prepared in identical conditions. Therefore, the equivalence between

vitrification and glass dynamics previously exposed to bulk amorphous polymers could not be considered in such a way for confined systems. This result implies that other factors, such as the geometric ones associated with confinement, are of utmost importance.

Furthermore, PS nanospheres have exhibited similarities with thin films with weak interactions polymer-substrate and freestanding films, in term of deviations in T_g and rate of physical aging. In particular, such systems, due to the high free surface area are able to maintain the thermodynamic equilibrium more efficiently than their unconfined counterparts. Therefore, they can access lower energy states otherwise not easily accessible in bulk systems, because of the long time scales required for reaching the thermodynamic equilibrium. By means of aging measurements below T_g, a complex recovery behavior of the thermodynamic properties has been observed, supporting the existence of multiple equilibrium recovery mechanisms at different time scales.

Moreover, in order to get establish an analogy between confined and bulk polymers, long-term physically aged amorphous polymers have been studied. By monitoring the physical aging at room temperature (R.T.) of bulk polymers with $T_g >>> T_{R.T.}$ for times up to tens of years, we have been able to corroborate the presence of those different mechanisms of enthalpy recovery, already seen in our nanospheres at relatively shorter times. This result reveals the universality of the complex nature of thermodynamic equilibrium present in glassy materials.

Apart from the kinetics of equilibrium recovery of glassy polymers below T_g, non-equilibrium effects above T_g have been considered too. To this aim, poly(tert-butylstyrene) (PTBS) thin films supported onto a substrate with weak interactions, have been employed to study the T_g by means of ellipsometric spectroscopy. In this study the importance of the adsorbed layer between the polymer and substrate has been highlighted. Moreover, it has been set the amount of free interfacial area, unslaved by an underlying adsorbing layer, as

the key factor in determining the enhanced efficiency of these systems to stay in thermodynamic equilibrium.

Finally, it is shown that exploring nanostructured polymer glasses allow us to access time scales amenable to the normal practice of the experimental work. Besides, the most significant and intriguing prospects of this work are the new possibilities opened by FSC. This technique allowed us to access very short time scales, by the application of high cooling/heating rates in the order of ~ 1000 K/s, enhancing the out-of-equilibrium dynamics not accessible until today. Furthermore, it is possible to obtain the structural relaxation kinetics, the fictive temperature, and the relaxation map, similar to the one obtained from purely relaxation techniques (*e.g.* dielectric spectroscopy), and provide information on the molecular dynamics of the studied systems. It is important to remark that, apart from the study of our simply model based on PS nanospheres, further investigation of other glassy polymers confined at lower nanoscale levels are required in order to understand how the role of chain conformations affect the glass transition.

APPENDIX

A.1. CHAPTER 3 – Vitrification and Molecular Mobility in Polystyrene Nanospheres and in Bulk

A.1.1. SAMPLES MORPHOLOGY

Sample masses were taken approximately in between from 100 to 500 ng and calculated based on the analysis of heat flow jump (ΔHF) at 373 K as shown from the heating scans at 1000 K/s in Figure A.1.[1] These results are summarized in Table A.1.

Table A.1 Obtained masses for all the studied PS systems calculated from the ΔHF.

System	*Mass (± 5 ng)*
Bulk	200
500 nm	500
320 nm	100
230 nm	100

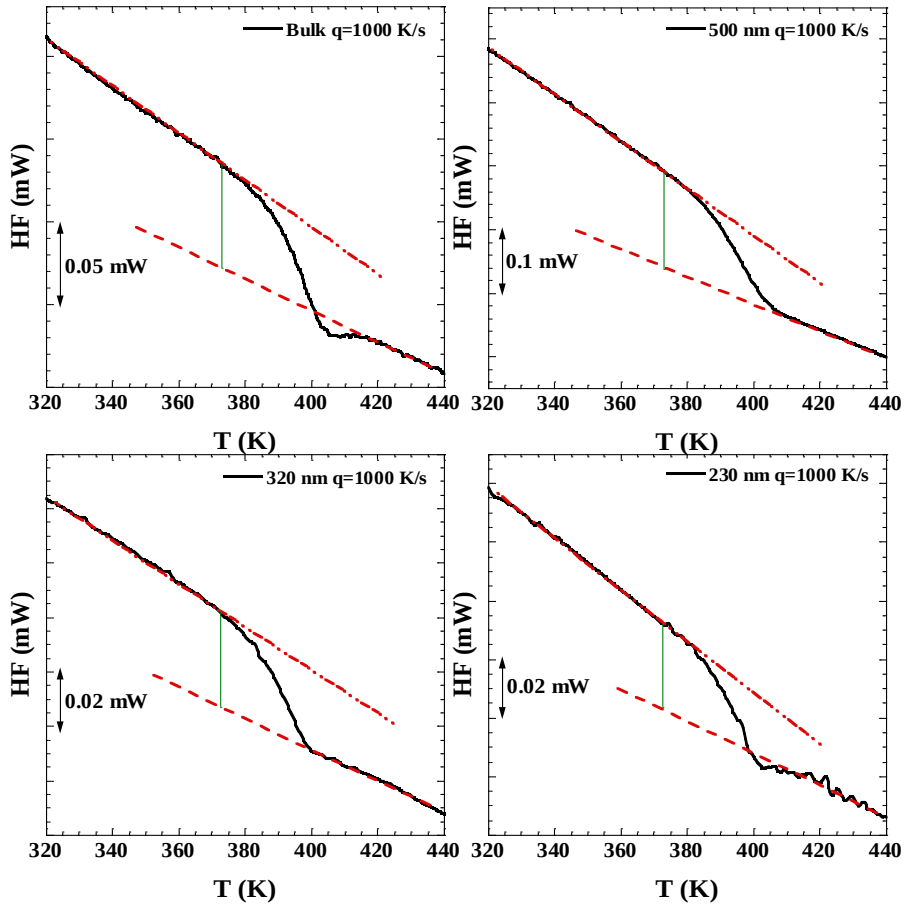

Figure A.1 Flash DSC 1 heat flow heating scans for bulk PS and 500-320-230 nm diameter PS nanospheres performed on heating at 1000 K/s after cooling at 1000 K/s. Red dashed lines correspond to the melt heat flow line and red dashed dotted lines to the glass heat flow line.

All the masses and thicknesses of PDMS layer in each chip configuration PS nanospheres/PDMS were calculated from the following equations (A.1) and (A.2). Table A.2 summarizes the obtained values.

$$m = \frac{\Delta H_{FDSC}}{\Delta h q} \quad \text{(A.1)}$$

$$h = \frac{m}{\rho \pi (d/2)^2} \quad \text{(A.2)}$$

where ΔH_{FDSC} is the enthalpy of the melting peak area; Δh is the specific enthalpy of melting, taken form the ATHAS data bank;[2] q is the cooling rate; h is the thickness; ρ is the density; d is the sample diameter, which corresponds to the diameter of the chip (0.5 mm).

Table A.2 PDMS masses on the chip membrane for 500, 320 and 230 nm PS nanospheres after an isotherm of 30 minutes at T= 173 K and q=1000 K/s

Sample	ΔH_{FDSC} (mJ/s)	*Mass* (ng)	*Thickness, h* (nm)
500 nm	29.42	2.4	19.8
320 nm	33.6	2.74	22.6
230 nm	26.97	2.2	18.1

A.2. CHAPTER 5 – Very long-term physical aging of glassy polymers

A.2.1. SIZE – EXCLUSION CHROMATOGRAFY (SEC / MALLS)

Figure A.2 shows the SEC/MALLS traces for bulk polymers of PSU, PAr and PC using as an eluent at a flow rate of 1 mL/min. All the solutions were prepared at 4 mg/ml in THF.

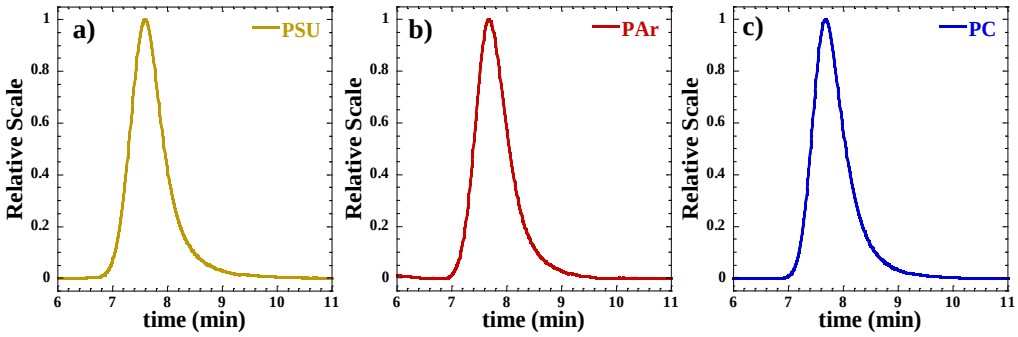

Figure A.2 Illustration of the Relative Scale of SEC/MALLS traces for a) Poly(arylate) (PAr); b) Poly(carbonate) (PC); c) Poly(sulfone) (PSU) as a function of the retention time in minutes.

A.2.2. SPECIFIC HEAT CAPACITY

Figure A.3 shows the specific heat capacity at T_g for PSU, PAr and PC samples. The specific heat capacity jump (Δc_p) was calculated at T_g, obtained from the half-height between the melt and glass lines.

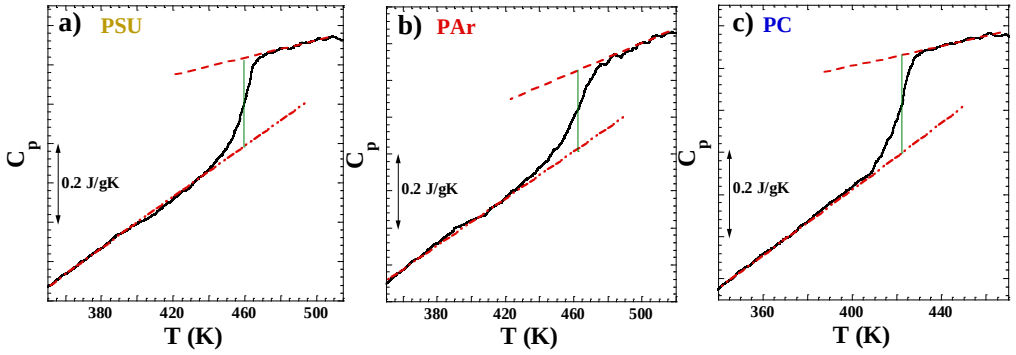

Figure A.3 *Standard* DSC specific heat capacity scans for PSU, PAr and PC performed on cooling at 20 K/min. Red dashed lines correspond to the melt specific heat line and red dashed dotted lines to the glass specific heat line.

A.3. CHAPTER 6 – Tuning confinement effects on PTBS thin films

A.3.1. CAUCHY EQUATION

Cauchy's equation is an empirical relationship between the refractive index and the wavelength of light for a particular transparent material. Three parameters (*A*, *B* and *C*) are used in the equation (A.3) for the Cauchy transparent model.[3]

$$n = A + \frac{B}{\lambda^2} + \frac{C}{\lambda^4} \qquad \text{(A.3)}$$

where *A*, *B* and *C* are the characteristic constants that describe the refractive index of the substance. In this case, we have employed the Cauchy model values belonging to PS in order to fit the ellipsometric angles (Ψ and Δ) of PTBS. Table A.3 shows the *A*, *B* and *C* employed values.

Table A.3 Cauchy transparent model parameters for polystyrene

	A	*B*	*C*
PS	1.5897330	-0.6218504	1.7228140

A is a dimensionless parameter; *B* (nm^2) affects the curvature and the amplitude of the refractive index for medium wavelengths in the visible; *C* (nm^4) affects the curvature and amplitude for smaller wavelengths in the ultraviolet.[4]

A.3.2. POLY(TERT-BUTYLSTYRENE) THERMAL STABILITY

Figure A.4 shows thermogravimetric (TG) analysis of PTBS under different atmospheric conditions. These experiments were performed in order to check the stability of PTBS under the imposed annealing protocol in the open air at 453 K. As can be observed from the weight loss analysis of Figure A.4, under

air atmosphere, that is, oxidative conditions, no degradation is observed until ~ 550 K.

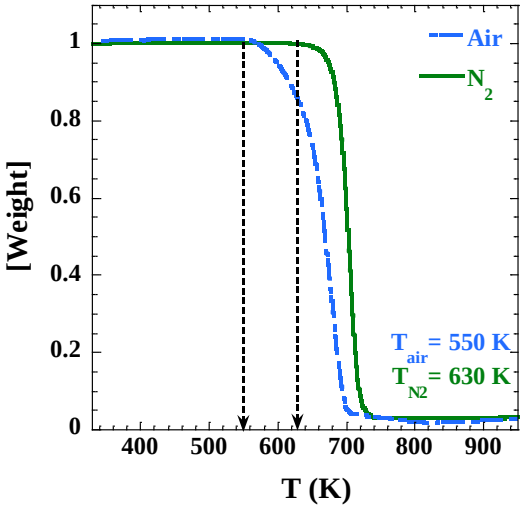

Figure A.4 TG curves for degradation of PTBS heated at 10 K/min under air (oxidative) and nitrogen (inert) atmospheres. Dashed blue line corresponds to the oxidative conditions and solid green line to inert conditions.

A.4. REFERENCES

(1) Schawe, J. E. K.; Pogatscher, S. Part I. Material Characterization by Fast Scanning Calorimetry: Practice and Applications. In *Fast Scanning Calorimetry*; Schick, C., Mathot, V., Eds.; Springer International Publishing, 2016; pp 3–80.

(2) Poly(dimethyl siloxane) (PDMS) Heat Capacity, Enthalpy, Entropy, Gibbs Energy - SpringerMaterials https://materials.springer.com/polymerthermodynamics/docs/athas_0119 (accessed Apr 13, 2018).

(3) Jenkins, F. A.; White, H. E. *Fundamentals of Optics*; International student edition; McGraw-Hill, 1976.

(4) Spectroscopic ellipsometry TN14 http://www.horiba.com.

PUBLICATIONS

This thesis has contributed to the following publications:

(1) Irreversible Adsorption Erases the Free Surface Effect on the Tg of Supported Films of Poly(4-Tert-Butylstyrene). Perez-de-Eulate, N. G.; Sferrazza, M.; Cangialosi, D.; Napolitano, S. *ACS Macro Lett.* **2017**, *6* (4), 354–358.

(2) Glass Transition and Molecular Dynamics in Polystyrene Nanospheres by Fast Scanning Calorimetry. Perez-de-Eulate, N. G.; Di Lisio, V.; Cangialosi, D. *ACS Macro Lett.* **2017**, *6* (8), 859–863.

(3) Double Mechanism for Structural Recovery of Polystyrene Nanospheres. Perez-De-Eulate, N. G.; Cangialosi, D. *Macromolecules* **2018**.

(4) The Very Long-Term Physical Aging of Glassy Polymers. Perez-de-Eulate, N. G.; Cangialosi, D. *Phys. Chem. Chem. Phys.* **2018**.

ACKNOWLEDGEMENTS / AGRADECIMIENTOS

Durante todos estos años de doctorado me llevo dos importantes cosas: por un lado, un trabajo que me ha aportado una experiencia y unos conocimientos enormes, los cuales me permitirán seguir progresando en mi vida profesional. Por otro lado, un grupo de gente excepcional que me ha aportado mucho apoyo y muy buenos momentos. A todas estas personas quiero darles las gracias.

En primer lugar me gustaría agradecer a mi director de tesis Daniele Cangialosi, por toda la ayuda brindada durante estos cuatro años. Muchas gracias por el apoyo y por el esfuerzo realizado sobre todo en este último tramo de tesis. También quisiera agradecer al Prof. Juan Colmenero de León el haberme dado la oportunidad de formar parte del grupo "Polymer and Soft Matter", y al resto de integrantes que en algún momento me han prestado su ayuda.

Mi agradecimiento a Simone Napolitano. Thank you very much for your support and for giving me the opportunity of doing my abroad research in your "Laboratory of Polymer and Soft Matter Dynamics". I would like to extend my gratitude to all the members of your group and to Pascal Pirotte for helping me with the ellipsometer. Furthermore, many thanks to Prof. Rodney Priestley for his supporting letter to obtain the recognition of 'International Thesis'.

Expreso mi agradecimiento a la Universidad del País Vasco (UPV/EHU), al Ministerio de Economía, Industria y Competitividad (MINECO) por la

concesión de la beca FPI (BES-2013-063947) y a la fundación de investigadores Materials Physics Center (MPC-BERC) por el contrato en el periodo final de la tesis.

Primeramente me gustaría agradecer a Isa el haber estado siempre a mi lado. Gracias por haber compartido conmigo los entresijos del laboratorio y por el día a día, sin ti esto no hubiera sido lo mismo. Me llevo a una gran amiga.

A mis chicas del despacho. Izaskun y Lucía, agradeceros a las dos todo vuestro apoyo, así como los buenos momentos vividos y ¡los que nos quedan por vivir! Me alegro de haberos conocido. Tampoco puedo olvidarme de mis antiguos compañeros: Luisa, gracias por haberme ayudado tanto al inicio y por estar a mi lado; Gerardo, a ti también agradecerte esas charlas de desconexión de media tarde. Igualmente ha sido un placer haber podido compartir un trocito de este camino con: Rubén, Alicja, Zita, Lisa, Jordana y Ana Lucía.

A Daniel Martinez-Tong, muchas gracias por tu constante ayuda y apoyo, sin duda pieza fundamental en este trabajo.

Por supuesto mencionar al resto de mis actuales compañeros: a Guido, Marina, Amaia, Paula, Bea y Edurne agradeceros vuestros consejos y fructíferas conversaciones, así como a Thomas, Jon, Jordan, Maud, Julen, Jorge, Xavier y Daniel. No puedo olvidarme de ti Valerio, muchas gracias por haberme enseñado tanto de calorimetría, grazie mille!

A los que no estáis aquí pero seguís continuamente a mi lado. Manuel desde China con tus visitas anuales, siempre es un placer compartir unas cañitas o vinos contigo. Irma, gran persona y me encanta que después de tantos años sigamos compartiendo buenos momentos. Por supuesto, no puedo olvidarme de ti Alex, has sido y sigues siendo un gran compañero dentro y fuera de este centro.

A mi entorno personal de amig@s que han vivido esta etapa desde muy cerca. Sois parte de mi vida, por lo que esta tesis es una pequeña parte de la vuestra.

A mi "cariño", que sepas que no me quedan palabras para agradecerte todo tu apoyo y constancia. Lo que puedo decirte es que tú me has enseñado a seguir el poema de Rudyard Kipling: "El éxito comienza en la voluntad".

Y por supuesto a mi familia, a mi hermana Susana y a mis aitas. Aita, ama gracias por confiar en mí ¡Esta tesis va por vosotros!

ESKERRRIK ASKO GUZTIOI!!!